UNIVERSITEIT VAN PRETORIA
UNIVERSITY OF PRETORIA
YUNIBESITHI YA PRETORIA

Brake Based Integrated Rollover Prevention and Yaw Control for an Off-Road Vehicle

by

Rénier Strauss

Submitted in partial fulfilment of the requirements for the degree

Master of Engineering

(Mechanical Engineering)

In the Faculty of

Engineering, Built Environment and Information Technology (EBIT)

at the

University of Pretoria,

Pretoria

December 2016

Summary

Title:	Brake Based Integrated Rollover Prevention and Yaw Control for an Off-Road Vehicle.
Author:	Rénier Strauss
Study Leader:	Prof. P. S. Els
Department:	Mechanical and Aeronautical Engineering, University of Pretoria
Degree:	Master of Engineering (Mechanical Engineering)

Sport utility vehicles typically feature high ground clearances that allow them to be used in off-road conditions. Their use is not limited to off-road conditions and they are often used as day-to-day family vehicles. On the road, where high friction surfaces are prevalent, their high centres of gravity can make them susceptible to un-tripped rollovers during severe dynamic manoeuvers such as an emergency obstacle avoidance. The detection of a high risk of rollover and the avoidance thereof has great potential to improve vehicle safety, as the consequences of rollover incidents are generally quite severe.

Rollover mitigation systems are triggered when a rollover threshold index is exceeded, indicating a high risk of rollover. The metric implemented in this study is known as the zero-moment point method, which allows for vehicle parameters and terrain to be taken into account. Previous research has indicated that mitigation systems that trigger braking intervention are some of the most successful methods in reducing rollover risk, as it not only stabilises the vehicle, but also reduces the speed.

Brake based rollover prevention systems typically implement electronic stability program methods that use yaw rate reduction as the primary tool for reducing rollover risk, which often comes at the expense of the vehicle's path following ability. This means that the stability control system may lead to the vehicle leaving the road and causing an even more severe accident. The control algorithm implemented in this study gives preference to reducing the forward speed of the vehicle which in turn reduces lateral acceleration, a major contributor to rollover propensity. Braking is however apportioned to all four wheels and distributed so as to achieve vehicle yaw rate targets. Emphasis is placed on maintaining good path following capability to prevent the vehicle from leaving the road.

The detection and mitigation system was tested on a Land Rover Defender 110 for a variety of manoeuvers in simulation as well as experimental testing. The results indicate that the rollover mitigation system managed to successfully reduce the rollover threshold index of the vehicle during the manoeuver whilst simultaneously maintaining the path following ability of the vehicle and improved the yaw rate tracking.

Acknowledgements

I would like to show my gratitude to:

- My parents Deon and Marié Strauss and sister Tanya, for their unconditional support and encouragement.
- Prof. Els for the opportunities, support and guidance during my time at the Vehicle Dynamics Group.
- My fellow post-graduate students Jacob Grobler, Brett Kent, Wietsche Penny, Glen Guthrie, Joachim Stallmann, Herman Hamersma and the rest of the VDG team for their advice, assistance and the comic relief.
- Carl Becker for his help during testing and Theunis Botha for all the knowledge sharing.
- Bernard Linstrom for the support through post-graduate studies and the encouragement to complete my master's degree.

Table of Contents

List of Figures

List of Tables

List of Abbreviations

$4S_4$	Four-State Semi-Active Suspension System
ABS	Anti-Lock Braking System
ADAMS	Automatic Dynamic Analysis of Mechanical Systems
CG	Centre of Gravity
DLC	Double Lange Change
ESC	Electronic Stability Control
ESC+RP	Electronic Stability Control with Rollover Prevention
ESP	Electronic Stability Program
FL	Front Left
FR	Front Right
GPS	Global Positioning System
IMU	Inertial Measurement Unit
LLTR	Lateral Load Transfer Ratio
MES	Manoeuver Entry Speed
MR	Magneto-rheological
MTF	Magic Tyre Formula
NHTSA	National Highway Traffic Safety Administration
NS	Neutral Steer
OA	Obstacle Avoidance
OEM	Original Equipment Manufacturer
OS	Oversteer
R^2	Coefficient of determination
RCF	Rollover Critical Factors
RI	Rollover Index
RL	Rear Left
RMS	Root Mean Square
RR	Rear Right
SSF	Static Stability Factor
SUV	Sport Utility Vehicle
TTR	Time-to-Rollover
US	Understeer
ZMP	Zero-Moment Point

List of Symbols

a_x	Longitudinal acceleration [m/s²]
$a_{y,c}$	Critical lateral acceleration [m/s²]
$a_{y,des}$	Desired lateral acceleration [m/s²]
a_y	Lateral acceleration [m/s²]
a_z	Vertical acceleration [m/s²]
C_1, C_2	Constants
C_α	Tyre cornering stiffness [N/°]
$C_{\alpha f}$	Cornering stiffness of front tyres [N/°]
$C_{\alpha r}$	Cornering stiffness of rear tyres [N/°]
$F_{x,fl}$	Front left tyre longitudinal force [N]
$F_{x,fr}$	Front right tyre longitudinal force [N]
$F_{x,rl}$	Rear left tyre longitudinal force [N]
$F_{x,rr}$	Rear right tyre longitudinal force [N]
F_{xf}	Font tyres longitudinal force [N]
F_{xr}	Rear tyres longitudinal force [N]
ΔF_x	Desired longitudinal force [N]
F_y	Lateral Force [N]
F_{y0}	Lateral tyre force with no longitudinal force [N]
F_{yf}	Front tyres lateral force [N]
F_{yr}	Rear tyres lateral force [N]
F_{yi}	Inner tyres lateral force [N]
F_{yo}	Outer tyres lateral force [N]
$F_{z,fl}$	Front left tyre vertical force [N]
$F_{z,fr}$	Front right tyre vertical force [N]
$F_{z,rl}$	Rear left tyre vertical force [N]
$F_{z,rr}$	Rear right tyre vertical force [N]
F_{zi}	Inner tyre vertical force [N]
F_{zo}	Outer tyre vertical force [N]
g	Gravitational acceleration = 9.81 [m/s²]
h	Height of centre of gravity [m]
h_f	Front roll centre height [m]
h_r	Roll centre height or rear roll centre height [m]
h_s	Distance between roll centre and CG [m]
I_{xx}	Roll mass moment of inertia [kgm²]
I_{yy}	Pitch mass moment of inertia [kgm²]
I_{zz}	Yaw mass moment of inertia [kgm²]
I_{xz}, I_{yz}	Mass product of inertia [kgm²]
k_1	Constant

$K_{\emptyset}$	Roll stiffness [N/rad]
$K_{\emptyset f}$	Front suspension roll stiffness [N/rad]
$K_{\emptyset r}$	Rear suspension roll stiffness [N/rad]
K_s	Suspension stiffness [N/m]
K_v	Understeer gradient
L	Distance between front and rear axle [m]
L_f	Distance from front axle to centre of gravity [m]
L_r	Distance from rear axle to centre of gravity [m]
m	Mass of vehicle [kg]
M_z	Yaw moment [Nm]
p	Brake pad pressure
q	Pitch rate [rad/s]
r	Yaw rate [rad/s]
r_o, r_i	Brake pad inner and outer radius [m]
r_t	Tyre rolling radius [m]
R	Radius of corner [m]
t	Time [s]
T	Track width [m]
T_b	Braking torque [Nm]
T_s	Distance between suspension struts [m]
V/V_x	Vehicle longitudinal velocity [m/s]
$V_{x,des}$	Desired vehicle longitudinal velocity [m/s]
$V_{x,m}$	Measured vehicle speed [m/s]
V_y	Vehicle lateral velocity [m/s]
W	Vertical tyre load [N]
x_{zmp}	Longitudinal position of zero moment point
y_{zmp}	Lateral position of zero moment point
β	Vehicle side-slip angle [rad]
β_f	Front tyres average slip angle [rad]
β_r	Rear tyres average slip angle [rad]
$\dot{\beta}$	Vehicle side slip rate [rad/s]
δ_{SIS}	Steady increasing steer angle [rad]
δ_{SS}	Steady state steering angle [rad]
μ	Road friction coefficient
μ_{bp}	Brake pad friction coefficient
η	Positive constant
$\emptyset/\emptyset_r$	Roll angle [rad]
$\emptyset_t$	Terrain roll angle [rad]
$\emptyset_{th}$	Roll angle threshold [rad]
$\dot{\emptyset}$	Roll rate [rad/s]
$\dot{\emptyset}_{th}$	Roll rate threshold [rad/s]

θ	Pitch angle [rad]
I_i	Inertia tensor [kgm²]
$\overrightarrow{M_A}$	Moments about point A
$\overrightarrow{a_i}$	Acceleration [m/s²]
$\vec{g}$	Gravitational acceleration [m/s²]
m_i	Mass of i^{th} body [kg]
$\overrightarrow{p_i}$	Position vector [m]
$\overrightarrow{\alpha_i}$	Angular acceleration [rad/s²]
$\overrightarrow{\omega_i}$	Angular velocity [rad/s]
$\vec{\imath}, \vec{\jmath}$	Component unit x- an y-vectors

1. Introduction

The sales of Sport Utility Vehicles (SUV's) have increased significantly in recent years. This is due to an increasing number of product offerings becoming available, the ground clearance they provide and the higher seating position that improves visibility and perception of safety. Where these vehicles use to be somewhat unrefined and purchased for their off-road capabilities, these vehicles have become more popular for everyday use as ride, handling and refinement improved. The characteristics that lead to their popularity also put them at risk of incidents such as rollovers. This is mainly due to their high centre of gravity and typically compliant suspension with large amounts of travel. The trend of fitting large low profile tyres, with high levels of grip, adds to the problem.

The National Highway Traffic Safety Administration (NHTSA, 2013) states that although rollovers account for a small percentage of total accidents, their fatality rate is among the highest. 2010 figures indicate that rollover account for only 2.1% of all passenger cars, SUV, pickup and van crashes, although they led to nearly 35% of all passenger vehicle deaths. In South Africa during 2009, rollovers were responsible for almost 24% of all fatal crashes and nearly 25% of all road fatalities, (Road Traffic Management Corporation, 2009). Tripped rollovers account for the majority of rollover incidents, although the mitigation of these incidents does not always lie with the vehicle characteristics itself, as will be explained later. The untripped rollover case is considered a factor that can be controlled to some large extent and it is therefore considered imperative to reduce the rollover propensity of these high centre of gravity vehicles.

This research will cover some of the recognised studies done on the topic of vehicle rollover and discuss the parameters that lead to rollover, the methods of detecting impending rollover as well as some of the methods available to mitigate rollover.

A zero-moment point based rollover index is developed in this report along with an associated braking based rollover prevention and yaw control system. The control methodology is tested in a simulation as well as experimental environment to establish its effectiveness at reducing rollover risk, whilst maintaining the path following and yaw response capabilities of the vehicle during an emergency evasive manoeuver.

Results indicate that the proposed system is feasible and has the potential to significantly reduce untripped rollover without significant additional vehicle cost and complexity.

2. Literature Study

The literature study aims to provide an overview of research that has been conducted previously on vehicle rollover.

The research can typically be categorised into the subsections of rollover detection and rollover prevention. Although these areas overlap in some instances, the development of these systems can be quite diverse.

The study will first provide an overview of the mechanism of rollover after which the detection and prevention studies are discussed. The standard industry tests for rollover propensity are also investigated.

2.1 Rollover Description

A vehicle subjected to some form of cornering manoeuvre along a curved path experiences acceleration towards the centre of the curved path. The tyres of the vehicle produce forces towards the centre of the turn which accelerates the vehicle centripetally.

The lateral tyre forces act in the ground plane, while the lateral acceleration of the vehicle towards the centre of the turn acts at the CG. This offset between the tyre forces and the vehicle CG leads to a moment on the vehicle which attempts to roll it towards the outside of the turn (Gillespie, 1992).

A roll angle between the sprung and unsprung mass is induced as well as a transfer of loads form the tyres on the inside of the turn towards the outside of the turn. This overturning moment leads to a rollover condition when the inside tyres are unloaded sufficiently (i.e. loses ground contact) before sliding occurs.

The situation described is what is known as an un-tripped rollover. The vehicle is overturned without the outside tyres making contact with an obstacle or digging into a soft surface. When the latter occurs it is considered to be tripped rollover and can occur when the vehicle slides. The tripped rollover phenomenon is a very complex one, as it very much depends on factors such as the obstacle with which the tyres makes the impact and subsequently the way in which the impact energy is dissipated (Gillespie, 1992). The study of tripped rollovers tend to focus less on the dynamics of the vehicle itself and the focus of this study will therefore be on un-tripped rollovers.

Figure 1 shows the basic mechanisms involved when analysing the lateral load transfer in the presence of a centrifugal inertia force. The load transfer is described by equation (2-1) as discussed by Gillespie (1992).

$$F_{zo} - F_{zi} = \frac{2F_y h_r}{T} + 2K_{\emptyset}\frac{\emptyset}{T} \tag{2-1}$$

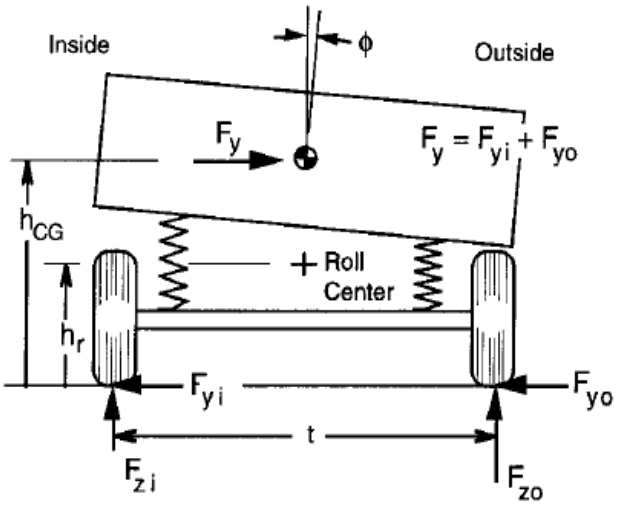

Figure 1 – Simple vehicle cornering model, (Gillespie, 1992)

Equation (2-1) considers the vehicle to be lumped to a single axle and shows the coupling between the sprung and unsprung masses. It is evident that the load transfer depends on two factors, the first term describing the effect of transferring the lateral force to the roll centre and the second term the moment produced around the roll centre. When the vehicle is considered as such a lumped system, the only factors that influence the load transfer are the height of the vehicle centre of gravity and the vehicle track width.

The effect of changing the roll stiffness only becomes apparent once the relationship between the front and rear roll stiffnesses are considered, which have the effect that different load transfers are experienced at the front and the rear of the vehicle (Milliken & Milliken, 1995). Increasing the overall vehicle roll stiffness has secondary effects such as that the lateral displacement of the centre of gravity is reduced when a roll angle is introduced by a certain lateral acceleration.

The onset off vehicle rollover requires sufficient friction between the tyres and the road. A high friction coefficient allows for large enough lateral acceleration and overturning moment to be produced that could lead to rollover. To illustrate this, the simple rigid vehicle model in Figure 2 is analysed.

$$\sum F_y = ma_y$$
$$F_{yi} + F_{yo} = ma_y \tag{2-2}$$

$$\sum F_z = ma_z$$
$$F_{zi} + F_{zo} = mg \tag{2-3}$$

If all tyres are considered to be in contact with the road, the maximum lateral forces that can be produced are:

$$F_{yi} = \mu F_{zi}$$
$$F_{yo} = \mu F_{zo} \tag{2-4}$$

$$F_{yi} + F_{yo} = \mu(F_{zi} + F_{zo})$$
$$ma_y = \mu mg \tag{2-5}$$

Therefore:

$$\left(\frac{a_y}{g}\right)_{slide} = \mu \tag{2-6}$$

By assuming that the vehicle is at the point of imminent rollover, the load on the inside tyres go to 0. Taking the sum of moments around the outside tyre contact patch:

$$mg\left(\frac{T}{2}\right) = ma_y h$$
$$\left(\frac{a_y}{g}\right)_{roll} = \frac{T}{2h} \tag{2-7}$$

The vehicle will slide before it rolls when $\left(\frac{a_y}{g}\right)_{roll} > \left(\frac{a_y}{g}\right)_{slide}$. This criteria for slide before roll can then also be written as:

$$\frac{T}{2h} > \mu \tag{2-8}$$

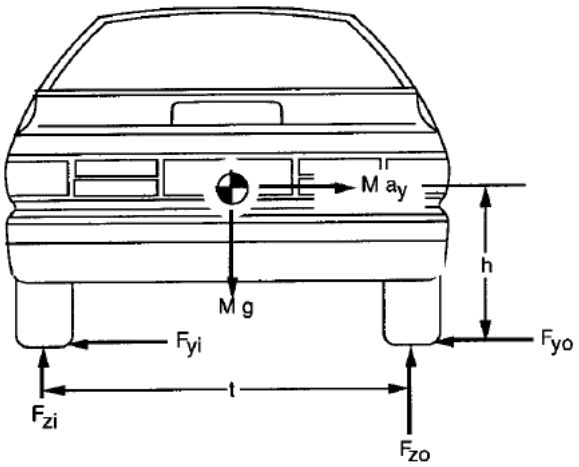

Figure 2 - Rigid vehicle model

2.2 Rollover Detection

The development of strategies aimed at reducing the risk of rollover as well as knowing the rollover risk of a particular vehicle requires an accurate metric that indicates under which conditions a rollover will occur. Quantifying the risk of a rollover has been the study of various authors.

The most basic metrics known as the Static Stability Factor (NHTSA, 1991) is based on the roll vs. slide criteria described in equation (2-8). Slide will hence occur before roll if equation (2-8) is satisfied

The factor $\frac{T}{2}/h$ in this equation is the Static Stability Factor (SSF) and is a basic metric used by the National Highway Traffic Safety Association to classify the rollover risk of a vehicle, (NHTSA, 1991). According to the SSF, the rollover risk of a vehicle is only dependent on the height of the vehicle centre of gravity and the track width in the presence of sufficient grip.

The use of the SSF to quantify the rollover risk is discussed by Hac (2002b) who illustrates its deficiencies in accurately predicting the lateral acceleration threshold that would lead to rollover. Hac goes on to expand the vehicle roll model, as illustrated in Figure 3, to include the effects of change in track width due to lateral tyre deflection and suspension kinematics as well as change in CG height from jacking forces and even wheel gyroscopic effects. A factor is also added to compensate for dynamic overshoot influenced by the damping of the suspension. The results indicate that these secondary factors can reduce the rollover threshold by as much as 20-25%, compared to the SSF, for a typical SUV.

The document presented by Li, et al. (2013) expands on the work done by Hac (2002b) to also include the effects of the road surface. This is achieved by taking the vertical displacement of the CG, caused by the vertical sprung mass vibration, into account. The shortcomings of the SSF are recognized and different indices called Rollover Critical Factors (RCF) are defined and compared for different dynamic tests. The results indicate that the RCF based on tyre, suspension and vibration effects is the most sensitive to detecting rollover and provides the highest safety margin.

The metrics discussed are capable of providing a real time rollover threat index by using measurements at the specific time instance. These rollover threat indices therefore require the measurement of factors such as lateral acceleration, sprung mass displacement as well as roll angle and roll acceleration. These parameters are readily available in simulation models although it could be costly to implement on a vehicle. The problem we also face with these rollover indices is that they are based on current conditions and does not provide any future predictions that will allow sufficient time for a roll prevention system to intervene.

A predictive rollover threat index that is commonly used as input to prevention systems is the Time-to-Rollover (TTR) index introduced by Chen & Peng (1999). The TTR index is based on the development of accurate yaw and roll models that are used to predict the threat of a rollover in the near future. The model is investigated for rollover cases and the clock is then rolled back to see what the vehicle conditions were at that time. Recognising these conditions can then predict an impending rollover.

The model was refined with a trained neural network to correct the errors between predicted TTR and actual TTR. Although this was successful for heavy trucks, the gains in accuracy were insignificant for implementation on a SUV. The tests by Chen & Peng proved to provide a TTR warning in the order of 0.3s.

The need for accurate estimation of the vehicle states which could lead to a rollover is also recognised by Hac, et al. (2004). The document states that measurements such as lateral acceleration and roll rate alone are not sufficient in accurately predicting an impending rollover. Road inputs such as changes in banking angle can cause false detections. For this reason the model also distinguishes between the vehicle with its tyres making contact with the road and a vehicle that is experiencing some wheel lift off. This is illustrated in Figure 3 where the instantaneous roll centre of the vehicle changes.

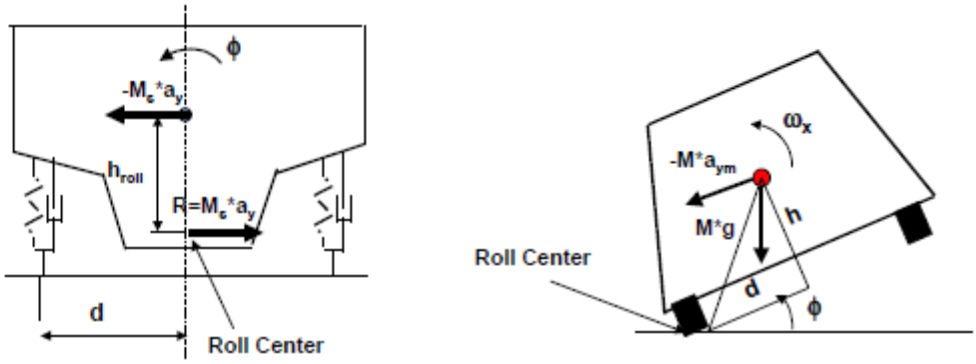

Figure 3 - Roll centre changes before and after wheel lift, (Hac, et al., 2004)

Hac, et al. then introduces a model-based closed-loop observer that uses sensor inputs such as lateral acceleration and roll rate to produce an accurate approximation of the relative roll angle and roll rate of the vehicle. The lateral acceleration, roll angle and roll rate are then combined into an overall Rollover Index (RI) that aims to predict a rollover condition. Results from the tested conditions appear to be successful in avoiding false detections.

An estimator based system using similar principles is developed and implemented by Yoon, et al. (2007). Simulation results show good performance of the rollover index in detecting rollover.

The Zero-Moment Point (ZMP) method is investigated by Lapapong (2010) for use as a vehicle rollover prediction metric. The ZMP is a method commonly used to determine the balance stability of biped robots. The zero-moment point is defined as the point on the ground where the sum of the tipping moments due to gravitational and inertial forces acting on an object is equal to zero. For an object to remain stable, the zero-moment point is required to be within the support polygon of the mechanism. This method is successfully validated by the author to predict vehicle wheel lift by using measurable parameters.

A new rollover index is developed by Phanomchoeng & Rajamani (2011) that claims to detect both tripped and un-tripped rollovers that are caused by both lateral as well as vertical vehicle inputs. The rollover index is produced by a non-linear observer in conjunction with inputs from vertical and lateral accelerometers. The model is tested using a scale vehicle with results proving to accurately detect the different rollover conditions. The development of this roll index appears to still be at an

infant stage with real vehicle simulation results not appearing to be available. The initial simulation and scale model results do appear to be very promising for further investigation.

2.3 Rollover Prevention

The prevention of the un-tripped rollover has been the focus of much research, with different methods showing various levels of success. The research typically addresses different primary and secondary factors that contribute to rollovers taking place. These include measures to reduce the lateral and yaw accelerations of the vehicle as well as reducing the body roll angle of the vehicle.

The typical methods utilised implement the different categories discussed below.

2.3.1 Controllable Suspension

The research done by many authors including that of (Gillespie, 1992), (Milliken & Milliken, 1995) and (Hac, 2002b) show that the lateral displacement of the vehicle CG from an induced roll angle is a major contributor to lateral load transfer when a vehicle experiences a lateral acceleration. By reducing the roll angle this factor can also be reduced, hence raising the rollover threshold.

As mentioned previously, the roll angle can be reduced by increasing the roll stiffness of the vehicle. By using the vehicle roll angle as a measure of the handling performance of the vehicle, Els (2006) developed a controllable suspension system known as the Four-State Semi-Active Suspension System ($4S_4$). The system is based on a hydro-pneumatic suspension principle and has the ability to switch between two discrete spring stiffnesses and two discrete damping characteristics. Figure 4 shows the system layout, with the different spring and dampers characteristics achieved are shown in Figure 5 and Figure 6 respectively.

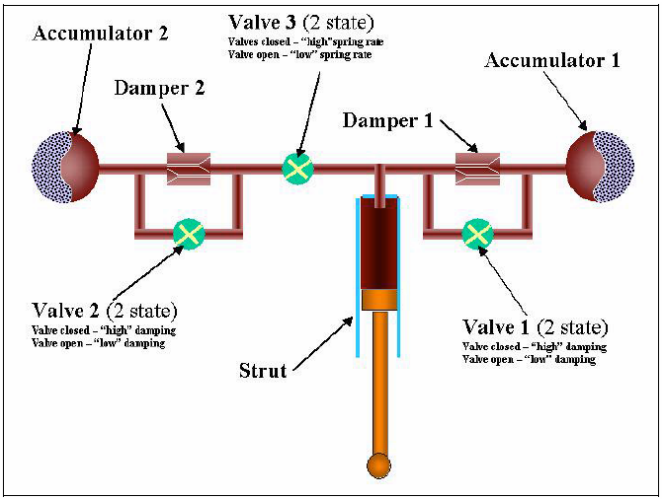

Figure 4 - $4S_4$ Suspension system circuit diagram, (Els, 2006)

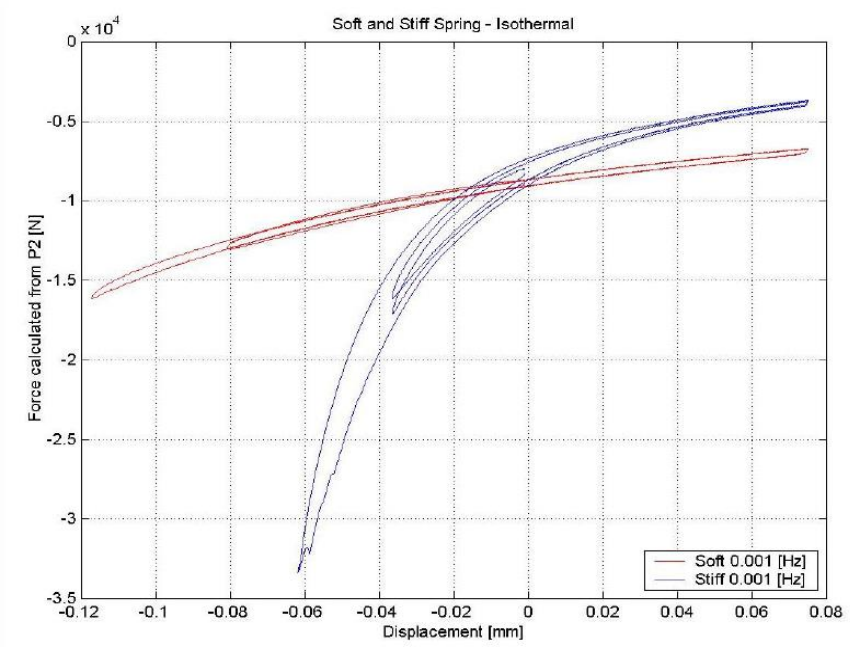

Figure 5 - 4S$_4$ Soft and Stiff spring characteristics, (Els, 2006)

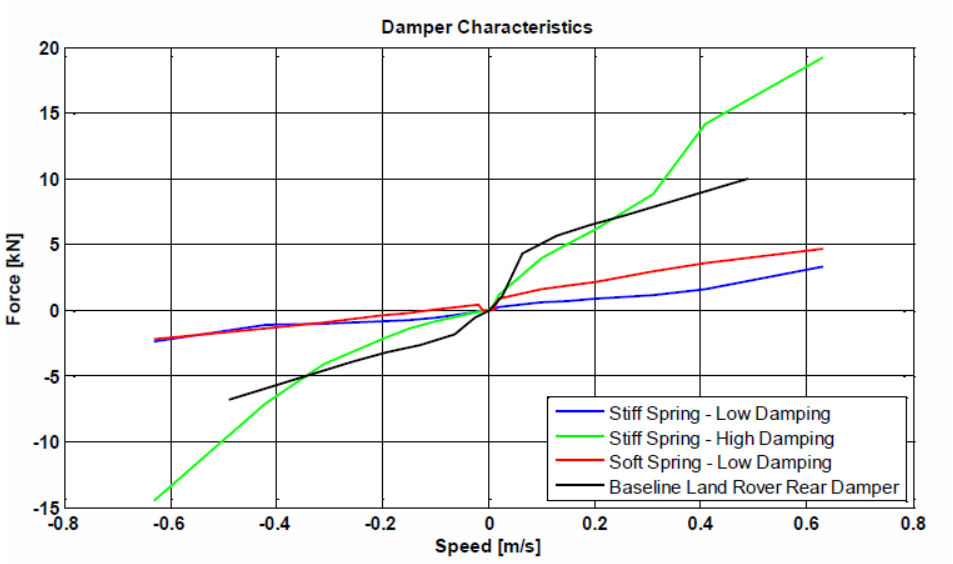

Figure 6 - 4S$_4$ Damping characteristics, (Els, 2006)

The system switches between a ride (soft spring and low damping) setting and a handling (hard spring and high damping) setting whenever the need for either is detected based on threshold Running RMS lateral and vertical acceleration values. The system is implemented on a Land Rover Defender 110 SUV.

It is shown that the system manages to successfully reduce the vehicle roll angle during a double lane change test by between 61 and 78%. The nature of the system also allows the ride height of the vehicle to be lowered by 50mm, a control measure that further reduces roll angle and load transfer during cornering.

The study on rollover performed by Uys (2007) on a Land Rover Defender 110 SUV highlights the importance of high damping on reducing roll velocity and wheel lift during a manoeuvre such as the NHTSA Fishhook test (Forkenbrock, et al., 2004).

The control over damping characteristics is achieved by semi-active systems such as the $4S_4$ system as well as various other widely implemented semi-active systems. One such system is a magneto-rheological damper that can achieve varying damping levels dependent on the electrical current supplied to its damping fluid that contains magnetic particles. The changing current varies the fluid viscosity and subsequently the damping characteristics of the suspension. Production examples include vehicles produced by Cadillac, Audi and Ferrari.

A system of controlling the vehicle stability and yaw response by changing the damping characteristics through MR damping is proposed by Bodie & Hac (2000). The mechanism behind the system is the influence of vertical tyre loads on the lateral force generation of the tyre. By changing the individual damping characteristics of the front and rear suspension, the lateral load transfer can be manipulated during dynamic manoeuvers. The tyre load-sensitivity effects (discussed in section 2.4.2) will then lead to varying over- or understeer characteristics. Simulations indicate that closed loop control can lead to a reduced yaw rate error from the desired yaw rate.

Other methods of damping control include the use of bypass valves to switch between different orifice sizes to allow for different damping characteristics. Manufacturers of such dampers include Ohlins, Bilstein and Koni.

A study on the effect of controlling roll angle on the Land Rover Defender 110 SUV was performed by Cronjé (2008). The study was based on the use of an active anti-roll bar fitted to the rear of the vehicle. The system showed an improvement in roll angle of 74% during the double lane change test at 70km/h. The fitment of the active anti-roll bar to only the rear of the vehicle does however decrease the yaw stability of the vehicle by increasing the rear lateral load transfer and hence the oversteer tendencies of the vehicle.

The ride height adjustment characteristic of the $4S_4$ system is utilised by Van Der Westhuizen (2012) to introduce vehicle levelling control to counter and reduce the roll angle of the vehicle. This control is achieved by pumping and draining oil from the respective corners of the vehicle. The results show a successful improvement in roll angle. The system is also claimed to have the benefit of improving pitch and dive behaviour of the vehicle.

A production example of a system aimed to achieve roll control without the use of a fixed anti-roll bar is the system utilised in the McLaren MP4-12C. This system was originally invented by Heyring (1995). It consists of double acting hydraulic cylinders that are diagonally linked to the unit on the corresponding opposite side of the vehicle. This means that a bump movement on the left wheel resists the rebound movement on the right wheel and visa-versa. This has an anti-roll effect, but with the added advantage that the flow between units can also be controlled.

2.3.2 Four Wheel Steering

The use of four wheel steer systems is typically implemented on vehicles to improve stability at high speeds and yaw response at lower speeds. It is however considered in the context of rollover mitigation by Hac (2002a). It is argued that the use of active rear steer can reduce the vehicle rollover threat by reducing the yaw acceleration of the vehicle and the tendency of the vehicle to oversteer. The instability induced by an oversteering vehicle is considered to be a risk that contributes to rollover.

The simulation results indicated that the implementation of active rear steer increased the rollover threshold of the vehicle over the base vehicle without control in a double lane change test. It was mentioned that the biggest improvement of rollover mitigation was produced when this system was combined with active brake control.

2.3.3 Braking Based Control

The use of braking systems to mitigate rollover has been studied by various authors and is also a system that has been implemented on a commercial level. The concept of anti-rollover braking was patented by Wielenga (2000) and similar concepts implemented by companies such as Bosch (Bosch, 2013) as part of their existing Electronic Stability Program that is used by many original equipment manufacturers (OEM's).

The idea behind the original concept by Wielenga (2000) was that the use of braking on the front most heavily loaded wheel addresses two factors that contribute to rollover. The application of the longitudinal braking force firstly imparts a yaw moment on the vehicle that counters the yaw from the steering input. This has the effect that the radius of the path the vehicle is following increases and hence reduces the lateral acceleration of the vehicle. The second factor is the effect of the braking force on the tyre. The concept of the friction circle, as illustrated in Figure 7 shows that the application of a braking torque creates a longitudinal tyre force that reduces the lateral force the tyre is capable of producing, due to only a finite amount of grip being available from the tyre at a specific load. This reduction in lateral force reduces the lateral acceleration of the vehicle.

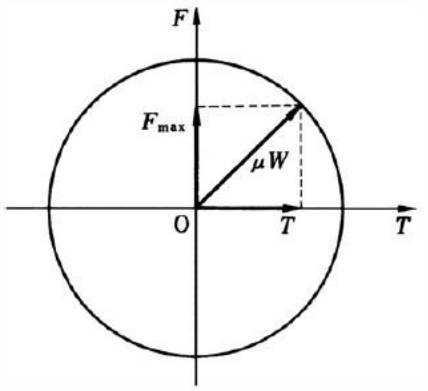

Figure 7 - Tyre friction circle, (Abe, 2009)

The study conducted by Chen & Peng (2010) argues that the use of braking based systems is one of the most economical to implement commercially due to the use of the same technology commonly available on a vehicle's stability control system. The authors utilise their TTR metric in conjunction with a differential braking system that applies a braking torque to the outside front wheel during cornering. The system reduces the longitudinal velocity, lateral tyre force and yaw rate; all factors that increase the risk of rollover. The simulation results show a successful reduction in the rollover risk. The system is also tested with human steering interaction. The results show that the system is still successful in reducing rollover risk although in an obstacle avoidance test drivers tended to increase the steering input in response to the understeer induced by the system, in effect negating some of the system control efforts.

The need for improved stability when applying differential braking is discussed by Cao, et al. (2013). They present an integrated control system that consists of roll stability control as well as yaw stability control. The TTR metric is used to detect impending rollover. The system induces understeer by braking the outside front wheel to reduce the lateral acceleration and applying braking to the inner wheel to reduce the yaw error of the vehicle.

A different approach to correct the yaw error created by differential braking is followed by Carlson & Gerdes (2003). The system uses steer-by-wire to correct the yaw error and follow the original intended path. This type of technology is still in its infancy on commercial level, although the results show that the system is capable of reducing the roll angle whilst still tracking the intended path.

A unified chassis control system that integrates rollover prevention with electronic stability control together with continuous damping control is proposed by Yoon, et al. (2009). A rollover index is monitored and a braking based system is triggered when the threshold is exceeded. The braking based system aims to reduce the rollover risk whilst simultaneously improving the lateral stability of the vehicle. The continuous damping control is used to control the roll response of the vehicle. The system was evaluated in the CarSim simulation software and proved to be very successful in reducing rollover risk as well as yaw and tracking error.

Evaluation of the previously developed unified chassis control system is continued by Yoon, et al. (2010). In this instance the system aims to integrate the active front steering with the electronic stability control as well as continuous damping control. The electronic stability control was expanded to include side-slip control. An overview is also given to illustrate the control hierarchy between traditional vehicle stability control and the rollover prevention system. The system is only tested in simulation.

An overview study on the success of various rollover mitigation systems was performed by Hac (2002a). The study does a comparison of systems such as braking based Vehicle Stability Enhancement, active rear steer and active anti-roll bar based Dynamic Body Control. Simulations are done on a SUV and results show that the most successful rollover prevention is achieved by the braking based stability control in conjunction with either one of the other systems. The improved yaw control introduced by the added active rear steer resulted in the most stable vehicle, whereas the active anti-roll bar merely improves the balance between ride and handling of the vehicle.

2.4 Tyre Models

The Pacejka '89 tyre model is also commonly known as the Magic Formula tyre model (Blundell & Harty, 2004). This formula uses the data gathered from experimental tyre tests that relates factors such as slip angle to lateral force at a given tyre load. These tests are usually performed at discrete loads. The Magic Formula uses coefficients calculated from a curve fit to relate lateral force to slip angle at specified loads other than that used to gather the experimental data. This tyre model is mainly used for handling simulations on smooth roads and is not very computationally expensive to implement. This model was used for the initial feasibility study and development of the control strategies discussed in this report.

FTire or Flexible Ring Tire Model is a full 3D physics based tyre model. The model is based on a tyre belt modelled as a flexible ring (Figure 8) that has defined structural dynamics properties (Cosin Scientific Software, 2015). This flexible ring is discretised into "belt elements" that are connected to their direct neighbours by springs in-plane and out-of-plane. The structural characteristics of these belt elements as well as the spring and damping characteristics of their association with the centre rigid hub are defined during extensive parameterisation based on physical testing of the tyre. This tyre model is claimed to be able to describe dynamic responses up to 200Hz as it is not based on empirical curve fitting of experimental data.

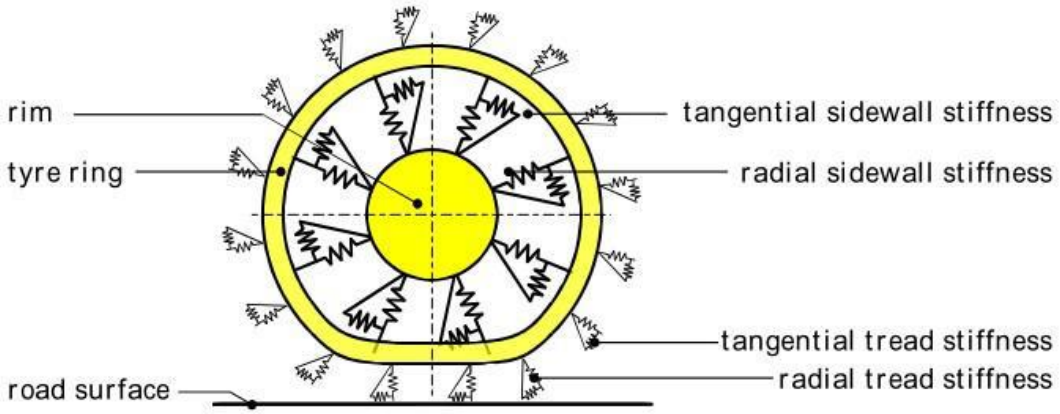

Figure 8 - FTire stiffness elements (Penny, 2015)

2.4.1 Friction Circle

The scenarios we are investigating where braking torques are applied to individual wheels require consideration of both the lateral and longitudinal tyre models. Many authors such as (Milliken & Milliken, 1995) and (Abe, 2009) discuss this topic as the concept known as the tyre friction circle or friction ellipse.

The friction circle is considered to be the limit of resultant force that a tyre can produce, based on the load applied to the tyre. This means that the vector combination of the lateral and longitudinal force the tyre is producing is limited by this available friction boundary. The maximum lateral force

that a tyre can produce is reduced as a result of a driving or braking torque that is applied to the wheel.

Abe makes the assumption that if the reduction in lateral force due to traction or braking is constant at any slip angle the following holds: The relationship between the lateral force at a given slip angle without a longitudinal force is related to the lateral force at the same slip angle in the presence of a longitudinal force by the below equation.

$$\frac{F_y}{F_{y0}} = \frac{\sqrt{\mu^2 W^2 - {F_x}^2}}{\mu W} \tag{2-9}$$

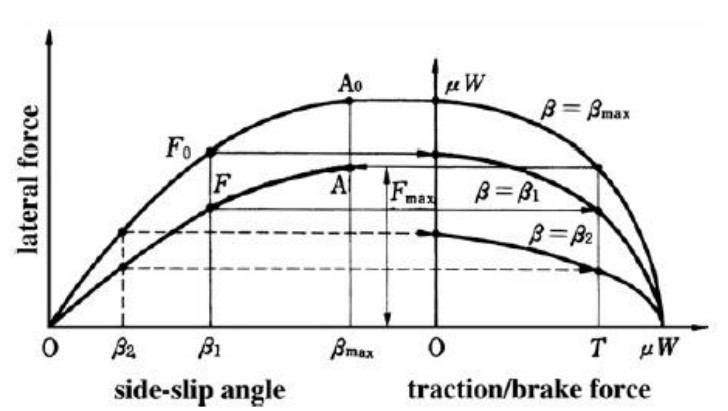

Figure 9 - Effect of braking/tractive force on lateral force generation, (Abe, 2009)

2.4.2 Tyre Load Sensitivity

Tyre load sensitivity is described as the characteristic of a tyre to experience a drop in the lateral friction coefficient that can be achieved as the vertical load on the tyre increases, (Milliken & Milliken, 1995). This effect is illustrated in Figure 10 that shows how lower friction coefficient peaks are produced with an increase in tyre load.

The significance of this phenomenon relates to the handling balance of a vehicle as well as the road holding capability of the vehicle. It is therefore evident that the distribution of loads on the four tyres of the vehicle will have an effect on the lateral force producing capabilities of the tyres. The effect of load transfer on the reduction of total available lateral force on a specific axle is shown in Figure 11.

The figure indicates that a higher total lateral force can be produced at an axle when no load transfer is present. The presence of load transfer reduces the total lateral force produced by the axle.

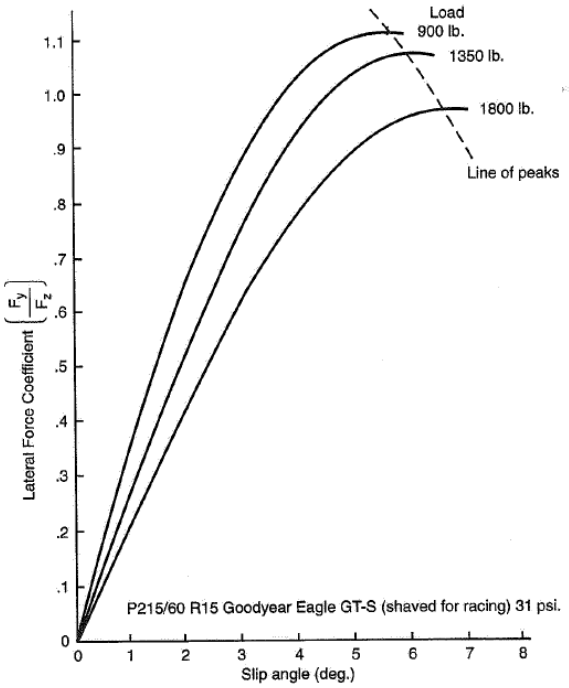

Figure 10 - Tyre load sensitivity, (Milliken & Milliken, 1995)

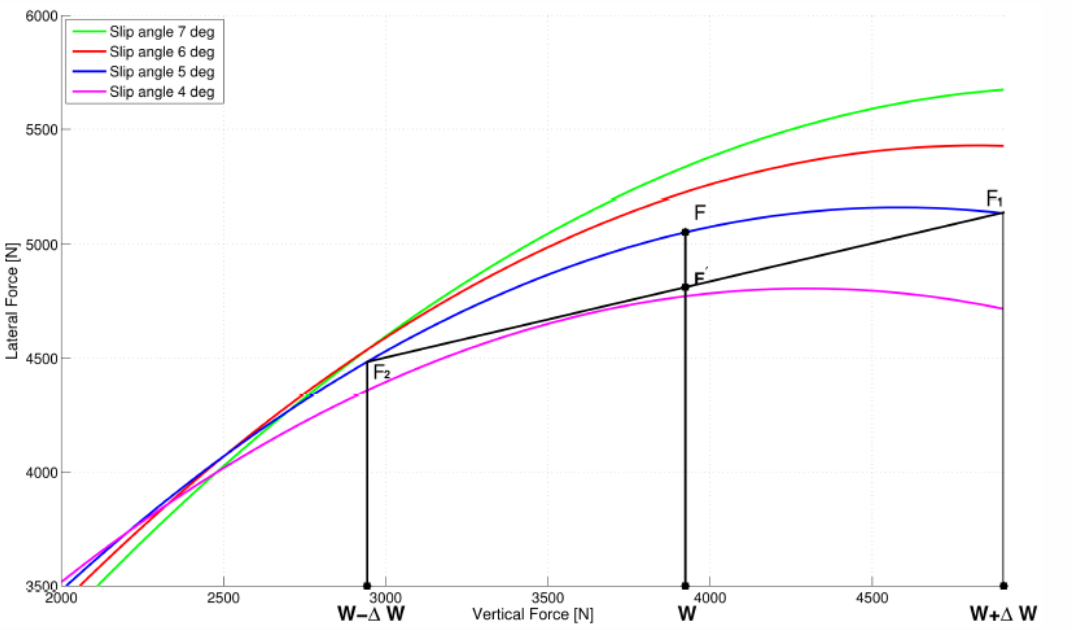

Figure 11 - Reduction in lateral force due to load transfer, (Botha, 2011)

2.5 Electronic Stability Control Overview

The yaw control systems typically found on production vehicles, typically employ systems such as the Bosch ESP system (Robert Bosch GmbH, 2005). The fundamental operation of such a system is the application of a braking force to the outer front wheel when oversteer is detected or braking the inner rear wheel when understeer is detected. The application of these braking forces produces a correcting moment to reduce the yaw error of the vehicle. These systems are very successful on passenger vehicles with low centres of gravity. The ability of these systems to curb under and oversteer in high centre of gravity vehicles might be limited.

Figure 12 from Chen & Peng (2010) illustrates the yaw moment change created by applying a braking force to different wheels. During a cornering manoeuver with simultaneous brake application, the following effects can be expected at each wheel:

Front outer wheel

Lateral load transfer from cornering has placed a heavy vertical load on this tyre. The higher normal force allows for large lateral and longitudinal forces to be produced by the tyre. The braking force creates a moment that corrects oversteer. Increasing the braking force until the lateral force is inhibited by the friction circle mechanism, more understeer is induced. Application of brakes on this wheel will therefore always help induce understeer.

Front inner wheel

Load transfer has reduced the vertical load on this tyre and the total grip available at this tyre has been reduced. The braking force on this wheel initially creates a yaw moment that pulls the vehicle into the corner and reduces understeer. Increasing the braking force will eventually decrease the lateral tyre force of this front tyre and lead to understeer.

Rear outer wheel

This wheel sees an increased normal load from load transfer. Initial brake application creates a yaw moment that induces understeer. Due to the friction circle, increasing the braking force will reduce the lateral force available from the tyre and start to cause oversteer of the vehicle.

Rear inner wheel

The normal load on this tyre has been greatly reduced by lateral load transfer and therefore has a relatively small amount of total grip available. Brake application at this wheel initially creates an understeer correcting moment. Increased braking force reduces the lateral force available at the tyre and creates oversteer.

It is shown that only braking of the outer front wheel and the inner right wheel is consistent in the yaw effects it produces on the vehicle. This is the reason why braking is usually applied at these wheels. It is however clear that the ability of an ESP system to correct understeer deteriorates as load transfer is increased. High centre of gravity vehicles have high load transfers and the low

normal load on the inner rear wheel makes it less effective at creating an understeer correcting moment.

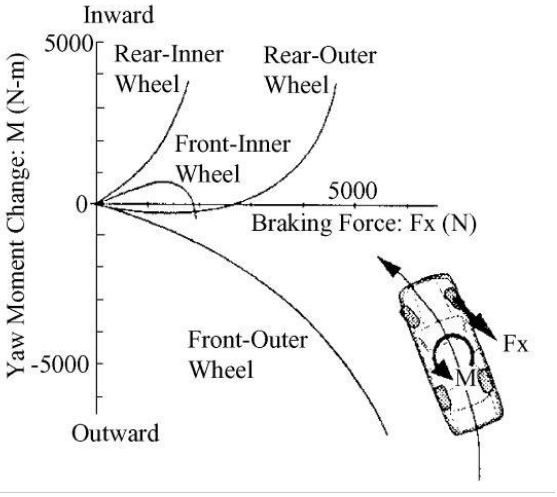

Figure 12 - Yaw moment change from brake application (Chen & Peng, 2010)

2.6 Handling and Rollover Testing

A set of standardised test are commonly used to characterise the handling characteristics and rollover propensity of a vehicle.

The handling is usually defined by tests such as the constant radius test, which provides insight into the steady state response of the vehicle, whereas the dynamic abilities are tested by the severe double lane change. The J-turn and Fishhook tests are designed more specifically to study the roll behaviour of vehicles.

2.6.1 Constant Radius Test

The steady state handling of a vehicle can be tested by driving the vehicle around a course of constant radius and gradually increasing the vehicle speed until the vehicle can't maintain the intended path. A minimum radius of 30m is recommended by Gillespie (1992). The test will give insight into the oversteer or understeer characteristics as well as steady state roll angles, slip angles and wheel loads if such measurements are available.

Figure 13 shows how an understeering vehicle requires additional steer input at increasing lateral acceleration and less steering angle for an oversteering vehicle.

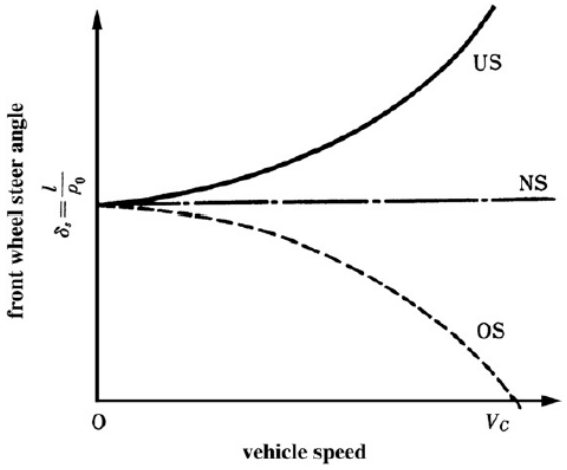

Figure 13 - Steer angles for constant radius test, (Abe, 2009)

2.6.2 Severe Double Lane Change

The severe double lane change test is set out as per the ISO 3888-1 standard (International Organisation for Standarisation, 1999). The test consists of a vehicle entering a course where it changes lanes to a lane parallel to its initial lane and then returns to its initial lane, all within a demarcated area as shown in Figure 14. The NHTSA came to the conclusion that the ISO 3888-1 tests are more suitable to handling evaluation due to the number of transient movements, although small amounts of time for stabilisation take place in the test (Forkenbrock, et al., 2005).

The test is performed by driving the vehicle through the course at increasing speeds until a clean run (not knocking the set out cones) is not achievable. This is a closed loop test and therefore strongly dependent on the driver skill.

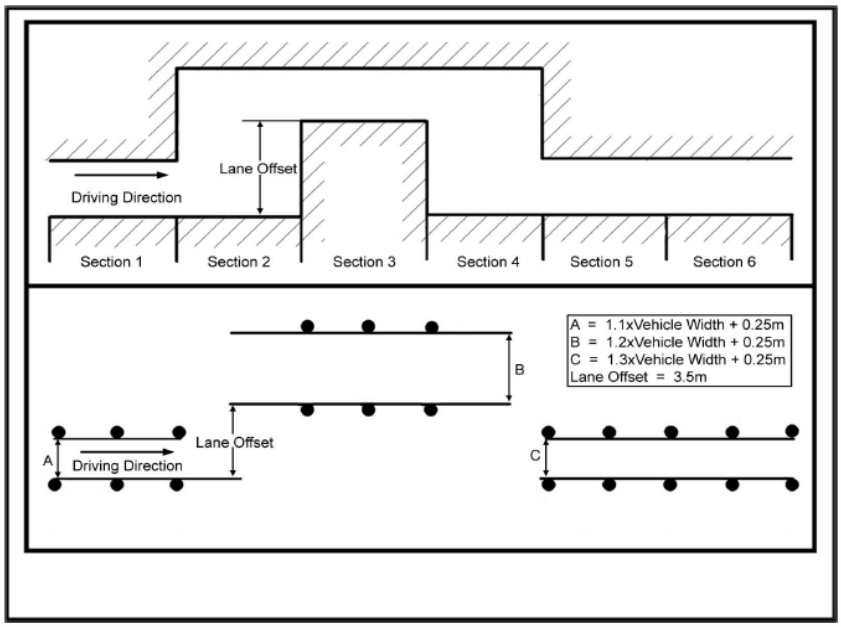

Figure 14 – ISO 3888-1 course layout, (Botha, 2011), (International Organisation for Standarisation, 1999)

2.6.3 Obstacle Avoidance Test

The obstacle avoidance test is also often referred to as the Elk-test, although its formal description is the ISO 3888-2 testing standard (International Organisation for Standarisation, 2011). The test is similar to the ISO 3888-1 configuration in that it features parallel lanes with widths that are a function of the vehicle dimensions. This track is however much shorter in length, which makes it more suitable to test the vehicle response to avoidance manoeuvers as opposed to vehicle handling.

The ISO 3888-2 test was initially part of Phase IV of the NHTSA Rollover Research Program (Forkenbrock, et al., 2005). The authors found that the test wasn't suitable to limit rollover resistance testing, mainly due to the second lane allowing for the vehicle to settle before steering back into the third lane. The NHTSA then proposed the modified ISO 3888-2 test course, which replaced the offset lane with only two cones to form a gate. Using a gate instead of a lane allows for a more severe transition during the manoeuver and not allowing the vehicle states to reach steady state.

The layout of the modified ISO 3888-2 test is shown in Figure 15. This test is commonly used by the NHTSA to perform effectiveness testing of vehicle Electronic Stability Control systems.

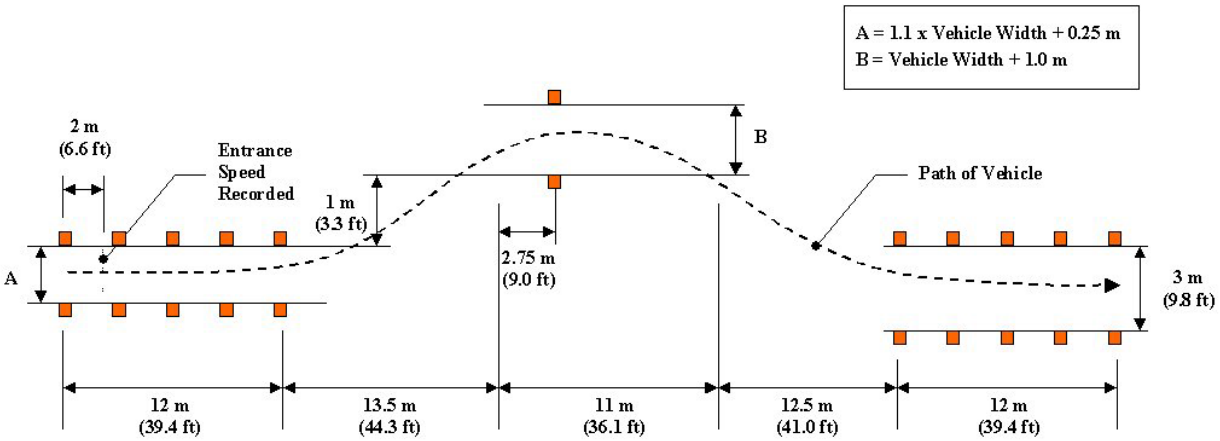

Figure 15 – Modified ISO 3888-2 course layout, (International Organisation for Standarisation, 2011)

2.6.4 Fishhook Test

The fishhook test is considered by the NHTSA to be one of the most severe tests of vehicle untripped rollover propensity (Forkenbrock, et al., 2005). This is due to the combination of sudden steering inputs as well as the sudden steering reversal. The name of the test originates from the shape of the path the vehicle follows, as illustrated in Figure 16.

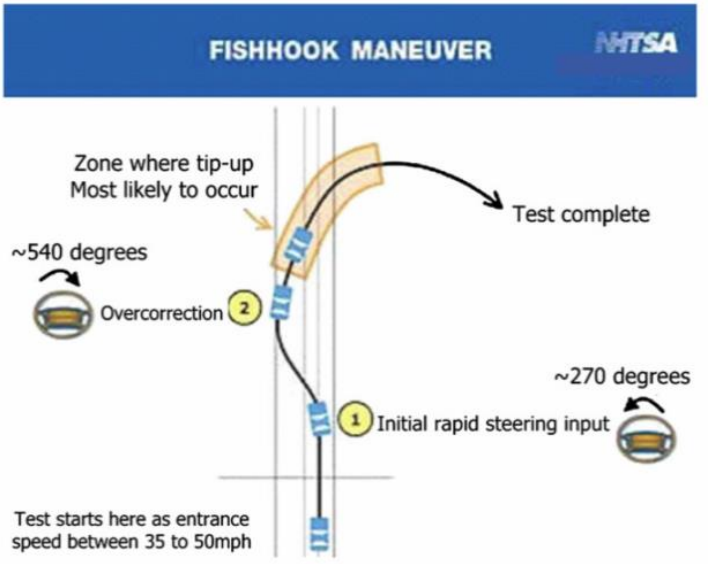

Figure 16 - NHTSA Fishhook manoeuver, (Yoon, et al., 2010)

The complete test consists of two phases. The first is a test to establish some of the vehicles handling parameters during a Slowly Increasing Steer test, the outputs of which are then used as input parameters to the fishhook test itself (Forkenbrock, et al., 2004) .

The Slowly Increasing Steer test first consist of maintaining a steady speed of 80 km/h with the steering wheel angle increased from 0 to 30° at a rate of 13.5°/s. A linear approximation is then made to establish the steer angle δ_{SIS} that would produce a lateral acceleration of 0.55g at 80 km/h.

The steering input as shown in Figure 17 at a speed of 80 km/h. The average value of the steering angle that achieved a lateral acceleration of 0.3g was then recorded, which then serves as input to the Fishhook test.

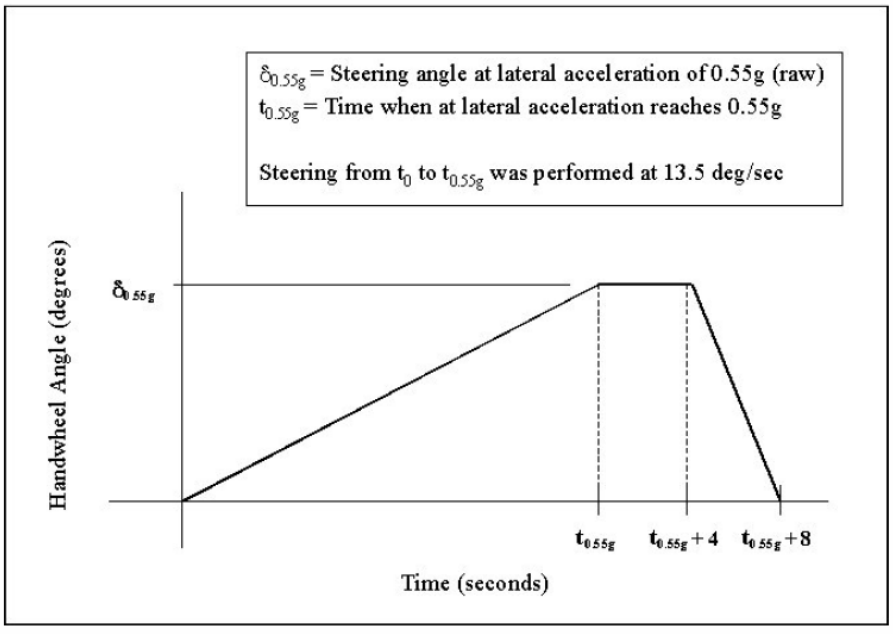

Figure 17 - Slowly increasing steer test, (Forkenbrock, et al., 2004)

Figure 18 shows the steering angle input profile for conducting the Fishhook test. The initial steer is performed at a steering wheel rate of 720°/s up to the maximum steering wheel angle (A) which equals the 0.3g steering angle established previously times a scalar value of 6.5. This steering wheel angle is then maintained until a roll rate of 1.5°/s is achieved. The steering wheel angle is then reversed at 720°/s to a steering wheel angle of –A and held for 3 seconds before ramping down to 0. The test is performed at different Manoeuver Entrance Speeds (MES) until simultaneous two-wheel lift in excess of 50.8mm is produced.

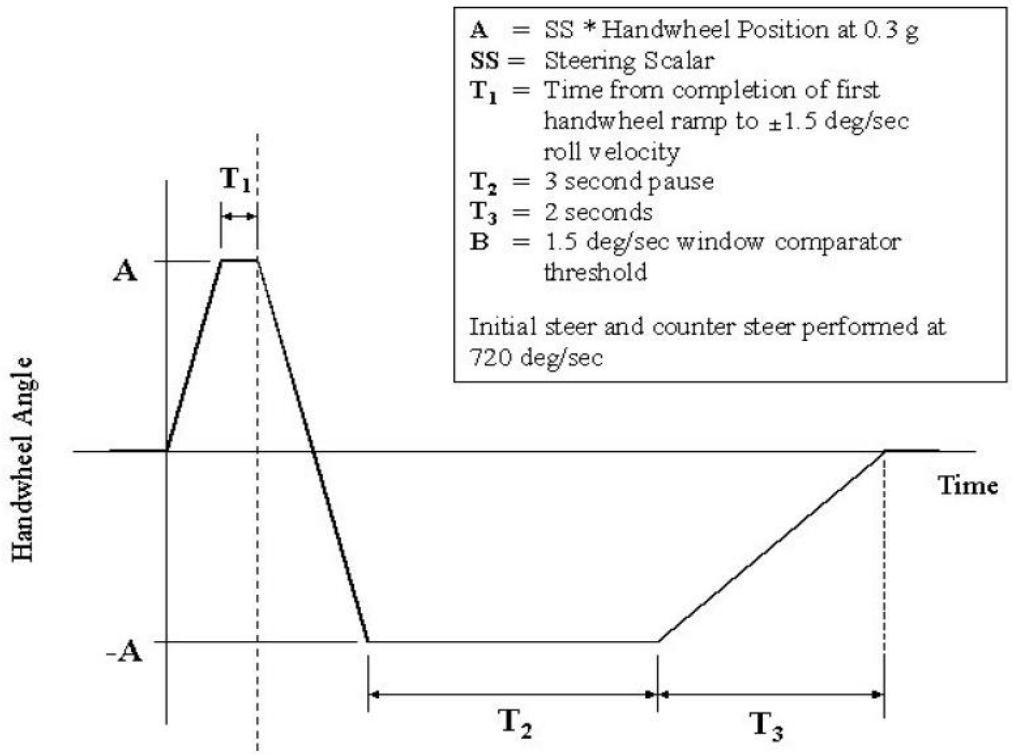

Figure 18 - Fishhook manoeuver steer input, (Forkenbrock, et al., 2004)

2.7 Conclusion

The study of literature on rollover detection and prevention has shown various approaches to the problem with varying levels of success. The untripped rollover case has received the most attention in the studies due to the situation being the most predictable and controllable with vehicle systems.

The literature on rollover detection systems has shown that model based predictive detection systems appear to be the most promising for future development. These detection systems rely predominantly on accurate vehicle models and sophisticated state estimators. The indication is that the further development of an accurate predictive detection system would require more focus on the control theory for the development of robust state estimators than focusing on the vehicle mechanisms itself. This particular study will however delve deeper into the prevention aspects of vehicle rollover. The zero-moment point method for rollover threat detection appears to be one of the more versatile and easily implementable detection systems

Different methods of rollover prevention were investigated in the literature. The most successful of these systems appear to be braking-based prevention systems. Other methods such as controllable suspension and active steering all contribute to reduce rollover risk, with the primary effect being the increase of vehicle stability in roll and yaw, whilst also contributing towards raising the rollover threshold.

This study will continue onto testing the contribution of some of these systems towards reducing rollover risk of a Land Rover Defender 110 SUV.

3. Rollover Threat Index

The activation of a rollover mitigation system requires a reliable method of establishing an imminent threat of rollover.

An absolute measurement of rollover can be based on the lateral load transfer ratio, which will indicate when weight has been transferred from the inside to the outside wheels during a manoeuver. Any further lateral inertial forces will then result in lifting of the inside wheels. Tyre normal forces and wheel lift can be very difficult to measure, especially on a commercial scale vehicle.

Load transfer can be approximated with an accurate vehicle model, although the secondary effects discussed by Hac (2002b) such as change in track width due to lateral tyre deflection and suspension kinematics together with change in CG height from jacking forces and dynamic overshoot should be taken into account.

Various authors such as Yoon, et al. (2007) have implemented a phase plane method that use the combined effects of roll angle, roll rate, lateral acceleration and time-to-wheel-lift to formulate the following rollover index:

$$for:\ \emptyset\left(\dot{\emptyset} - k_1\emptyset\right) > 0:$$

$$RI = C_1\left(\frac{\left(|\emptyset(t)|\dot{\emptyset}_{th} + |\dot{\emptyset}(t)|\emptyset_{th}\right)}{\emptyset_{th}\dot{\emptyset}_{th}}\right) + C_2\left(\frac{|a_y|}{a_{y,c}}\right) + (1 - C_1 - C_2)\left(\frac{|\emptyset(t)|}{\sqrt{\left(\emptyset(t)\right)^2 + \left(\dot{\emptyset}(t)\right)^2}}\right) \quad (3\text{-}1)$$

$$for:\ \emptyset\left(\dot{\emptyset} - k_1\emptyset\right) \leq 0: \qquad RI = 0$$

As this formulation indicates, the accurate estimation of the rollover threat index requires lateral acceleration and especially roll angle thresholds to be predetermined and constants be defined, which can prove to be difficult. These measures also do not account for road inclination angles and variations in road characteristics.

The method that was selected to determine the rollover threat is known as the zero-moment point based rollover index. This method requires vehicle inertial properties and monitoring of measurable acceleration parameters. This method can also account for road conditions such as banking angles.

3.1 Zero-Moment Point

The zero-moment-point (ZMP) is a concept that is widely utilised in the robotics industry for determining the balance stability of biped robots. The zero-moment point is defined as the point on the ground where the sum of the tipping moments due to gravitational and inertial forces acting on an object is equal to zero. The tipping moments are defined as components of moments that are

tangential to the supporting surface. For an object to remain stable, the zero-moment point is required to be within the support polygon of the mechanisms.

The general representation of the zero moment point problem is indicated in Figure 19. The masses m_i in the kinematic chain is assumed to have a velocity $\overrightarrow{v_i}$, acceleration $\overrightarrow{a_i}$, rotate at angular velocity $\overrightarrow{\omega_i}$ and angular acceleration $\overrightarrow{\alpha_i}$. The centre of mass of each body relative to an inertial frame is at position $\vec{r_i}$. The moments induced by inertial and gravitational forces about point A can then be described by the following relationship:

$$\overrightarrow{M_A} = \sum_i (\overrightarrow{p_i} \times m_i \overrightarrow{a_i}) + \sum_i (I_i \overrightarrow{\alpha_i} + \overrightarrow{\omega_i} \times I_i \overrightarrow{\omega_i}) - \sum_i (\overrightarrow{p_i} \times m_i \vec{g}) \tag{3-2}$$

Where $\overrightarrow{p_i} = \vec{r_i} - \vec{r}_{zmp}$ and $\vec{g}$ is gravitational acceleration. If $\overrightarrow{M_A} = [0\ 0\ \overrightarrow{M_{A_z}}]^T$, point A becomes a zero-moment point.

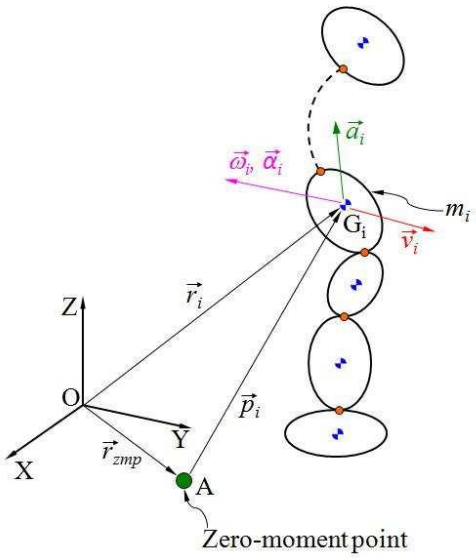

Figure 19 - Kinematic chain (Lapapong, 2010)

3.2 Zero-Moment Point Applied to Vehicle

The zero-moment point method is applied to a rigid vehicle model by Lapapong (2010) to provide an index for determining impending rollover. As per the definition of the zero-moment point, the vehicle is considered to approach an unstable condition once the zero-moment point reaches the track and wheelbase limits of the vehicle.

Figure 20 indicates the rigid vehicle model used to calculate the zero-moment point as indicated by point Q on the ground plane. The reference coordinate system is fixed at the vehicle centre of gravity. Figure 20 also indicates how the effect of road inclination is incorporated in the calculation of the zero-moment point. This implies that road profile data can be used to give greater accuracy to the rollover threat index.

The vehicle inertial properties together with angular velocity, angular acceleration and linear acceleration are used to calculate the position $\vec{p}$ from the general formulation:

$$M_{Q_z}\vec{k} = \vec{p} \times m\vec{a}_G + I\vec{\alpha} + \vec{\omega} \times I\vec{\omega} - \vec{p} \times m\vec{g} \tag{3-3}$$

Equating the $\vec{\imath}$ and $\vec{\jmath}$ components in the above equation to zero, we can express the x and y positions of the zero-moment point as x_{zmp} and y_{zmp}. Since we are concerned with the lateral dynamics to calculate the threat of rollover, we only consider the position of y_{zmp}. If the position of y_{zmp} approaches the half-track width of the vehicle, the vehicle will become unstable and produce wheel lift.

Performing the derivations produces the following formulation for calculating y_{zmp}:

$$\begin{aligned} y_{zmp} = \{&mgcos(\theta)\sin(\emptyset_r)[T|\tan(\emptyset_r - \emptyset_t)|+2h] - ma_{G_y}[T|\tan(\emptyset_r - \emptyset_t)|+2h] \\ &-2I_{xx}\alpha_x + 2I_{xz}\alpha_z + 2I_{yz}(q^2 - r^2) + 2(I_{xz} + I_{yy} - I_{zz})qr\} \\ /\{&2m\left[gcos(\theta)\cos(\emptyset_t)\sec(\emptyset_r - \emptyset_t) - a_{G_y}\tan(\emptyset_r - \emptyset_t) - a_{G_z}\right]\} \end{aligned} \tag{3-4}$$

The formulation indicates that the lateral position of the zero-moment point can be calculated with knowledge of vehicle inertial properties and measurable acceleration parameters. The zero-moment point is defined as a position on the ground plane and therefore the contributions of tyre lateral and longitudinal forces produces no moments around this point, which simplifies the problem.

The rollover index is subsequently defined as the ratio between the y_{zmp} and the half-track width. A zero index indicates the y_{zmp} position to be on the vehicle centreline and an index of 1 indicating the y_{zmp} position on the half-track and impending rollover.

Research done by Lapapong (2010) also included a study of increasing the accuracy of the rollover index by expanding the vehicle model into a coupled sprung and unsprung mass with separate inertial properties. The results indicated a slight improvement in mimicking measured wheel lift, although the improvement was negligible when the greater simplicity of the rigid vehicle model is considered.

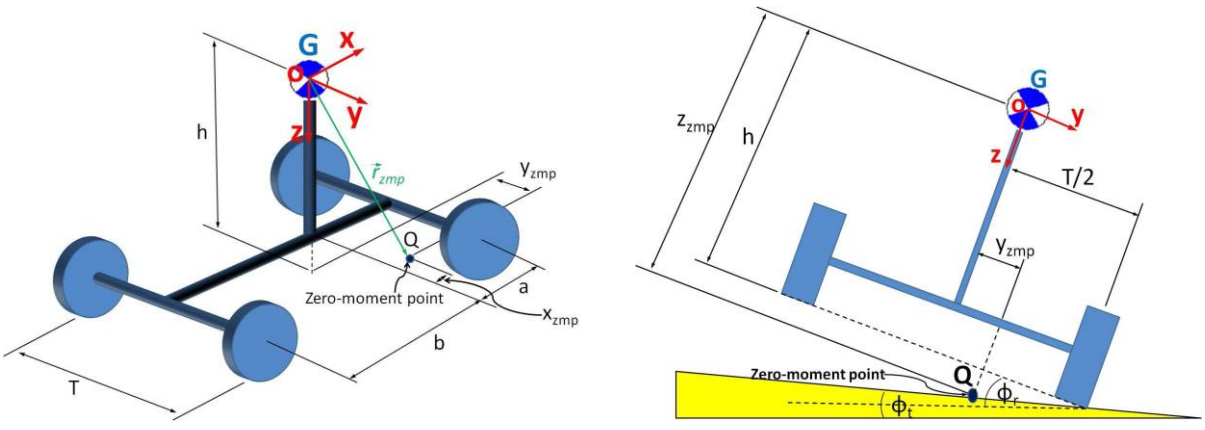

Figure 20 - Rigid vehicle model (Lapapong, 2010)

3.3 Zero-Moment Point vs Lateral Load Transfer

The zero moment based rollover index is compared to the lateral load transfer ratio based rollover index. The LLTR rollover index is defined in equation (3-5). The LLTR rollover index captures the fundamentals of the rollover problem, as it indicates when load has been transferred from the inner to the outer tyres during a cornering manoeuver.

$$RI_{LLTR} = \left| \frac{F_{z,fl} + F_{z,rl} - F_{z,fr} - F_{z,rr}}{F_{z,fl} + F_{z,fr} + F_{z,rl} + F_{z,rr}} \right| \tag{3-5}$$

Figure 21 shows a comparison of typical rollover indices calculated from the 2 methods for a double lane change manoeuver. Results were produced using an ADAMS simulation of the test vehicle.

The results indicate that the ZMP based rollover index mimics the rollover index from the lateral load transfer. In most instances it also appears that the ZMP method produces its peaks slightly ahead of time. This characteristic is advantageous in that it leads to a slight preview, which allows the safety system to intervene earlier. There is a difference in magnitude between the two methods with the ZMP method appearing to be more sensitive. This phenomenon isn't of concern. A rollover index threshold has to be assigned at which the safety system needs to be triggered. The magnitude of this threshold is therefore a parameter that is tuned to suit the desired response of the system.

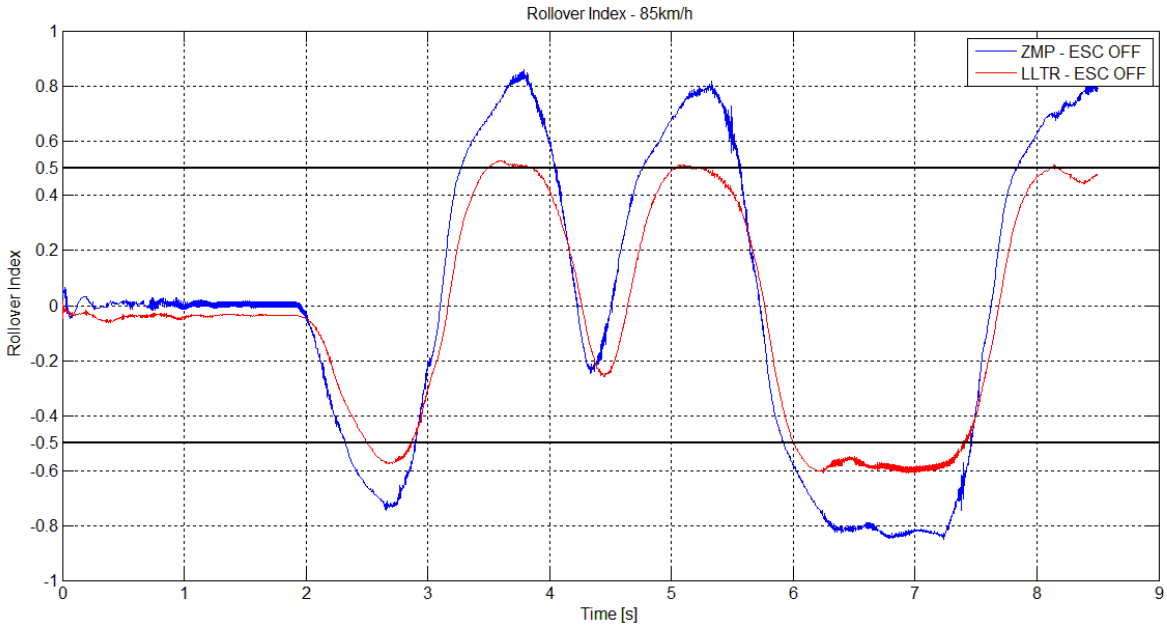

Figure 21 - Zero-moment point RI vs Lateral Load Transfer Ratio RI

3.4 Sensitivity Analysis

A sensitivity analysis was performed on the zero-moment point formulation in order to establish the effect of the contributions of the various parameters on the rollover index. The dynamic parameters in the ZMP rollover index formulation relies on accurate measurements constantly taken on the vehicle. The sensitivity analysis was performed to identify parameters that have a small effect on the rollover index and can likely be omitted. Omitting certain parameters can reduce the complexity of the system as well as the number of sensors required on the vehicle.

The results of the sensitivity analysis of the RI for a 60 km/h obstacle avoidance manoeuver is summarised in Table 1 below.

Table 1 - RI parameter sensitivity

				Parameter Change			
				+10%		-10%	
Parameters	Baseline Value		Rollover Index				
			Base	Value	% Change	Value	% Change
Roll Angle	-3.63	°	1.01	1.0219	0.84%	1.0048	-0.85%
Pitch Angle	2.75	°		1.0137	0.03%	1.013	-0.04%
Lateral Acceleration	-7.23	m/s²		1.1077	9.31%	0.9182	-9.39%
Roll Rate	-0.67	°/s		1.0135	0.01%	1.0132	-0.02%
Pitch Rate	1.00	°/s		1.0135	0.01%	1.0133	-0.01%
Yaw Rate	-31.86	°/s		1.0135	0.01%	1.0133	-0.01%
Roll Acceleration	67.43	°/s²		1.0072	-0.61%	1.0195	0.60%
Yaw Acceleration	0.02	°/s²		1.0135	0.01%	1.0132	-0.02%
Mass	2047	kg		1.0191	0.56%	1.0063	-0.70%
Ixx	839	kgm²		1.007	-0.63%	1.0197	0.62%
Iyy	2471	kgm²		1.0132	-0.02%	1.0135	0.01%
Izz	2057	kgm²		1.0135	0.01%	1.0132	-0.02%

The sensitivity analysis indicates that the pitch angle and pitch rate have negligible contributions. The vertical acceleration is also excluded, as the system will be tested on a level road and in which case the road banking angle is also considered to be 0.

The results in Table 1 indicate that the lateral acceleration, roll angle, roll acceleration, mass and roll inertia have the most noticeable contributions to the RI and all these parameters are used in the yaw ESC+RP control system and are therefore included. The RI appears to be reasonably robust with regards to the accuracy of the vehicle inertia properties, which makes it easily implementable.

The vehicle parameters that need to be known are the following:

- Mass
- Pitch, roll and yaw inertia
- Track width

The following measurements will be taken from sensors on the vehicle and included in the calculation of the RI:

- Roll angle, roll rate and roll acceleration
- Lateral acceleration
- Yaw rate and yaw acceleration

Figure 22 shows the contributions of the different terms in the ZMP RI equation. These terms are indicated as:

Mass Term

Lateral Acceleration Term

$$y_{zmp} = \{mgcos(\theta)\sin(\emptyset_r)[T|\tan(\emptyset_r - \emptyset_t)|+2h]\} - [ma_{G_y}[T|\tan(\emptyset_r - \emptyset_t)|+2h]$$

Roll Acceleration Term

$$-2I_{xx}\alpha_x + 2I_{xz}\alpha_z + 2I_{yz}(q^2 - r^2) + 2(I_{xz} + I_{yy} - I_{zz})qr\}$$

$$/\{2m\left[gcos(\theta)\cos(\emptyset_t)\sec(\emptyset_r - \emptyset_t) - a_{G_y}\tan(\emptyset_r - \emptyset_t) - a_{G_z}\right]\} \quad (3\text{-}6)$$

The lateral acceleration is by far the most significant contributor to the RI, which agrees with the report by Lapapong (2010). Lapapong also indicated that although the contribution of the vehicle mass term is relatively small, the effect becomes much more pronounced in the presence of a road banking angle as well as a larger vehicle roll angle.

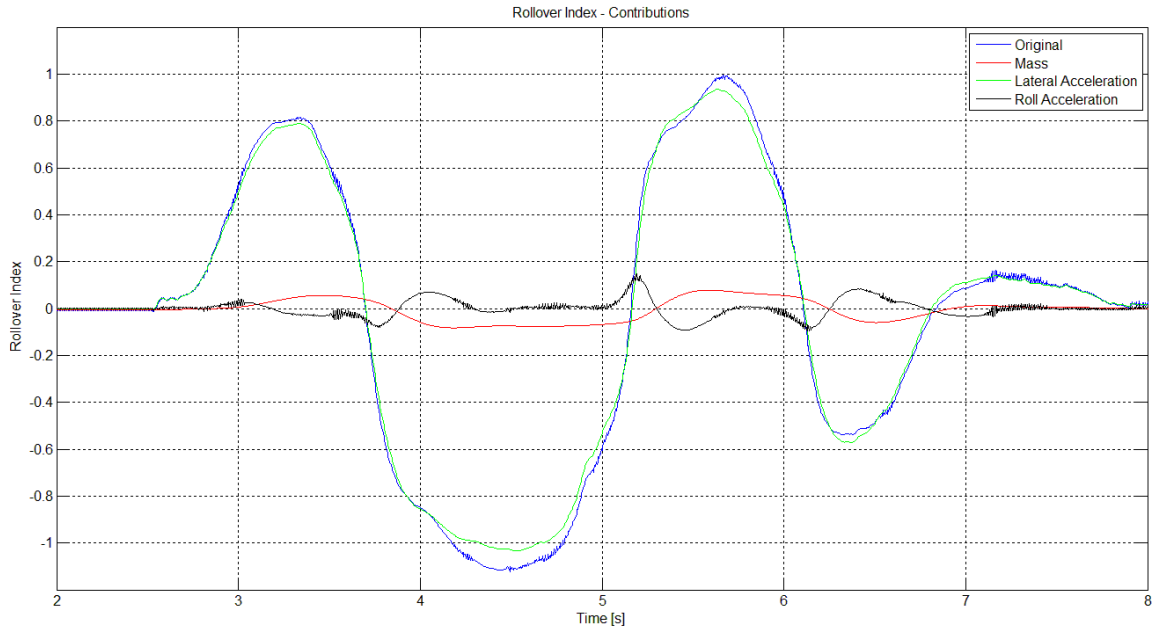

Figure 22 - Rollover Index parameter contributions

4. Control Strategy

The Electronic Stability Control with Rollover Prevention (ESC+RP) algorithm developed in this report consist of several subsystems that combine to control the individual brake pressures of each wheel in order to reduce the rollover risk of a vehicle in an extreme manoeuver. The main aim of the system is to reduce the risk of rollover whilst still allowing the driver to maintain steering control in order to navigate the vehicle along the intended path.

The high level control is responsible for setting the overall dynamics objectives of the vehicle. In this instance these objectives include a desired longitudinal velocity and a desired yaw rate. These two objectives are then expanded down to a level where individual wheel brake pressures are specified that would alter the vehicle response to meet the control objectives. The low level controller in turn, is responsible for managing the braking system to produce desired individual wheel brake pressures.

After an introduction to the sliding mode control methodology implemented, the following subsystems of the ESC+RP system are discussed in further detail:

High level control:

- Rollover Index
- Desired Velocity
- Speed Controller
- Desired Yaw Rate
- Yaw Control

Low level control:

- Brake Pressure Control

4.1 Sliding Mode Control

The behaviour of the dynamics of vehicles is considered to be non-linear, partly due to the non-linear forces developed by the tyres at different load and slip conditions. A vehicle dynamics control system has to be able to deal with this non-linear behaviour. The sliding mode control methodology is one of the ways to achieve control over nonlinear dynamic systems and is typically implemented in vehicle yaw rate and slip angle control by authors such as Rajamani (2006). An introduction to the sliding mode controller is provided by Slotine & Li (1991).

The sliding mode control methodology is based on the notion that it is much simpler to control an equivalent first order system, be they non-linear, than to control n^{th}-order systems. The sliding mode control method also makes the assumption that the system model contains inaccuracies that need to be accounted for. This robustness of the sliding mode control methodology to deal with

nonlinearities and less precise models make it very suitable for application in vehicle dynamics control.

The sliding surface $S(t)$ in the state space that specifies the error between single order variables x, are typically defined by the following scalar equation:

$$s = x - x_{desired} \tag{4-1}$$

The control law, that will achieve the target of keeping the scalar s equal to zero, is defined as:

$$\frac{1}{2}\frac{d}{dt}s^2 = s\dot{s} \leq -\eta|s| \tag{4-2}$$

where η is a strictly positive constant. Equation (4-2) states that the squared "distance" to the sliding surface, as measured by s^2, decreases along all system trajectories. Thus, it constrains trajectories to point towards the surface $S(t)$ (Slotine & Li, 1991).

To account for model uncertainties and disturbances, a discontinuous term is added to the equivalent control law. This discontinuous term is typically defined as a sgn function:

$$\begin{array}{ll} sgn(s) = +1 & \text{If } s > 0 \\ sgn(s) = -1 & \text{If } s < 0 \end{array} \tag{4-3}$$

The introduction of the discontinuous term, does however lead to the problem of "chattering", as illustrated in Figure 23. To reduce this effect, the discontinuous term is smoothed, by replacing the sgn function with a saturation function defined as:

$$\begin{array}{ll} sat(s/\Phi) = s/\Phi & \text{If } abs(s/\Phi) \leq 1 \\ sat(s/\Phi) = sgn(s/\Phi) & \text{If } abs(s/\Phi) > 1 \end{array} \tag{4-4}$$

with Φ a positive constant specifying the thickness of the boundary layer surrounding the sliding surface.

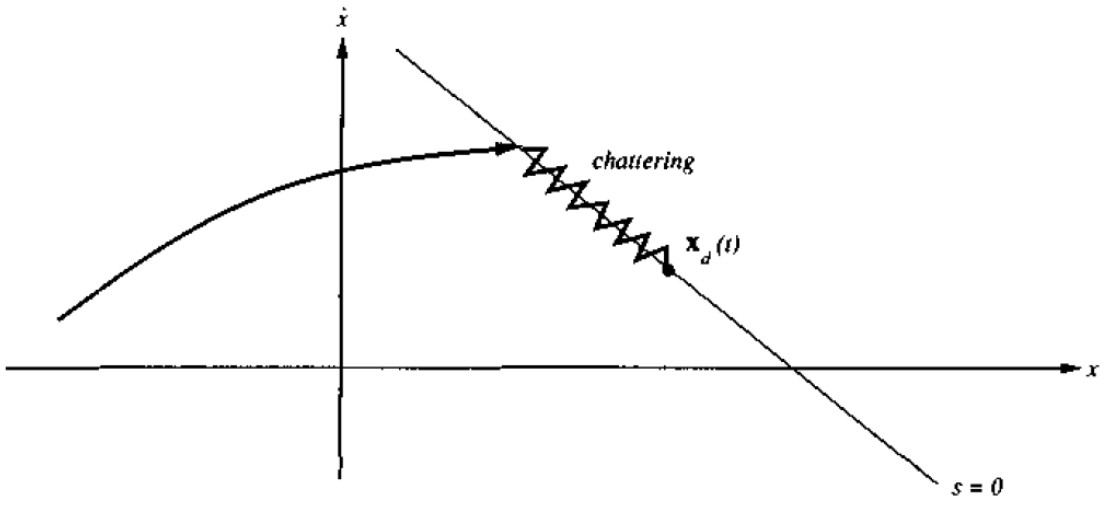

Figure 23 - Chattering from imperfect control switchings (Slotine & Li, 1991)

4.2 High Level Control

4.2.1 Rollover Index

The rollover index discussed in section 3.2 is utilised as the trigger for intervention from the rollover prevention system. The threshold limit can be predefined and determined from a combination of objective and subjective measures. A rollover index threshold can be selected as a balance between the calculated margin to rollover, as well as an acceptable intervention point based on the vehicle manoeuver severity perceived by the driver. Intervention at the relatively low threshold might be undesirable and unsettling to a driver if the vehicle is still perceived to be stable and in control.

For the purposes of the simulations and experiments in this report, a rollover index threshold and target of 0.5 was selected. This enables more severe intervention from the system at lower speeds and therefor allows for easier and safer experimental evaluation of the performance.

4.2.2 Desired Velocity

The sensitivity analysis of the ZMP based rollover index, performed in section 3.4, indicated that the parameter with the largest effect on the rollover index is the lateral acceleration of the vehicle. Equation (4-5) provides the relationship between vehicle velocity, yaw rate and lateral acceleration:

$$a_y = V(\dot{\beta} + r) \tag{4-5}$$

This indicates that the lateral acceleration can be reduced by reducing the velocity or the yaw rate of the vehicle. The latter being the approach typically followed by Wielenga (2000) and Chen & Peng (2010) as well as the systems available on certain vehicles fitted with a typical ESP system. Analytical as well as real world results indicate that this works effectively in reducing the risk of rollover. Figure 24 illustrates such a system in action, as fitted to a Porsche Macan.

An ESC based system will typically apply a large brake pressure to outer front wheel. This braking force will create a yaw moment on the vehicle that induces understeer by reducing the yaw rate of the vehicle as well as by reducing the lateral force generation capability of the tyre. The large longitudinal force shifts the tyre's operating point closer to the edge of the friction circle and reduces the tyres ability to produce lateral force, inducing understeer. The combination of these mechanisms reduce the lateral acceleration of the vehicle and hence the risk of rollover.

The side-effect of inducing understeer and saturating the front tyre's lateral force generating ability is a compromised ability to maintain the intended directional response of the vehicle. In an emergency evasive manoeuver the driver will apply a large steering wheel input to swerve away from an obstacle. The ESC system detects a risk of rollover and a sudden braking force is applied to the outer front wheel. The yaw rate and lateral acceleration reduces and the vehicle continues on a path straighter than intended. In order to avoid the obstacle, the driver will have to increase the

steering angle to attempt to stay on the originally intended path. This was one of the observations made by Wu, et al. (2010) with a driver-in-the loop test setup.

Figure 24 - Porsche Macan Moose Test (Teknikens Varld, 2014)

The ESC+RP system discussed in this report aims to also reduce or eliminate the loss of directional control during intervention of the rollover mitigation system. The approach is to firstly focus on reducing the velocity component that contributes to the lateral acceleration indicated in equation (4-5).

The zero moment point rollover index is inversed to calculate the required lateral acceleration by specifying a desired rollover index. Considering the planar motion of the vehicle and assuming the same vehicle slip rate, equation (4-6) can be used to express the relationship between the current and the desired vehicle velocity.

$$V_{x,des} = \frac{1}{r}\{a_{y,des} - (a_{y,m} - V_{x,m}r)\} \tag{4-6}$$

This desire vehicle velocity is then fed to a sliding mode based speed controller that calculates the overall longitudinal force required to decelerate the vehicle at the required rate.

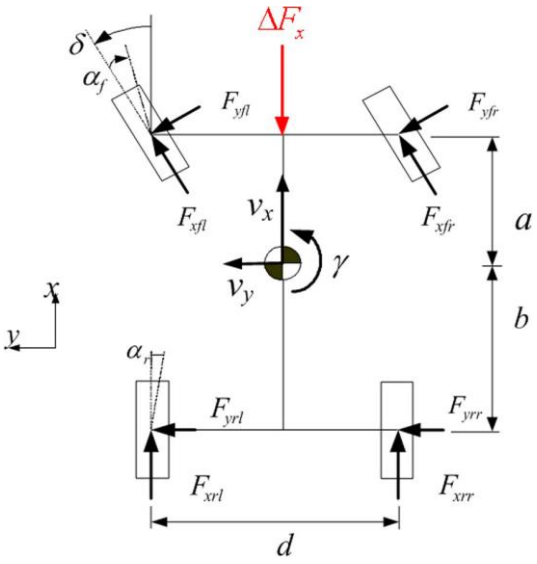

Figure 25 - Planar vehicle model with total braking force (Yoon, et al., 2009)

4.2.3 Speed Controller

The sliding mode control methodology is implemented to reduce the forward velocity of the vehicle to the desired velocity. Figure 25 shows the planar vehicle model that describes the following equation for the longitudinal acceleration of the vehicle:

$$ma_x = F_{xr} + F_{xf}cos\delta - F_{yf}sin\delta + mv_y r - \Delta F_x \tag{4-7}$$

Assuming a small steering angle, the longitudinal acceleration equation simplifies to:

$$a_x = \frac{1}{m}\left(F_{xr} + F_{xf} - F_{yf}\delta\right) + V_y r - \frac{1}{m}\Delta F_x \tag{4-8}$$

The sliding mode controller is considered to be stable when the equality of equation (4-2) is satisfied, with s and $\dot{s}$ defined as:

$$s = V_x - V_{x,des} \tag{4-9}$$
$$\dot{s} = a_x - \dot{V}_{x,des} \tag{4-10}$$

From equation (4-8) and (4-10) we get the following:

$$\dot{s} = \frac{1}{m}\left(F_{xr} + F_{xf} - F_{yf}\delta\right) + V_y r - \frac{1}{m}\Delta F_x - \dot{V}_{x,des} \tag{4-11}$$

The equivalent control input that would result in $\dot{s} = 0$ is the following:

$$\Delta F_{x,eq} = \left(F_{xr} + F_{xf} - F_{yf}\delta\right) + m(V_y r - \dot{V}_{x,des}) \tag{4-12}$$

The control input, that takes model uncertainties into account, is then given by:

$$\Delta F_x = \Delta F_{x,eq} - Ksgn(s) \tag{4-13}$$

Equation (4-2) can then be rewritten as:

$$s\left\{\frac{1}{m}\left(F_{xr} + F_{xf} - F_{yf}\delta\right) + V_y r - \frac{1}{m}\Delta F_x - a_{x,des}\right\} \leq -\eta|s| \tag{4-14}$$

High frequency chatter caused by the control input can be reduced by approximating the function $sgn(s)$ with a saturation function to give the desired braking force as:

$$\Delta F_x = \Delta F_{x,eq} - Ksat\left(\frac{V_x - V_{x,des}}{\Phi}\right) \tag{4-15}$$

Where Φ is used to specify the tolerance band for the control input. The gain K can be calculated from equations (4-13) and (4-14) to be the following:

$$K \leq -\eta M \tag{4-16}$$

The sliding mode control of vehicle speed assumes that a drive force $(F_{xr} + F_{xf})$ is present. The combination of the positive driving force and the braking control ensures the target speed is maintained. For the specific application there is only a braking force providing a deceleration and the braking force is very dominant when compared with the other longitudinal forces in equation (4-12). The controller is therefore simplified to equation (4-17). The positive constant η in equation (4-16) is considered a "convergence factor", which affects the rate at which the control parameter approaches the sliding surface. In this case it is simply the desired deceleration of the vehicle.

A proportional gain is applied to the value of η and in doing so varying the longitudinal acceleration specified to reach the desired velocity. The required longitudinal acceleration is low when the rollover index threshold is only marginally exceeded, but grows as the rollover index grows.

The saturation function of the sliding mode controller is maintained to smooth the response close to the target speed and reduce chatter of the control input when there is slight deviation from the target speed.

The output of the speed controller is the necessary total braking force required to achieve the desired velocity.

$$\Delta F_x = -Ksat\left(\frac{V_x - V_{x,des}}{\Phi}\right) \tag{4-17}$$

4.2.4 Desired Yaw Rate

The desired velocity and braking force calculated by the speed controller is required to reduce the lateral acceleration of the vehicle during the manoeuver and in turn reduce the rollover index. The system under investigation aims to maintain path following and steering control of the vehicle and hence sufficient yaw response. It is therefore required to provide the control system with a target yaw rate that needs to be achieved. The derivation of the target yaw rate for typical implementation in a vehicle ESC system is well documented by Rajamani (2006). This same process of derivation was followed in the present study.

It was shown that the steady state steering angle to follow a road of radius R is given by the following equation:

$$\delta_{ss} = \frac{L_f + L_r}{R} + K_v a_y \tag{4-18}$$

Where the understeer gradient K_v is given by:

$$K_v = \frac{L_r m}{2C_{\alpha f}(l_f + l_r)} - \frac{L_f m}{2C_{\alpha r}(l_f + l_r)} \tag{4-19}$$

$C_{\alpha f}$ and $C_{\alpha r}$ are defined as the linearized cornering stiffness of the front and rear tyres respectively, as indicated in Figure 26. The tyre slip angles are determined from the current load conditions, as described in paragraph 4.2.6. With knowledge of the tyre loads and slip, a finite difference method is used in conjunction with the Magic Formula tyre model, as indicated in equation (4-20), to calculate the tyre cornering stiffness (Botha, 2011).

$$C_\alpha = \frac{MTF(\beta + \Delta\beta, F_z) - MTF(\beta, F_z)}{\Delta\beta} \tag{4-20}$$

With $a_y = \frac{V^2}{R}$ and $r = V/R$, substituting and rearranging the above equations brings us to the relationship for the desired steady state yaw rate:

$$r_{des} = \frac{V}{R} = \frac{V\delta}{L_f + L_r + \frac{mV^2(L_r C_{\alpha r} - L_f C_{\alpha f})}{2C_{\alpha f} C_{\alpha r} L}} \tag{4-21}$$

Rajamani (2006) also expands on the yaw control model to develop a target vehicle slip angle. The priority between target yaw and slip angle is weighted to suit the desired response of the vehicle. Slip control is especially beneficial on low friction surfaces where it is not possible to achieve the target yaw rate and vehicle stability is to be maintained. The focus of this study is predominantly on the yaw response of the vehicle on high friction surfaces that could induce un-tripped rollover. Slip control is excluded from the control system. The effect of slip control integration can be investigated during further research.

Equation (4-21) shows the calculation of the desired vehicle yaw rate and indicates the parameters that are required. These parameters include real-time measurements such as steering angle and vehicle speed. The desired yaw rate calculation includes the understeer gradient of the vehicle that requires knowledge of the cornering stiffness of the front and rear tyres respectively. The cornering stiffnesses of the tyres are calculated from a mathematical vehicle model in conjunction with a Pacejka lateral tyre model. These models are used to estimate the current tyre forces and slip angles that can be used to determine the cornering stiffness of the tyres.

A desired yaw rate limit is imposed in the calculation. This limit is calculated from equation (4-22). The upper and lower bounds on the yaw rate dictates that the desired yaw rate should still be within the lateral grip levels of the vehicles. The yaw rate bounds are based on an assumed surface friction coefficient of the terrain.

$$a_y = Vr + \tan(\beta)\, a_x + \frac{V\dot{\beta}}{\sqrt{1 + \tan^2\beta}} \tag{4-22}$$

The equation for calculating the yaw rate bounds include terms for the slip angle and slip rate of the vehicle. Rajamani indicates that these terms contribute only approximately 15% to the overall yaw rate bound value and instead simplifies the equation to the following:

$$r_{upper\_bound} = 0.85\frac{\mu g}{Vx} \tag{4-23}$$

The tyre cornering stiffness that forms the understeer gradient term in the desired yaw rate equation is calculated by a simplified vehicle- and Pacejka tyre model. These models are discussed in section 4.2.6 and 4.2.7.

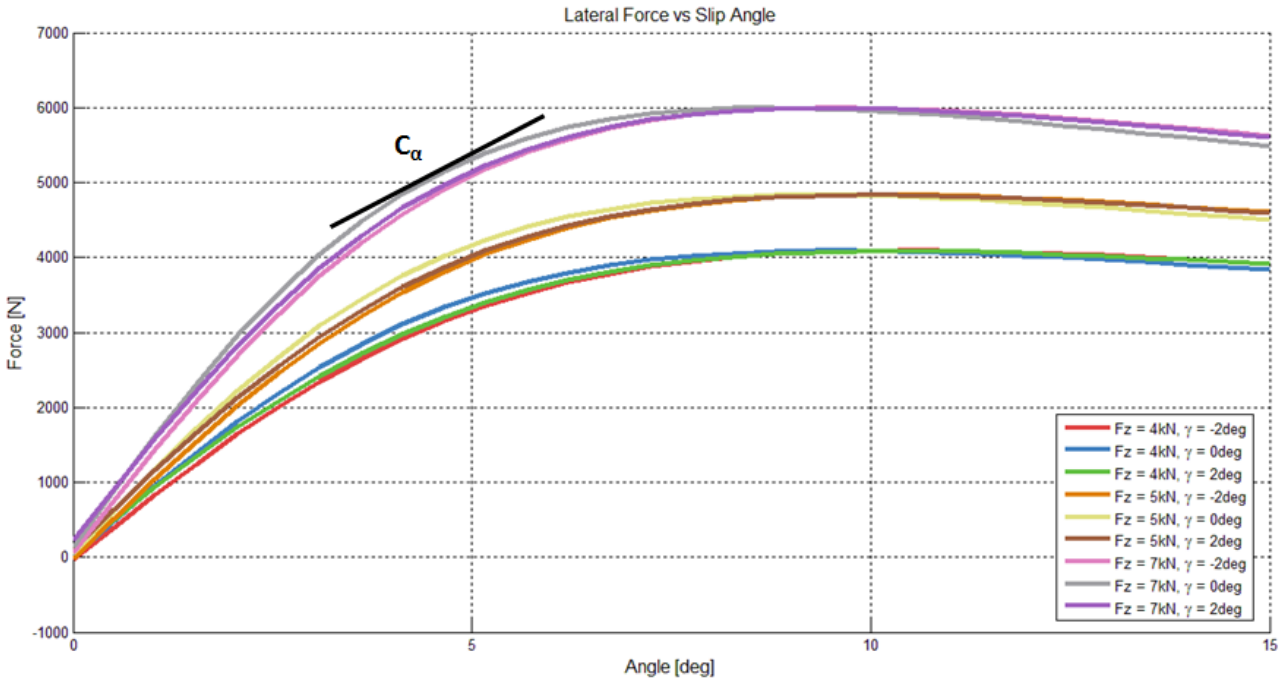

Figure 26 - Typical Pacejka tyre model data

4.2.5 Yaw Control Methodology

The yaw control algorithm is designed to distribute the total braking force suitably amongst the four wheels in order to achieve the calculated target yaw rate. This distribution of the braking force aims to keep the tyre forces within the friction circle and by doing so ensure that the objectives of speed reduction and path following is achieved as far as possible. To achieve these objectives, sufficient knowledge of the vehicle states are required. Vehicle, suspension and tyre models are incorporated in the algorithm for this purpose.

4.2.6 Tyre Model

The Land Rover Defender test vehicle is fitted with 235/85 R16 Michelin LTX AT² tyres that have been characterised for side force against slip angle. From this data a Pacejka '89 lateral force vs slip angle tyre model was created. The tyre model provides the lateral force produced by the tyre based on the vertical load and slip angle of the tyre.

The tyre model is used in the yaw control algorithm to determine the slip angle of the tyres. The lateral force produced by the tyres as well as the vertical loads on the tyres are determined from the

vehicle model and sensor outputs. These states are then used to estimate the slip angles of the tyres. A Newton-Raphson numerical method is implemented to solve for the slip angle in the Pacejka Magic formula. This proved to be significantly more computationally efficient as opposed to interpolating the slip angle from the curve.

With knowledge of the wheel load states, the cornering stiffnesses of the tyres at the current conditions are determined. The cornering stiffness of the tyre is the gradient of the lateral force vs slip angle curve at the given vertical load.

4.2.7 Vehicle and Suspension Model

Suspension Model

The Land Rover Defender test vehicle is fitted with the $4S_4$ semi-active suspension system developed by Els (2006). The system is able to switch each strut between discrete states and combinations of low or high damping as well as soft of stiff spring settings. The struts are hydro-pneumatic units and inherently provide a non-linear force response to displacement and velocity inputs, as indicated previously in Figure 5 and Figure 6.

A mathematical model of the pneumatic springs is based on the assumption that the process is adiabatic. The investigation by Van der Westhuizen & Els (2014) indicates that significant improvements in the accuracy of the spring model can be achieved by implementing a real gas model together with the energy equation. The ESC+RP algorithm is implemented on the vehicle in real time where computational efficiency is important. An adiabatic ideal gas model is implemented for its simplicity. It is however noted that it may produce inaccuracies at lower suspension input frequencies.

The damper model is based on lookup tables formulated from experimental data with force being a function of velocity. Friction is incorporated from lookup table, with friction force also a function of velocity.

Load Transfer Model

A lateral load transfer model is utilised to calculate the vertical tyre loads by providing the measured lateral acceleration of the vehicle CG as input to the model. An iterative process is used to calculate the front and rear roll stiffnesses. This is achieved by calculating front and rear spring stiffnesses by the backward difference method by assuming a deflection at the point in time. These stiffness values are used to calculate the roll stiffness from equation (4-24) after which the roll angle is recalculated from equation (4-25). This process is repeated iteratively until the strut deflection, roll angle and roll stiffness converge. These results are then used in equation (4-26) and (4-27) to produce the change in vertical loads at each tyre (Milliken & Milliken, 1995).

$$K_{\emptyset} = K_s \frac{{T_s}^2}{2} \tag{4-24}$$

$$\emptyset = \frac{m h_s a_y}{K_{\emptyset f} + K_{\emptyset r} - m g h_s} \tag{4-25}$$

$$\Delta F_{zf} = \frac{K_{\emptyset f}\emptyset + \frac{m L_r}{L_f + L_r} a_y h_f}{T} \tag{4-26}$$

$$\Delta F_{zr} = \frac{K_{\emptyset r}\emptyset + \frac{m L_f}{L_f + L_r} a_y h_r}{T} \tag{4-27}$$

The load transfer is considered to be at steady state and the damping forces are therefore neglected. Accurate measurement of the roll rate could however be included in the model to calculate the additional damping force during dynamic manoeuvers where strut velocities become significant.

Planar Model

A planar model as shown in Figure 27 is used to calculate vehicle states that dictate the lateral and yaw response of the vehicle. This is similar to the approach used by Linstrom (2015) and Botha (2011).

As discussed previously, once knowledge of the vertical and lateral tyre forces are known, the tyre slip angles can be estimated. With the vertical load calculated by the load transfer model, the lateral forces can be calculated from the lateral and yaw acceleration by using the relations in equation (4-29) and (4-30). The derivations are shown below.

From Figure 27, the individual tyre slip angles are defined as follows:

$$\begin{aligned} \beta_{fl} &\approx \frac{V\beta + L_f r}{V - T_f r/2} - \delta \\ \beta_{fr} &\approx \frac{V\beta + L_f r}{V + T_f r/2} - \delta \\ \beta_{rl} &\approx \frac{V\beta - L_r r}{V - T_r r/2} \\ \beta_{rr} &\approx \frac{V\beta - L_r r}{V + T_r r/2} \end{aligned} \tag{4-28}$$

It is assumed that second order terms of $|\beta|, \left|\frac{L_f r}{V}\right|, \left|\frac{T_f r}{2V}\right|, \left|\frac{T_r r}{2V}\right| \ll 1$ and can be ignored.

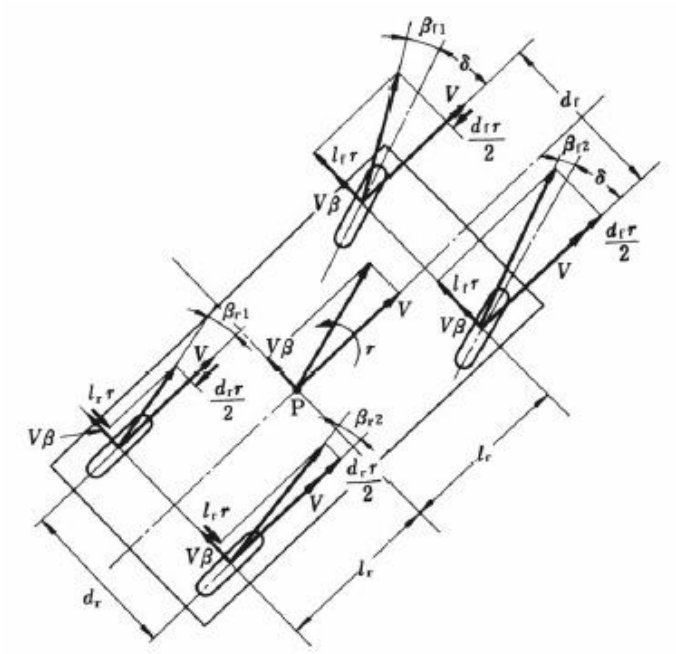

Figure 27 - Planar vehicle model slip angles (Abe, 2009)

These equations can be linearized to be approximately equal to:

$$\begin{aligned} \beta_{fl} &\approx \beta + \frac{L_f r}{V} - \delta \\ \beta_{fr} &\approx \beta + \frac{L_f r}{V} - \delta \\ \beta_{rl} &\approx \beta - \frac{L_r r}{V} \\ \beta_{rr} &\approx \beta - \frac{L_r r}{V} \end{aligned} \tag{4-29}$$

The left and right slip angles on each axle are therefore assumed to be equal:

$$\begin{aligned} \beta_f &\approx \beta + \frac{L_f r}{V} - \delta \\ \beta_r &\approx \beta - \frac{L_r r}{V} \end{aligned} \tag{4-30}$$

The lateral acceleration and yaw acceleration are defined by the equations of motion to be the following:

$$ma_y = F_{y,fl} + F_{y,fr} + F_{y,rl} + F_{y,rr} \tag{4-31}$$

$$I_{zz}\dot{r} = (F_{y,fl} + F_{y,fr})L_f - (F_{y,rl} + F_{y,rr})L_r - \frac{T_f}{2}(F_{x,fl} - F_{x,fr}) - \frac{T_r}{2}(F_{x,rl} - F_{x,rr}) \tag{4-32}$$

Rearranging equations (4-31) and (4-32), the front and rear lateral tyre forces is calculated by the following:

$$F_{y,f} = \frac{ma_y L_r + I_{zz}\dot{r}}{L_f + L_r} \tag{4-33}$$

$$F_{y,r} = \frac{ma_y L_f - I_{zz}\dot{r}}{L_f + L_r} \tag{4-34}$$

During experimental work, the lateral acceleration is measured directly, whereas yaw acceleration is derived from the yaw rate measured by the IMU.

The slip angles are calculated from the Pacejka tyre model as explained in section 4.2.6 and the vehicle side slip is calculated from the relations in equation (4-35) derived from equation (4-28):

$$\beta = \frac{\beta_f - \frac{L_f r}{V} + \delta + \beta_r + \frac{L_r r}{V}}{2} \tag{4-35}$$

4.2.8 Yaw Controller

A sliding mode control method is used to calculate the required yaw moment to correct the error between the current yaw rate and the calculated desired yaw rate. The planar vehicle model is used to establish the vehicle yaw and slip rate in response to a directly applied yaw moment. Adding this direct yaw moment to the model modifies equation (4-32) to take the following form of equation (4-36).

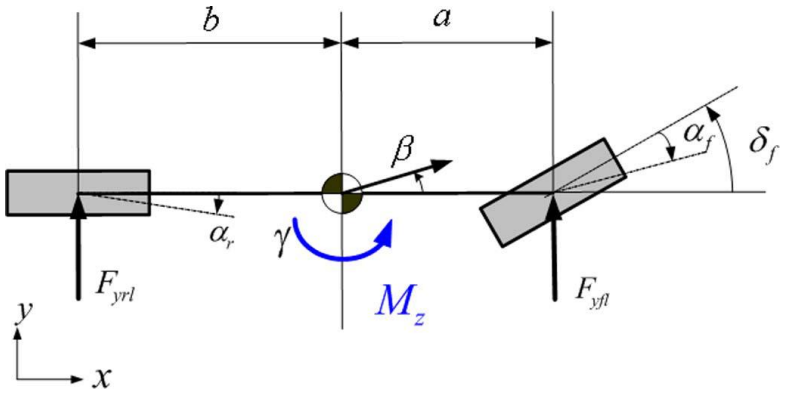

Figure 28 - 2-D Planar vehicle model with yaw moment (Yoon, et al., 2009)

$$I_{zz}\dot{r} = (F_{y,fl} + F_{y,fr})L_f - (F_{y,rl} + F_{y,rr})L_r - \frac{T_f}{2}(F_{x,fl} - F_{x,fr}) - \frac{T_r}{2}(F_{x,rl} - F_{x,rr}) + M_z \tag{4-36}$$

The lateral force produced by the tyre is related to the tyre slip angle and linearized cornering stiffness by:

$$F_y = C_\alpha \beta \tag{4-37}$$

By substituting the relationship between the individual tyre slip angles and the steering angle from equation (4-30) leads to the planar equation of motion for the yaw rate of the vehicle:

$$I_{zz}\dot{r} = -2L_f C_{\alpha f}\left(\beta + \frac{L_f r}{V} - \delta\right) + 2L_r C_{\alpha r}\left(\beta + \frac{L_r r}{V}\right) \tag{4-38}$$

$$\dot{r} = \frac{2\left(-L_f C_{\alpha f} + L_r C_{\alpha r}\right)}{I_{zz}}\beta + \frac{2\left(-L_f^2 C_{\alpha f} + L_r^2 C_{\alpha r}\right)}{I_{zz}V} r + \frac{2L_f C_{\alpha f}}{I_{zz}}\delta_f + \frac{1}{I_{zz}} M_z \tag{4-39}$$

The sliding surface for the sliding mode controller is defined as shown in equation (4-40) below, subject to the condition in equation (4-2). The desired yaw rate is the value calculated from equation (4-21).

$$s = r - r_{desired} \tag{4-40}$$

Differentiating s gives the following:

$$\dot{s} = \dot{r} - \dot{r}_{desired} \tag{4-41}$$

Considering that the desired yaw rate is based on a steady state condition, the derivative thereof is 0. The equivalent control input that achieves $\dot{s} = 0$ is then calculated as per equation (4-42) after substituting equation (4-39) into equation (4-41) to produce the following:

$$M_{z,eq} = -I_{zz}\left(\frac{2\left(-L_f C_{\alpha f} + L_r C_{\alpha r}\right)}{I_{zz}}\beta - \frac{2\left(L_f^2 C_{\alpha f} + L_r C_{\alpha r}\right)}{I_{zz}V} r + \frac{2L_f C_{\alpha f}}{I_{zz}}\delta\right) \tag{4-42}$$

A discontinuous term is added to equation (4-42) to account for model uncertainties, which leads to the following control input:

$$M_z = M_{z,eq} - K sat\left(\frac{r - r_{desired}}{\emptyset}\right) \tag{4-43}$$

The saturation function is once again used to eliminate chatter around the target parameter. The sliding condition can also be expressed by substituting equation (4-39) into equation (4-41) and subsequently into equation (4-2). Equation (4-42) is then substituted into the sliding condition to produce the following equation for calculating the gain K:

$$K = I_{zz}\left\{F_{y,f}\left|-\frac{L_f}{I_{zz}}\beta - \frac{L_f^2}{I_{zz}} r + \frac{L_f}{I_{zz}}\delta\right| + F_{y,r}\left|\frac{L_r}{I_{zz}}\beta - \frac{L_r^2}{I_{zz}} r\right| + |\dot{r}_{desired}| + \eta\right\} \tag{4-44}$$

The parameters η and $\emptyset$ can be tuned to achieve a desirable response. Where $\emptyset$ is used to define the tolerance band around the desired yaw rate.

4.2.9 Brake Force Distribution

Equation (4-43) provided us with a formulation to calculate the required yaw moment on the vehicle. In section 4.2.3 the total braking force required to reduce the vehicle lateral acceleration and rollover index respectively, was calculated. By combining these results, the distribution of the braking forces between the four tyres can be determined.

By once again viewing the vehicle in plane, the total force distribution between the right and the left of the vehicle can be determined:

$$\Delta F_x = \Delta F_{x,left} + \Delta F_{x,right} \tag{4-45}$$

$$M_z = \Delta F_{x,left}\frac{T}{2} - \Delta F_{x,right}\frac{T}{2} \tag{4-46}$$

By rearranging we get:

$$\Delta F_{x,left} = \frac{1}{2}\Delta F_x + \frac{M_z}{T} \tag{4-47}$$

$$\Delta F_{x,right} = \frac{1}{2}\Delta F_x - \frac{M_z}{T} \tag{4-48}$$

These braking forces assume that the required braking force can be achieved, however this might not be the case. The tyre contact patch has a finite level of grip available and the combined lateral force and braking might exceed this level. The tyre friction circle indicates that the vector sum of the lateral and longitudinal tyre forces are not allowed to exceed the total available friction force.

In section 2.4.1 it was shown that the addition of braking or traction forces reduces the maximum lateral force that a tyre can produce. Since the dominant longitudinal tyre force can be generated by the drivetrain or brakes, the maximum lateral force that a tyre can produce before friction limits are exceeded, is typically calculated as:

$$F_{y,max} = \sqrt{(\mu F_z)^2 - F_x^2} \tag{4-49}$$

For application in the yaw control system, this same methodology is used to put a limit on the braking force applied to the tyre at a known lateral force. Equation (4-49) is then modified to calculate the limit in longitudinal force that can be applied to the tyre at the current lateral force to not exceed the total available friction force, shown in (4-50). It is noted by Abe (2009), as indicated in Figure 9, that a reduction in lateral force can also be expected if the slip angle remains unchanged.

Implementing the interaction between accurate lateral and longitudinal tyre models can better improve this estimation.

$$\Delta F_{x,max} = \sqrt{(\mu F_z)^2 - F_y^2} \tag{4-50}$$

The braking force distribution between the front and rear tyres on the left and right respectively, is then calculated. The ratios between the maximum allowable braking forces of the front and rear tyres are determined and the braking distribution is apportioned accordingly:

$$Distribution_{left} = \frac{|F_{x,rl,max}|}{|F_{x,fl,max}|} \tag{4-51}$$

$$Distribution_{right} = \frac{|F_{x,rr,max}|}{|F_{x,fr,max}|} \tag{4-52}$$

Then,

$$F_{x,fl} = \frac{\Delta F_{x,left}}{1 + Distribution_{left}} \tag{4-53}$$

$$F_{x,rl} = \Delta F_{x,left} - F_{x,fl} \tag{4-54}$$

$$F_{x,fr} = \frac{\Delta F_{x,right}}{1 + Distribution_{right}} \tag{4-55}$$

$$F_{x,rr} = \Delta F_{x,right} - F_{x,fr} \tag{4-56}$$

The calculated individual brake pressures will then be the lower of the ideal calculated value and the maximum braking force allowed by the tyre friction circle.

With the individual wheel braking forces calculated, the wheel braking torques are calculated by applying the effective tyre rolling radius:

$$T_b = F_x r_t \tag{4-57}$$

4.2.10 Brake Pressures

The desired braking torques are used to calculate the required pressures in the braking circuit, which forms the system control input. The Land Rover Defender test vehicle is fitted with front and rear disc brakes that were characterised by Penny (2015) during the development of an ABS system for the vehicle. Table 2 shows the physical properties of the brake discs and pads.

Table 2 - Brake Geometry

	Front Brakes	Rear Brakes
Inner Diameter	0.1 m	0.1 m
Outer Diameter	0.149 m	0.149 m
Radial Angle	65°	35°

Budynas & Nisbett (2008) explains how braking torque can be related to an applied braking pressure by the following equation:

$$T_b = \int_{\theta_1}^{\theta_2} \int_{r_i}^{r_o} \mu_{bp} p r^2 dr d\theta \tag{4-58}$$

The equation can be simplified by assuming the conditions of either uniform wear of the pads or uniform pressure. It is shown by Budynas & Nisbett (2008) that sufficiently accurate results can be achieved by simply assuming constant wear, which leads to the following relation:

$$T_b = \frac{1}{2}(\theta_2 - \theta_1)\mu_{bp} p_a r_i \left(r_o^2 - r_i^2\right) \tag{4-59}$$

where p_a is the maximum allowable pressure at the inner radius of the brake pad.

The friction coefficient of the brake pads is an unknown in this equation. The study by Penny (2015) established the linear relationship between the applied hydraulic pressure and the torque produced by the front brakes. This empirical fit shown in Figure 29 shows a gain value between pressure and torque of 266. Using this value in the uniform wear equation calculated a friction coefficient of 0.384, which agrees with typical friction coefficient values in literature.

This friction coefficient was used to calculate the hydraulic pressure from the desired braking torque for the rear brakes. The rear brake pads cover a smaller radial angle and will hence require a larger pressure to produce the same torque as the front brakes.

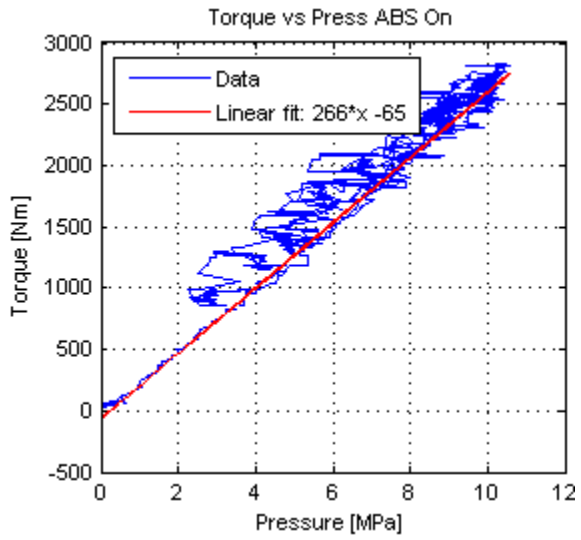

Figure 29 - Pressure to braking torque relation (Penny, 2015)

4.3 Low Level Control

The low level controller is responsible for managing the braking system to produce desired individual wheel brake pressures. The hardware used as well as the control implementation is discussed in greater detail.

4.3.1 ABS Hydraulic Modulator

The hydraulic layout of a typical 4-channel ABS modulator is shown in Figure 30. It is shown that each brake channel features inlet and outlet solenoid activated valves. A total of 8 valves are therefore used to control the individual wheel brake pressures. These valves are all either normally open or normally closed and cannot perform proportional control.

The inlet and outlet valves for each caliper can be switched individually to create the following distinct states:

- Pump mode: Inlet open, outlet closed - Pressure from master cylinder and/or pump is fed to the brake caliper.
- Hold mode: Inlet closed, outlet closed - Fluid is isolated at the caliper and pressure is maintained.
- Dump mode: Inlet closed, outlet open – Pressure at caliper is released and fluid flows towards pump and accumulator.

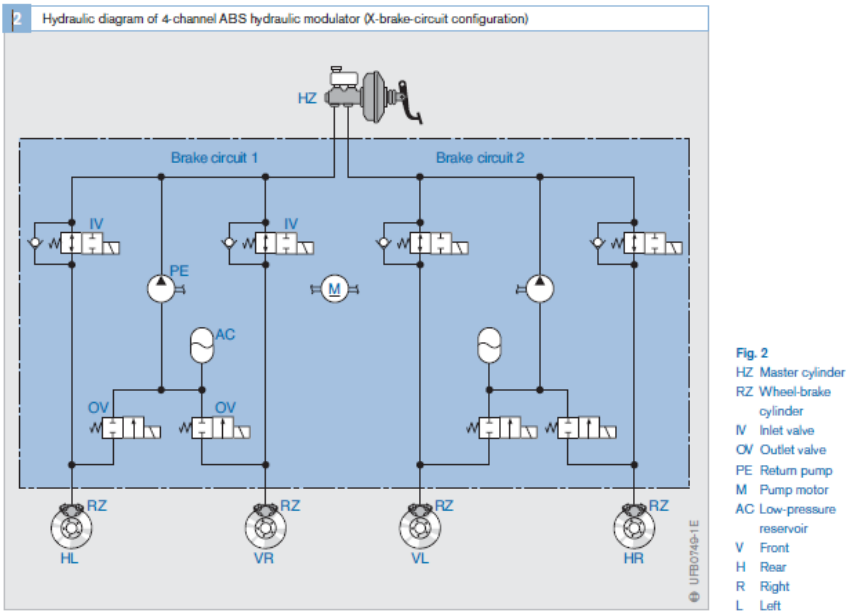

Figure 30 - ABS Hydraulic Layout (Robert Bosch GmbH, 2005)

The pressure at each brake caliper is controlled by switching between these discrete states and using the measured pressure as feedback. Due to the fact that proportional control is not possible with the solenoid valves of the ABS unit, the control methodology is limited to the rather crude bang-

bang type control. In simple terms, when the brake pressure is too low, the pressure is increased. When the pressure is within bounds, pressure is maintained. When the pressure is too high, the pressure is released.

It was shown by Penny (2015) that initialising the pump or dump modes lead to very large rates of pressure change. These large rates are undesirable in the sense that the target pressures can be very easily overshot and more gradual pressure changes are also often desired.

From experimental testing it was determined that the front and rear brake pressures rise at an average rate of approximately 110 MPa/s and 140 MPa/s respectively. The ABS valves are triggered by relays that are limited to a 100Hz activation rate. The solenoids are hence triggered at most every 10ms. This means that at each trigger of the valve solenoids, a jump of between 1.1 and 1.4 MPa of pressure has taken place.

Similarly the dump pressure drop rates are in the order of 150 MPa/s and 220 MPa/s for the front and rear brakes respectively. It is however noted that the rate at which the pressure drops decreases exponentially. The determined rates are therefore only considered to be applicable in the linear range where the brake pressures are to be modulated. These dumping rates then equate to pressure steps of 1.5 to 2.2 MPa between consecutive solenoid switches.

An algorithm was implemented by Penny (2015) where the pump and dump modes were instead applied in a stepwise manner. When a pressure increase is required, the pump mode is activated for a few time steps followed by the hold mode for a few time steps. This creates a step-wise increase in pressure. The same applies to the dump mode where the pressure is stepped down as indicated in Figure 31. These are called the pump-hold and dump-hold modes.

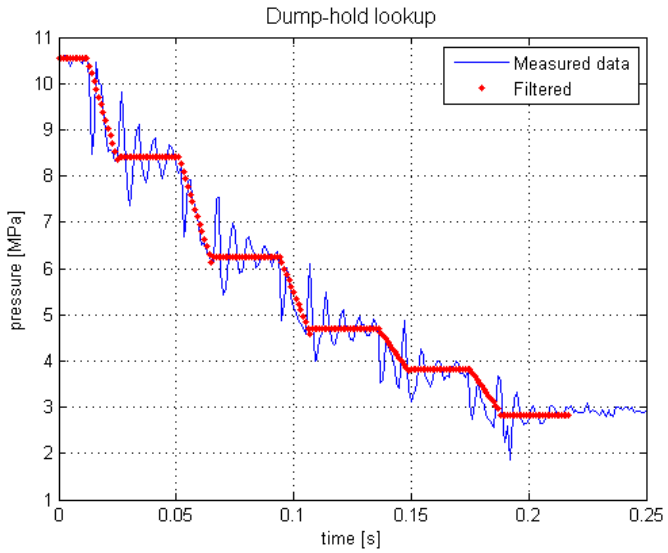

Figure 31 - Dump-hold pressure drop (Penny, 2015)

4.3.2 Hardware Limitations

The Land Rover Defender test vehicle is fitted a standard ABS modulator that is capable of controlling the braking pressure in 4 channels. For the operation of ABS braking, the initial brake pressure is always supplied to the system from the brake pedal actuated master cylinder. The fluid in the circuit is then controlled by the ABS solenoid valves, pump and accumulator in order to control the brake pressures. Although the main mechanism of pressure control is the same in an ABS and ESP modulator, there are some differences. The hydraulic circuit of a typical ESP modulator is shown in Figure 32.

The key difference between these two types of actuators is the ability of the ESP modulator to create hydraulic pressure without the brake pedal being pressed. This is achieved through the additional switchover and high pressure switching valves present in the ESP modulator. These valves allow the return pump to draw fluid from the master cylinder brake fluid reservoir and create or increase pressure in the circuit independent of the brake pedal application.

For the purpose of testing the stability control based rollover prevention system, the way in which pressure is supplied to the ABS modulator fitted to the vehicle was manipulated. The vehicle was fitted with a pneumatic actuator on the brake pedal that initially "loads" the modulator circuit without supplying pressure to the calipers. The ABS return pump is then used to increase the pressure to the calipers in a similar fashion to an ESP modulator.

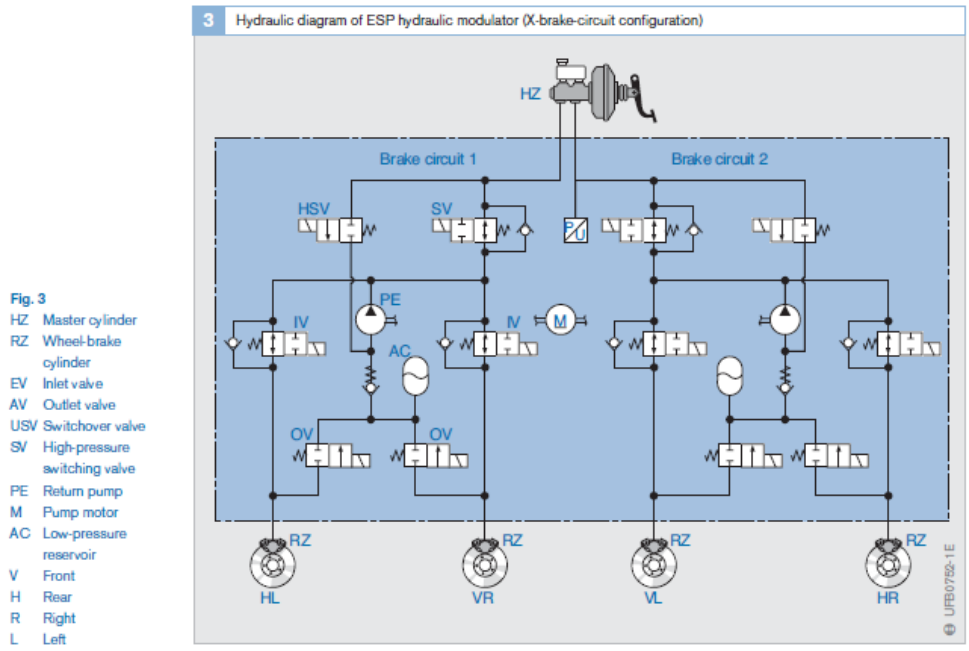

Figure 32 - Hydraulic layout of ESP modulator (Robert Bosch GmbH, 2005)

4.3.3 Pressure Control

The pressure control algorithm monitors the difference between the desired brake pressure and the measured brake pressure in each of the 4 brake channels. Based on these errors in brake pressure, each channel is assigned with a phase number, which in turn dictates the control inputs. Together with Figure 33, the phases are described as follows:

Phase 0:
The control algorithm is initialised and all inputs are in an inactive state.

Phase 1:
This is the standby mode which prepares the ESC+RP to act when required. The braking robot depresses the brake pedal. The desired brake pressures in all channels are 0 in this phase and the dump mode control signal is sent to the ABS modulator. Even though the brake pedal is depressed, the brake pressure is dumped past the caliper and the fluid moves to the internal accumulator.

Phase 2:
The desired pressure is larger than the current brake pressure. The ABS pump is switched on, the pump-hold mode control signal is sent to the ABS modulator and the brake pressure is stepped up.

Phase 3:
The measured brake pressure is within a tolerance band around the desired brake pressure. The hold mode control signal is sent to the ABS modulator and the brake pressure is maintained.

Phase 4:
The desired brake pressure is lower than the current brake pressure. The dump-hold mode control signal is sent to the ABS modulator and the brake pressure is stepped down.

The tolerance band in phase 3 was selected from experimental testing as well as taking the pressure steps at each solenoid switching interval into consideration. A very narrow tolerance band would lead to significant oscillation of the pressures. This is observed when the pressure overshoots the band during phase 2 and the subsequent phase 4 then drops the pressure to below the band before the next solenoid time step.

A tolerance band of 1.3 MPa was selected experimentally, as it proved sufficient to avoid oscillation fairly consistently. In most occasions, the pressure would settle in the tolerance band during phase 4 even if phase 2 caused overshoot. The tolerance band was apportioned to 0.8 MPa above the nominal value and 0.5 MPa below. This bias was selected on the basis that more braking would be safer than less in most occasions.

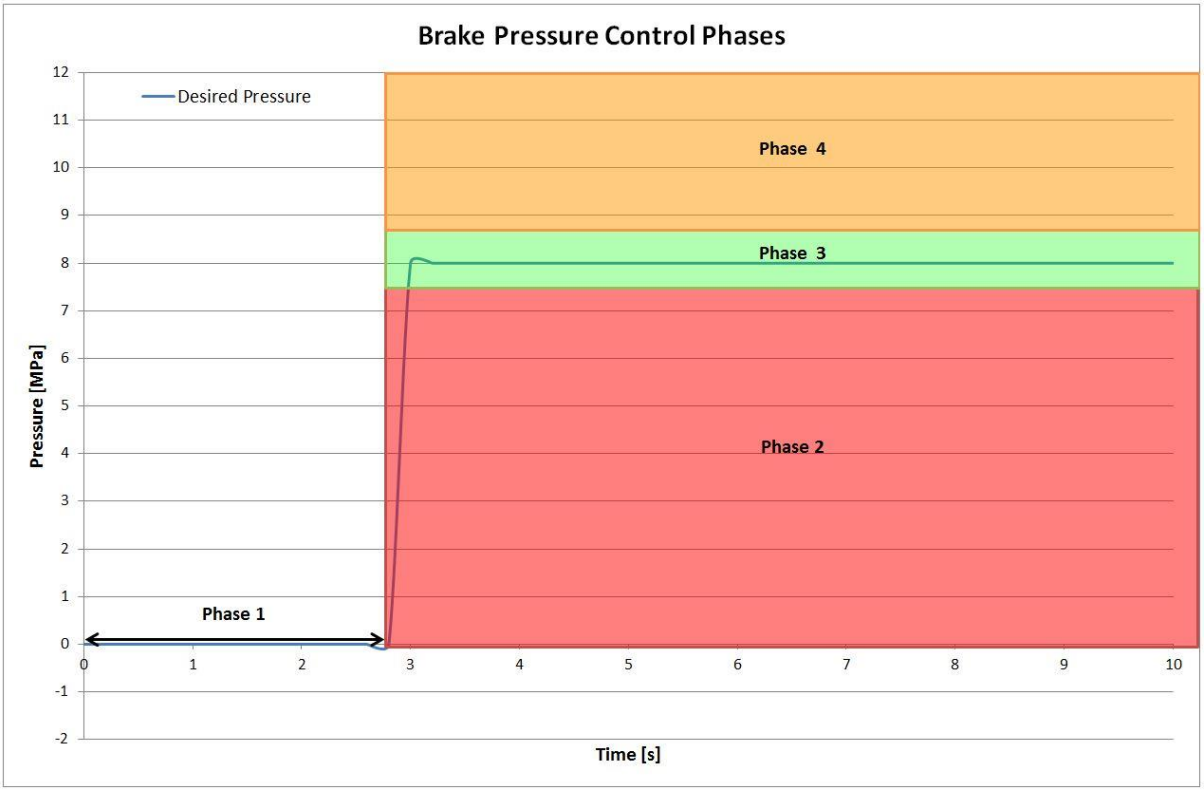

Figure 33 - Brake pressure control phases

5. Test Vehicle and Simulation Model

The vehicle used during experimental testing, the control and data acquisition equipment as well as the full vehicle simulation model is discussed in this chapter.

5.1 Test Vehicle

The Vehicle Dynamics Group at the University of Pretoria has a 1997 Land Rover Defender 110 SUV that has been used for testing and evaluation of vehicle dynamics systems for a number of years. The vehicle is fitted with an array of sensors for data capturing as well as the $4S_4$ semi-active suspension system as discussed in section 2.3.1.

The discussion regarding the rollover detection and control strategies has led to the identification of required measurements on the vehicle. These measures, as well as the equipment used to measure the parameters, are indicated in Table 3.

Table 3 - Vehicle Measurements

Parameter	Sensor	Parameter			
		Rollover Index	Desired Speed	Desired Yaw Rate	Yaw Control
Roll Angle	IMU – Novatel Span-CPT	O	O		
Roll Rate	IMU – Novatel Span-CPT	O	O		
Roll Acceleration	--	O			
Lateral Acceleration	IMU – Novatel Span-CPT	O	O	O	O
Yaw Rate	IMU – Novatel Span-CPT	O	O	O	O
Yaw Acceleration	--	O	O		O
Vehicle Speed	IMU – Novatel Span-CPT		O	O	O
Steering Angle	Encoder – Eltra EML50A			O	O
Brake Pressures	Pressure Transducers - Wika				O

As indicated in Figure 34, the vehicle is fitted with an Inertial Measurement Unit (IMU) that combines an antenna based GPS system as well 3-axis accelerometers and 3-axis gyroscopes. A potentiometer is fitted to the front right kingpin to measure steering angle and a Wika pressure transducer is fitted at each of the 4 brake calipers.

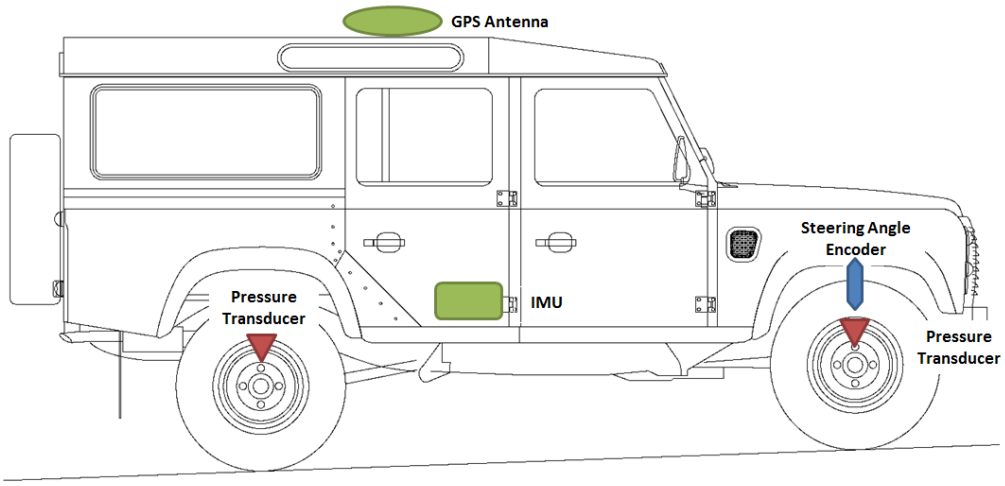

Figure 34 - Vehicle Instrumentation

5.2 Data Transmission

The vehicle is fitted with a Diamond Systems PC/104 computer that runs a Linux based operating system. The computer receives analogue inputs from the steering angle and brake pressure transducers which are captured at a 1000Hz sampling rate. The IMU transmits serial data at a rate of 20Hz for the acceleration and gyroscope data and 50Hz for the GPS based data.

Digital control outputs are relayed to the ABS modulator whilst analogue output is used to actuate the braking robot. The architecture of the data transmission is shown in Figure 35.

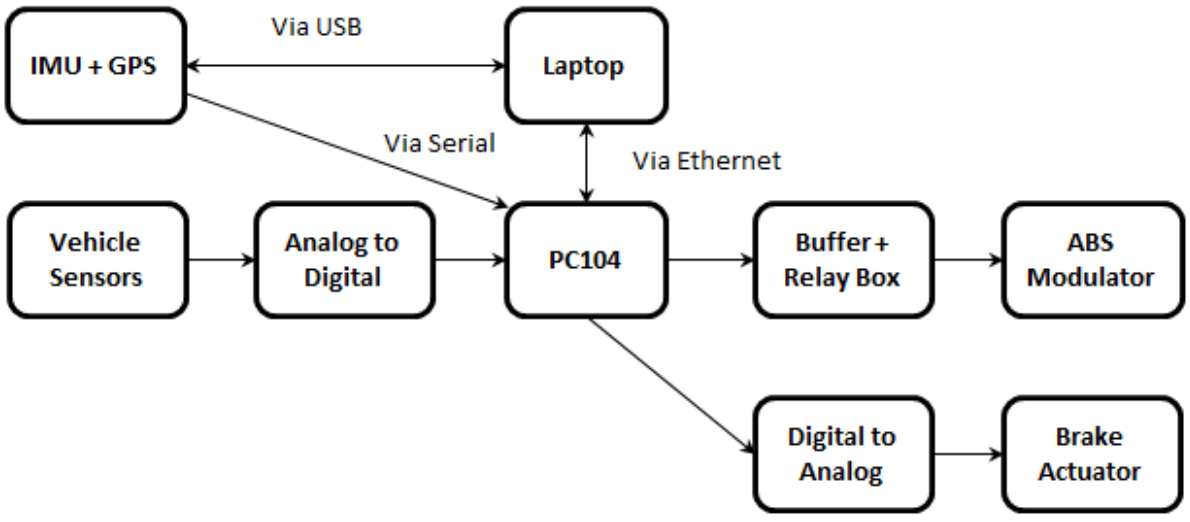

Figure 35 - Data acquisition and control block diagram

5.3 Full Vehicle Simulation Model

The proposed control systems were all initially tested and developed using an ADAMS 16 degree of freedom full vehicle model of the Land Rover Defender. This model was initially developed by (Thoresson, 2007) and later updated by (Uys, et al., 2007) and (Cronjé, 2008). The non-linear hydro-pneumatic $4S_4$ suspension system is included in the model.

A graphic of the overall model is shown in Figure 36. The rigid front axle is longitudinally fixed to the chassis with leading arms and rubber bushes. A Panhard rod locates the axle laterally. The rear solid axle features two trailing arms for longitudinal support, whilst the lateral constraint is provided by an A-arm pivoting on a spherical joint on the axle and bushes on the chassis. The body of the vehicle is also split into two sections and includes a torsional spring between the two units to model the chassis flexibility.

The ADAMS model is linked to a Matlab Simulink environment to perform co-simulation of the vehicle model in parallel with the numerical suspension strut models as well as the vehicle dynamics control systems. A closed-loop driver model developed by Botha (2011) is also included to perform simulations requiring the vehicle to following a predefined path such as double lane changes.

Initial control system development was performed using the ADAMS model together with a Pacejka '89 tyre model. This tyre model solves significantly faster than the more complex FTire tyre model used in later simulations. These tyre models are now briefly discussed.

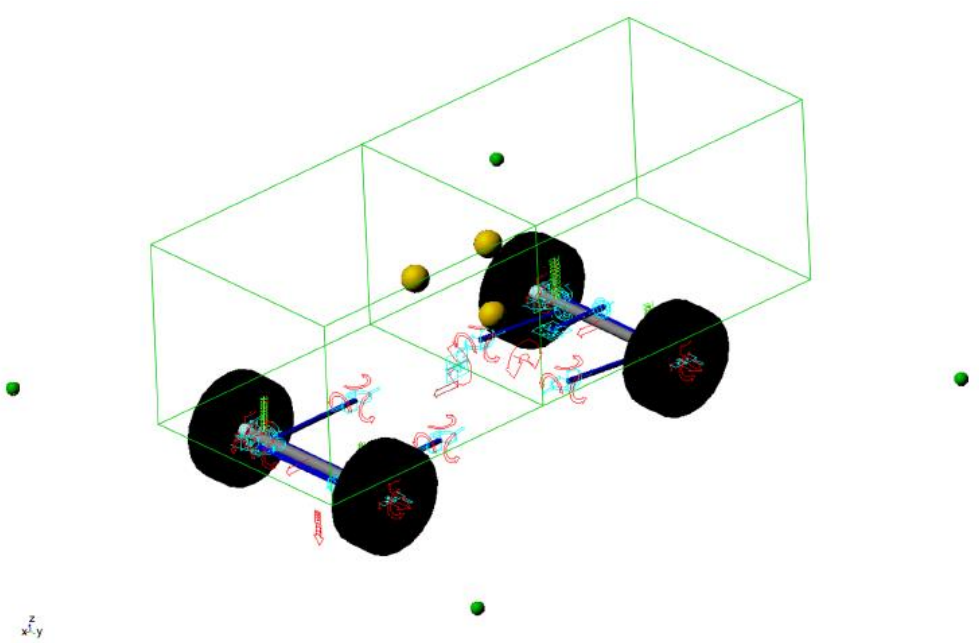

Figure 36 - Full vehicle ADAMS model representation

5.4 Tyre Models

Table 4 summarises the applicability of using different tyre models in ADAMS to simulate certain events or manoeuvers. It is shown that it is possible to implement the Pacejka '89 tyre model for simulation of steady state cornering, lane change, vehicle roll-over and braking/power-off during a turn. Even though it is possible for the latter 2 events, this tyre model is not the best for simulating these events.

Table 4 - ADAMS Tyre Model Applicability

		ADAMS Tyre		
		PAC2002	**PAC89**	**FTire**
HANDLING	Stand still and start	+	o/+	+
	Parking (standing steering effort)	+	-	+
	Standing on tilt table	+	+	+
	Steady state cornering	+	o/+	o/+
	Lane change	+	o/+	o/+
	ABS braking distance	+	o/+	+
	Braking/power-off in a turn	+	o	o/+
	Vehicle roll-over	+	o	+
	On-line scaling tire properties	+	-	o

-	Not possible/Not realistic
o	Possible
o/+	Better
+	Best use

It can be seen that the Pacejka 2002 and FTire models are more applicable for use in simulations of the typical manoeuvers under investigation.

The University of Pretoria has parameterised and validated an FTire model of the Michelin LTX 235/85 R16 tyre fitted to the Land Rover Defender test vehicle and this was implemented during the simulation studies.

5.5 Simulation Model Validation

The ADAMS model used for vehicle simulations has been extensively implemented for the testing of vehicle dynamics systems at the University from Pretoria. The model has been validated for lateral dynamics by various authors including Linstrom (2015). Linstrom implemented task specific sensors such as a side slip angle sensor and laser displacement sensors to measure roll angle. It was shown that the ADAMS model correlated very well with the experimental testing when performing ISO 3888-1 (International Organisation for Standarisation, 1999) double lane changes at speeds of 49, 61, 70 and 78 km/h.

The coefficients of determination calculated by Linstrom for the various model metrics are shown in Table 5.

Table 5 - ADAMS Model correlation (Linstrom, 2015)

	Coefficient of Determination (R^2)					
Speed [km/h]	Path	Slip-angle	Yaw Rate	Roll Rate	Roll Angle	Lateral Acc
49	0.99	0.84	0.91	0.17	0.65	0.95
61	0.98	0.84	0.92	0.42	0.80	0.96
70	0.98	0.93	0.92	0.48	0.76	0.96
78	0.96	0.91	0.90	0.59	0.67	0.97

As was previously discussed, the experimental testing described in this report utilised a central Inertial Measurement Unit to record the inertial data at a fairly low sampling frequency. Some of the metrics such as roll angle and roll rate is expected to not be as accurate as the displacement sensors utilised by Linstrom.

Initial baseline tests were however performed without the ESC+RP system in place and compared to results obtained by the path following controller with the ADAMS vehicle model. A typical comparison of metrics such as yaw rate, lateral acceleration, roll angle, roll rate, speed, path, steering angle and slip angles are shown for a 68 km/h double lane change in Figure 37.

The comparison shows a fairly good correlation between the measured and simulated data. As expected the roll data is not as accurate as desired, with the roll rate proving to be the least accurate. The maximum percentage relative error of the peaks for the double lane change manoeuver at 68km/h is summarised in Table 6.

The steering input correlation between the simulation and experiment was the strongest during the first half of the manoeuver and the correlation of the other measures was therefore also the strongest during this part.

The slip angles shown were calculated with the ESC+RP algorithm based on the planar vehicle model kinetics, but the parameters used to calculate the slip angles were measured on the vehicle.

Table 6 - Maximum relative error of correlation data peaks for the two halves of the manoeuver - DLC at 68km/h

	Maximum Relative Error	
Measures	**First Half**	**Second Half**
Steering Angle	5.9%	17.2%
Lateral Acceleration	11.8%	24.0%
Yaw Rate	12.7%	18.5%
Roll Angle	27.1%	38.4%
Roll Rate	50.7%	67.6%
Slip Angle Front	7.0%	12.8%
Slip Angle Rear	43.8%	16.1%

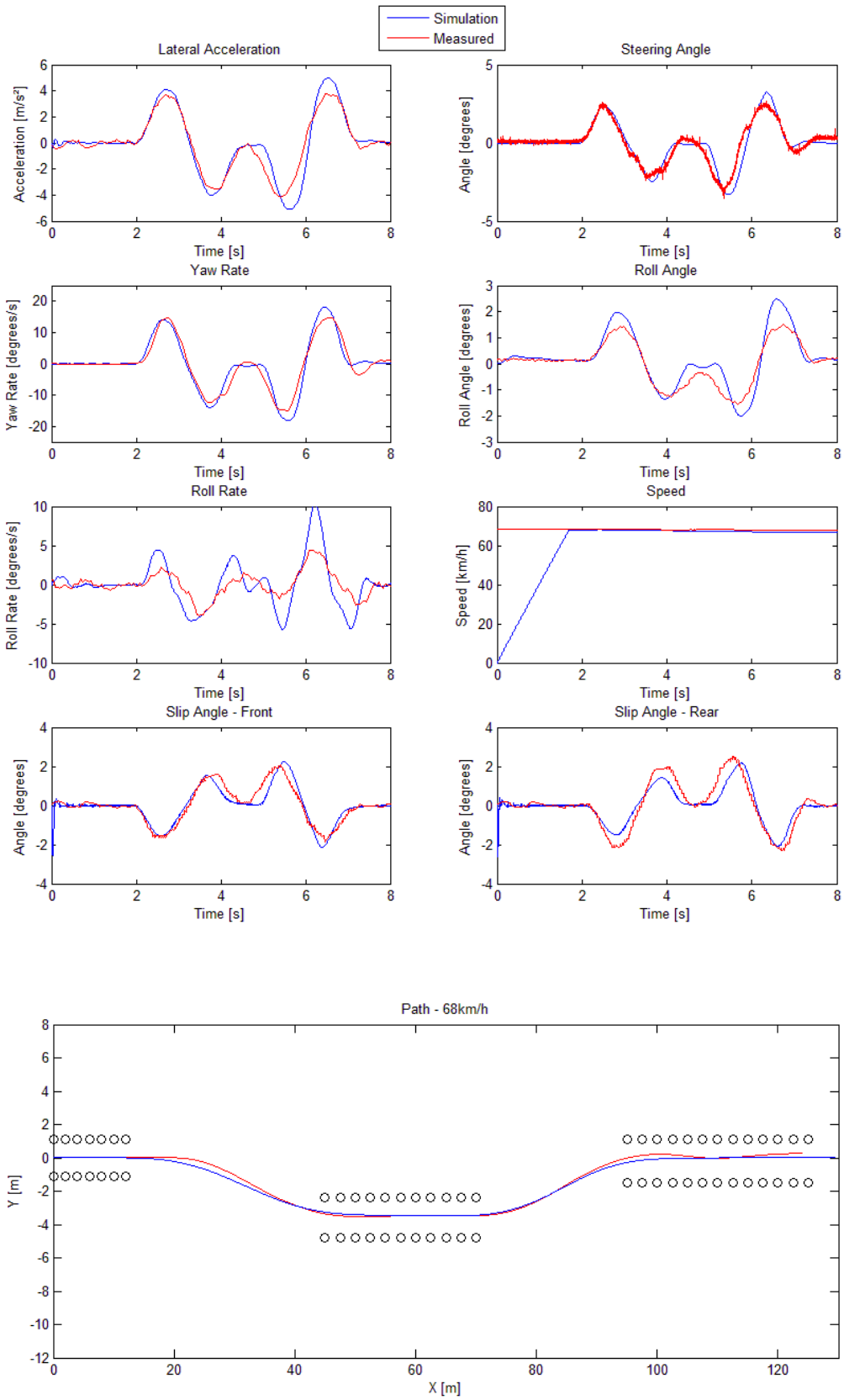

Figure 37 - Simulation vs experimental data - DLC at 68km/h

5.6 Slip Angle Estimation

In section 4.2.4 it was discussed that commercial ESC systems often implement a weighted combination of yaw rate error and side slip angle error to define the stability control parameter (Rajamani, 2006). To achieve this, an accurate estimation of the vehicle side slip angle is required. Sensors to measure vehicle slip directly are very expensive and impractical for implementation on a vehicle and mathematical approximation methods are therefore preferred.

The yaw control algorithm in this report used yaw- and lateral acceleration measurements in combination with the Pacejka tyre model to approximate the slip angles at each axle. The relationship in equation (4-35) is then used to calculate the overall vehicle slip. A comparison of typical calculated and measured vehicle side slip in simulation is shown in Figure 38. A fairly good correlation is achieved, with a maximum peak relative error of 35%, although a phase shift is also evident. This method can be considered to be fairly successful, although a well parameterised tyre model is necessary.

In the absence of a tyre model, the side slip needs to be calculated otherwise. A typical approach was discussed by Cheli, et al. (2007). They identified that the kinematics derived from the planar vehicle model can accurately approximate side slip during transient conditions, whereas a Kalman filter state observer shows good results during steady state conditions. A fuzzy-logic procedure is used to identify the steady state or transient conditions.

The combination of the kinematic and state observer approximations also allows for the tyre cornering stiffness values to be updated. This is especially beneficial when changing road surface conditions are encountered and the conditions under which the tyre model was developed is no longer representative.

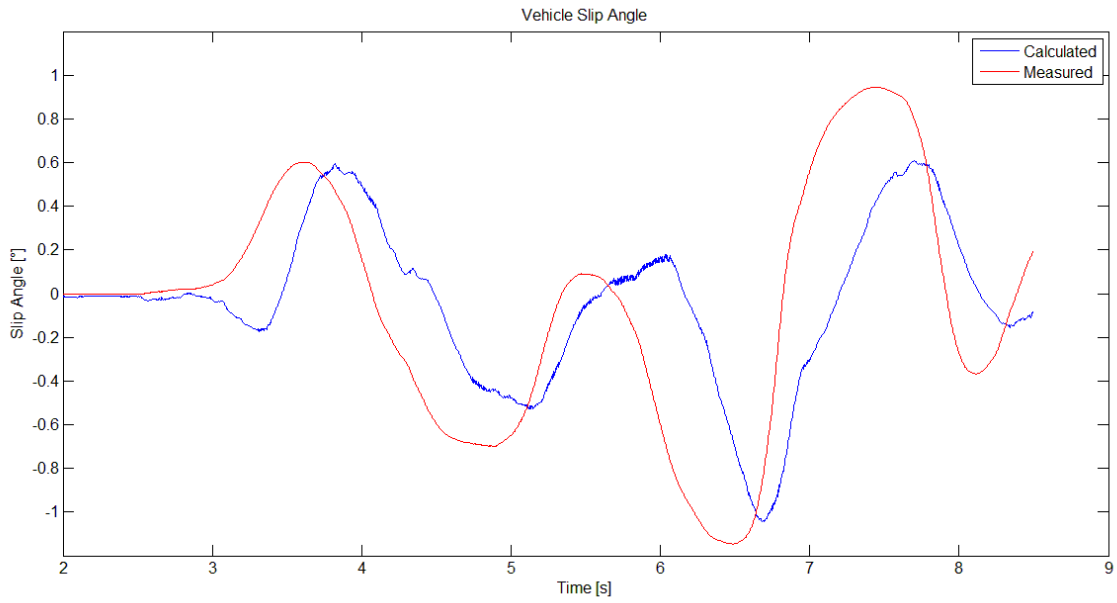

Figure 38 - Calculated vs. Measured Vehicle Slip Angle - DLC Simulation at 68km/h

6. Simulation Results

Initial simulations were performed to evaluate the effectivity of the different rollover prevention and yaw control strategies. Simulations were performed with the ADAMS model, implementing the FTire tyre model, in co-simulation with the Matlab and Simulink based control system. The path following steering controller was used to determine the steering input based on the specified path.

6.1 Braking Based System

The braking based system was tested in the ISO 3888-1 (International Organisation for Standarisation, 1999) double lane change manoeuver as well as the NHTSA fishhook test. The ISO 3888-1 and ISO 3888-2 (International Organisation for Standarisation, 2011) tests were also performed experimentally as discussed later in section 7.1 to 7.4. The fishhook test requires a very large section of flat road to conduct the test safely. The Gerotek Test Facilities (Gerotek Test Facilities, 2015), where the other tests were performed does not have a sufficiently large section of flat road to accommodate this test. The fishhook test was therefore limited to the simulation environment.

6.2 Double Lane Change – ISO 3888-1

The ISO 3888-1 double lane change (DLC) was used to perform initial verification and performance testing of the ESC+RP rollover prevention system. The DLC consists of a predefined course that the vehicle is required to follow, with the layout previously shown in Figure 14. The vehicle enters through an initial lane after moving across into a second lane, so as to simulate a severe overtaking manoeuver, and then return to the original line through the third lane. This is a test that requires closed loop steering inputs and the steering controller developed by Botha (2011) is used in the simulations.

The simulations were performed at three speeds, namely 68km/h, 77km/h and 85km/h, both with and without the ESC+RP system. These speeds were the measured entry speeds during certain experimental runs discussed in section 7 and was selected for simulation to provide an accurate comparison.

Figure 39 shows the paths that the vehicle followed for the different entry speeds and ESC+RP configurations. The vehicle left the course for the 85km/h case with the ESC off, whilst the ESC+RP system managed to keep the vehicle within the course. The vehicle would probably have knocked over some cones on entry to the third lane. The 77km/h vehicle would have also knocked the cones without the ESC+RP system, whilst the ESC+RP system assisted in keeping the vehicle in the centre of the lanes.

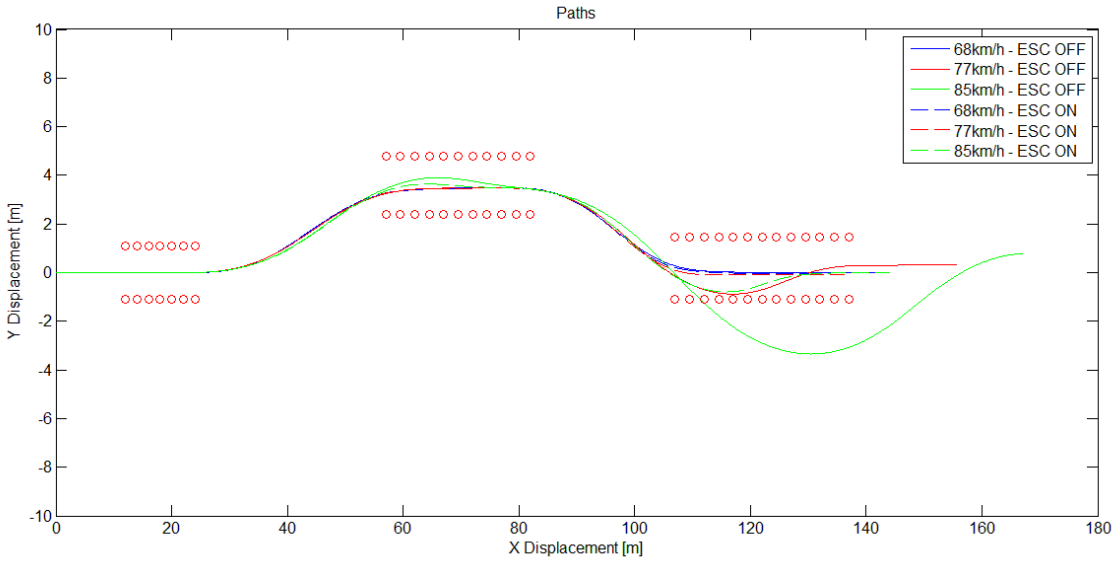

Figure 39 - DLC Simulations Paths

The rollover indices generated at the different entry speeds and ESC+RP configurations are shown in Figure 40, Figure 41 and Figure 42. The results obtained from the zero-moment point (ZMP) based rollover index are also compared to the lateral load transfer ratio (LLTR) based rollover index. These two rollover indices are shown to follow very similar trends, although the ZMP method produces much higher peaks and also earlier peaks. This holds the advantage that, because the ZMP RI increases earlier and more rapidly, the ZMP can be implemented to allow for earlier intervention from the ESC+RP system.

The simulation results indicate that for each case, the ESC+RP system has managed to reduce the rollover index peaks produced during the manoeuver. This reduced risk of rollover has not compromised the path following of the vehicle, as is also illustrated in the typical yaw rate data shown in Figure 43.

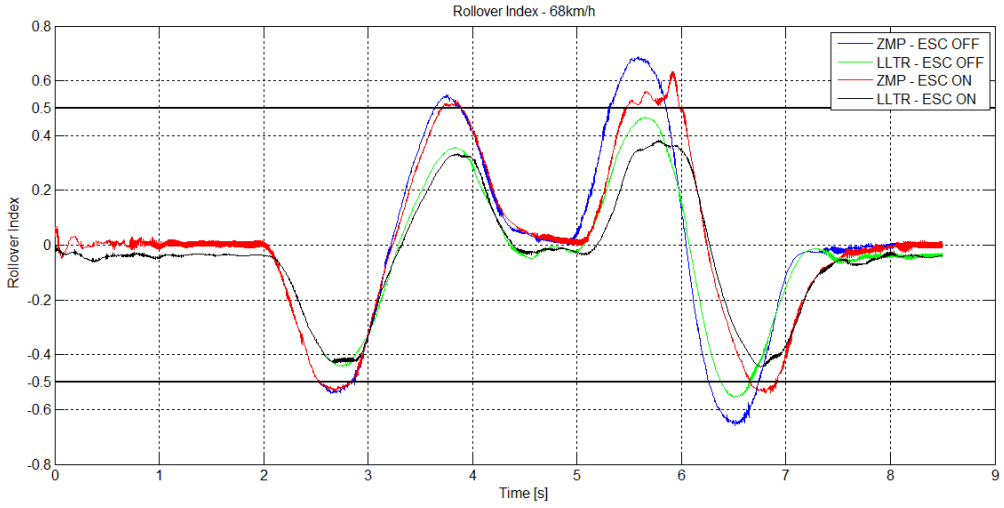

Figure 40 - RI for 68 km/h DLC

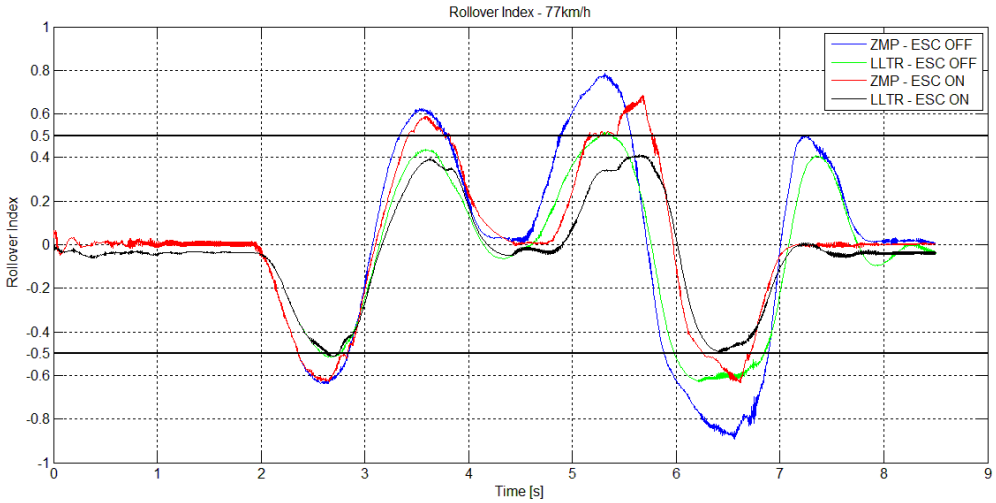

Figure 41 - RI for 77 km/h DLC

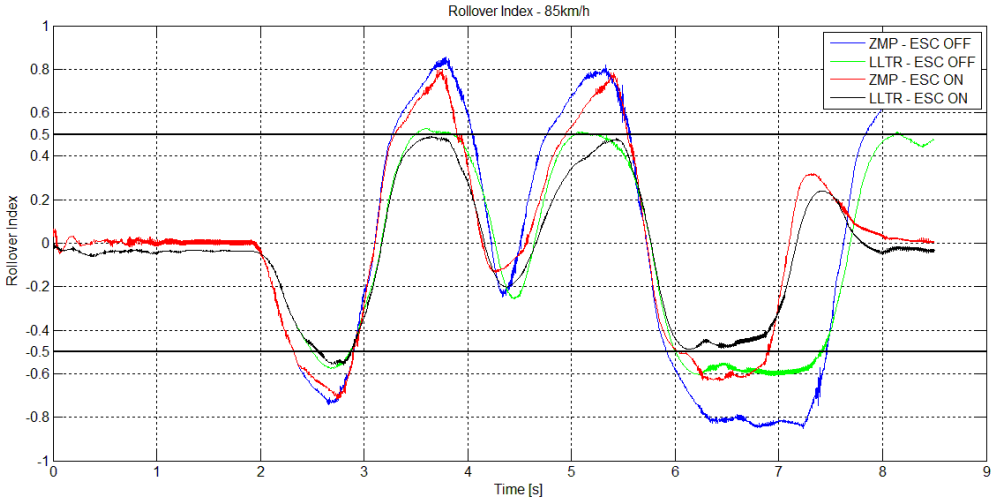

Figure 42 - RI for 85 km/h DLC

The yaw rate data for the 85km/h speed (Figure 43) shows that the desired yaw rate for the non-ESC+RP case becomes rather erratic. The desired yaw rate is a function of the cornering stiffness which is in turn calculated from interpolated slip angle values. The manoeuver induces large slip angles, which in turn led to some numerical instability of the desired yaw rate calculation. This problem was later eliminated on the test vehicle by imposing some limits on the front to rear slip angle relationship.

It is however evident that the run with the ESC+RP system activated shows a significantly improved yaw rate response where the desired yaw rate is followed much more closely.

Figure 44 shows the effect of ESC+RP on the tyre normal load distribution. The normal loads of the tyres are more closely spaced around the centre owing to a reduced lateral load transfer, partly due to the lower lateral accelerations experienced with the ESC+RP on, as shown in Figure 45.

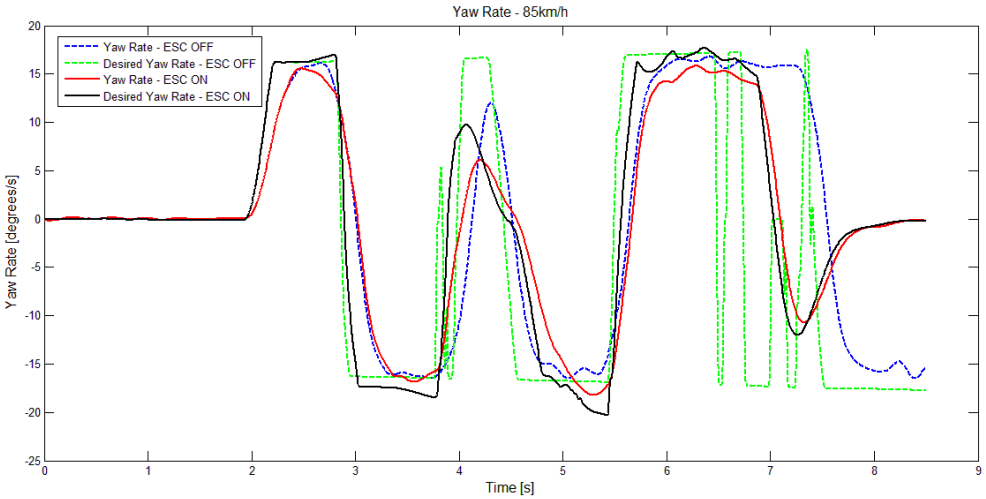

Figure 43 - Yaw rates for 85 km/h DLC

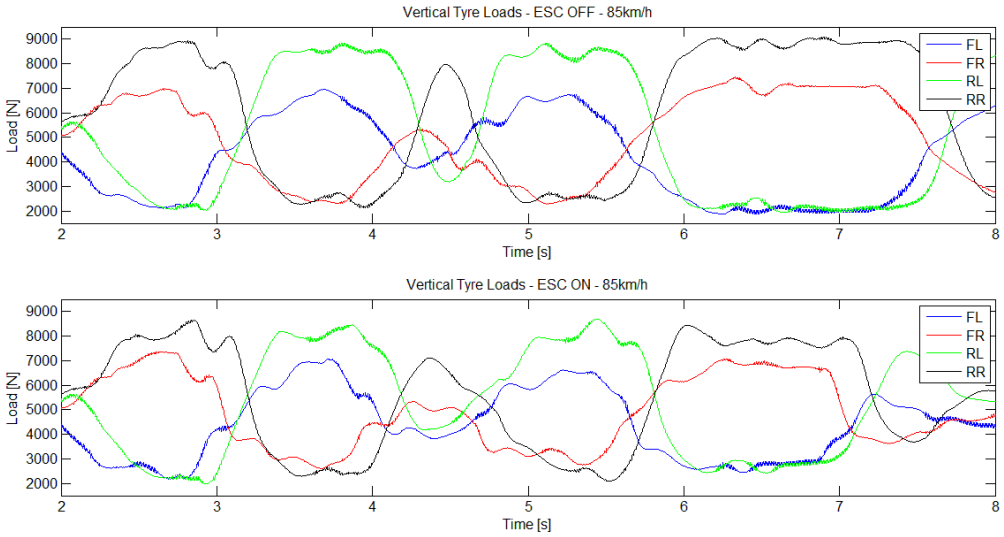

Figure 44 - Tyre normal loads for 85 km/h DLC

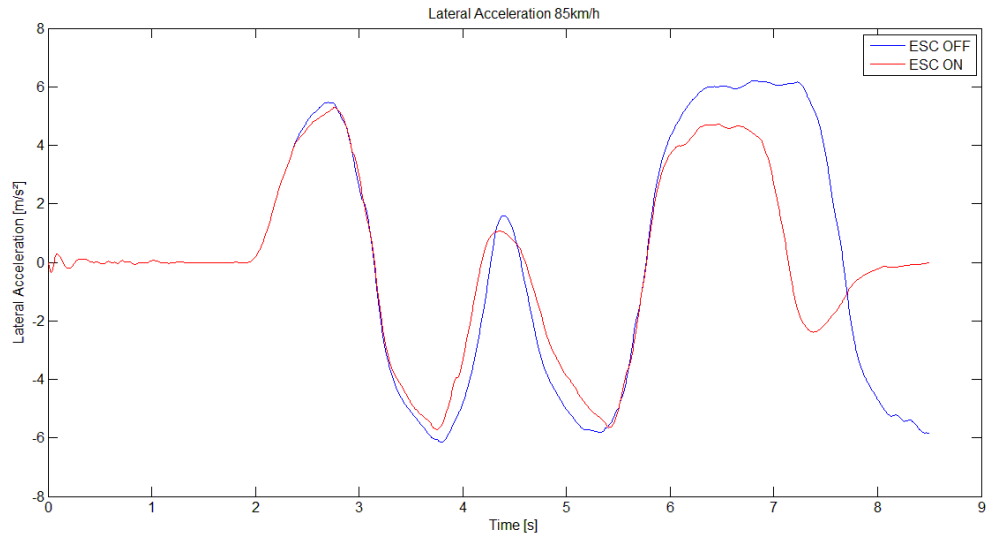

Figure 45 - Lateral acceleration for 85km/h DLC

The operation of the ESC+RP is best understood when the brake pressures generated at each wheel are analysed in conjunction with the steering input and yaw rate. The brake pressures generated by the intervention of the ESC+RP system for the 85km/h entry speed case are shown in Figure 46. The desired brake pressures calculated by the control system as well as the simulation generated brake pressures are shown. The "actual" brake pressures shown are generated to mimic the response of the ABS modulator. The same low level control methodology as described in section 4.3.3 was used. The phase 2 and phase 4 responses were modelled as the average rates of the measured increasing and decreasing pressure of the pump-hold and dump-hold responses respectively.

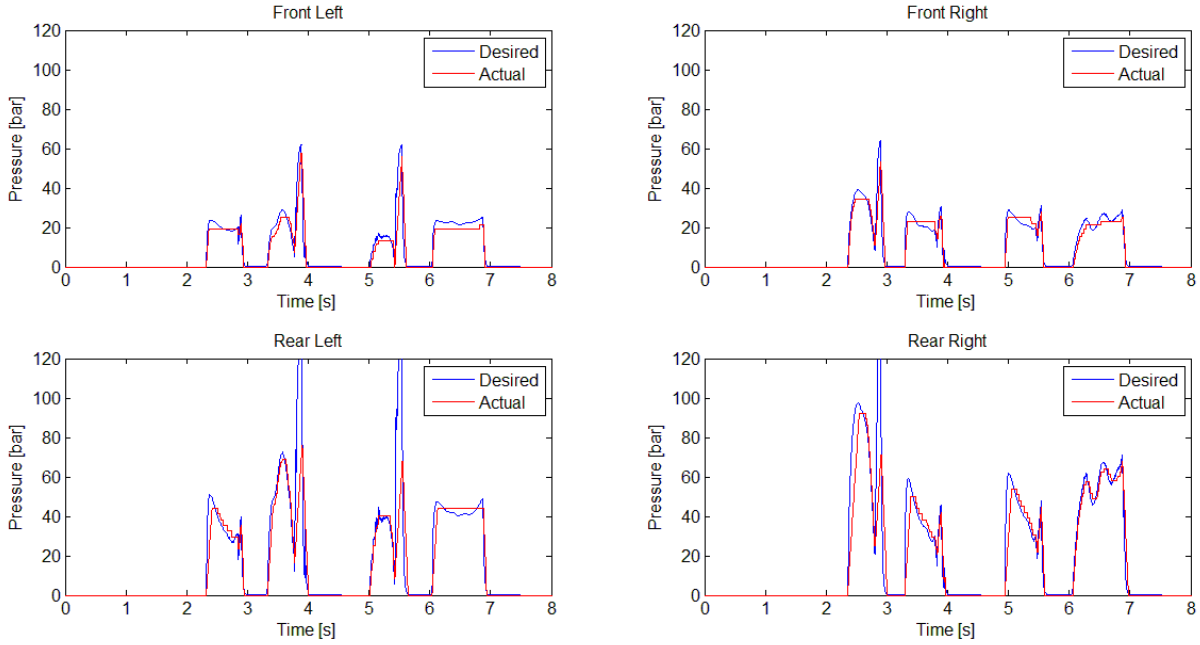

Figure 46 - Brake pressures for 85 km/h DLC

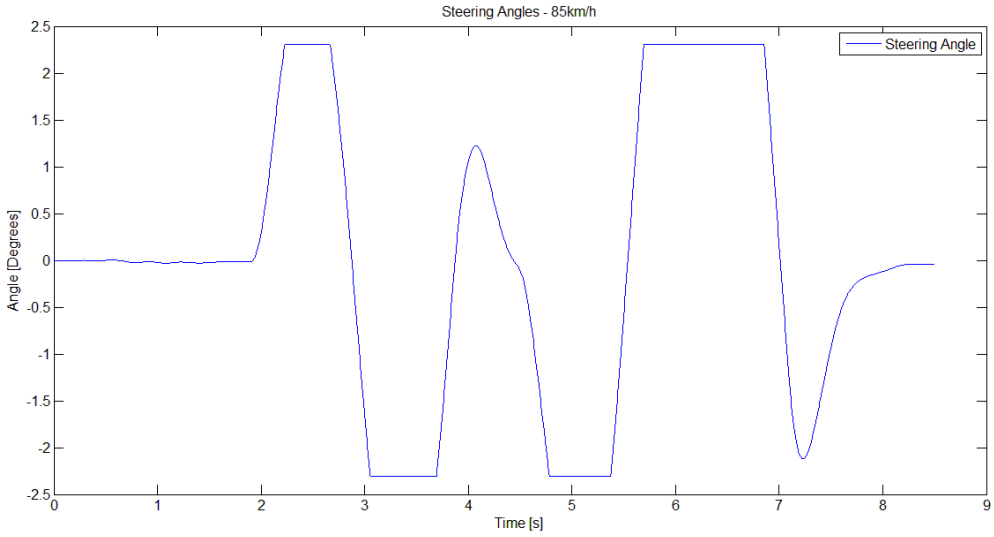

Figure 47 - Steering angles for 85 km/h DLC

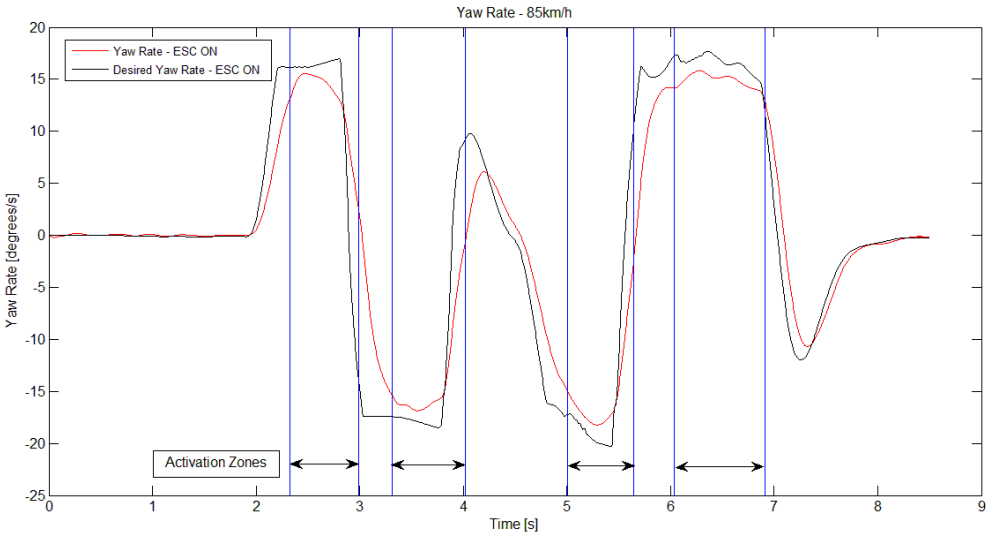

Figure 48 - Desired vs actual yaw rate for 85km/h DLC

The sliding mode controller used to control the yaw moment, features a saturation function that allows for a yaw rate error tolerance band to be specified. This tolerance band reduces chatter and overshoot from the controller. The ESC+RP activation zones are indicated in the yaw rate plot in Figure 48. It is seen that the yaw rate is initially too low, but is approaching the desired value. The brake pressure on the right (Figure 46) is therefore increasing to reduce the rate at which the yaw rate approaches the desired value. The pressure on the right then drops off when the actual yaw rate crosses the desired and the yaw rate is found to be too high. The spike in pressure at the right just before the 3s mark is aimed to increase the yaw rate while the vehicle is turning right towards the second lane in the DLC manoeuver. The brake pressures for the other zones can be analysed similarly. The braking applied resulted in the vehicle exiting the manoeuver at about 57 km/h as indicated in Figure 49.

The simulation results for the ISO 3888-1 double lane change indicate that the rollover indices as well as the yaw rate errors were reduced by the introduction of the ESC+RP rollover prevention system. The vehicle with the ESC+RP system activated showed lower risk towards rollover whilst the path following ability was maintained.

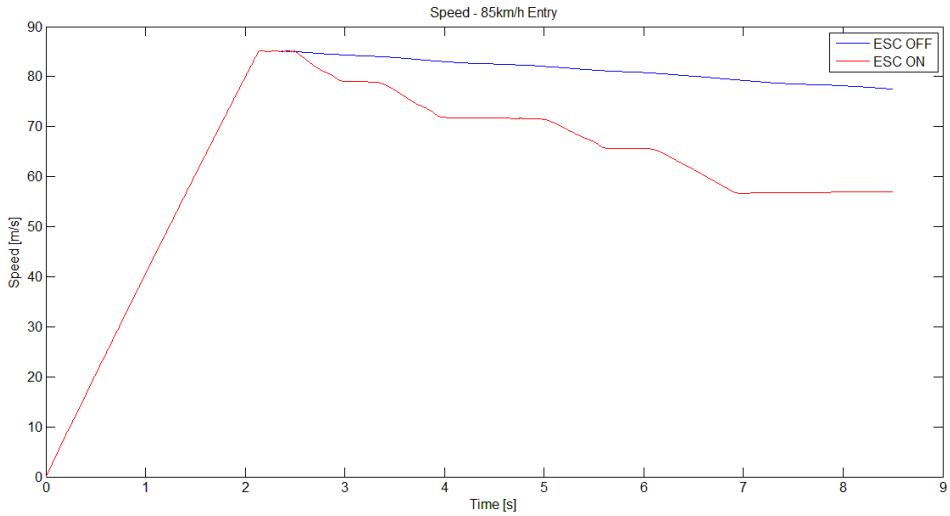

Figure 49 - Speed profile for 85km/h DLC

6.3 NHTSA Fishhook Test

The NHTSA Fishhook test is considered by the NHTSA to be the most severe test for determining the rollover resistance of a vehicle. The test consists of a vehicle driven at a speed slightly higher than the predetermined manoeuver entry speed. The driver releases the throttle and initiates the steering input when the target entry speed is reached. A large steer rate and then reversing steer rate is applied to the vehicle as indicated in Figure 50. The vehicle is considered to have passed the test at the specific entry speed when wheel lift is not induced during the manoeuver. The vehicle entry speed is increased until wheel lift is exhibited.

This test is considered to be very successful at establishing the rollover resistance of a vehicle. Once active safety systems are introduced, the validity of the test does become questionable. The steering input is open loop and the vehicle is therefore not required to follow a predefined path. Safety systems such as actives steering can simply prevent the vehicle from reacting to the steering wheel input and therefore reduce the curvature of the vehicle path. This will reduce the likelihood of rollover, but the path of the vehicle is completely discarded.

This test is simulated to establish the effect of the braking based rollover prevention system on the rollover propensity. The simulations were done at entry speeds of 50, 60 and 70km/h with the ESC+RP system off and then at 50, 60, 70 and 80km/h with the system on. In each case the ESC+RP system is triggered when the rollover index exceeds a threshold of 0.5.

Figure 50 indicates the steering inputs at the 50, 60 and 70 km/h entry speeds. The steering inputs are near identical. The slight deviation is attributable to the only closed loop feedback of the roll rate that determines the point at which the steering input is reversed.

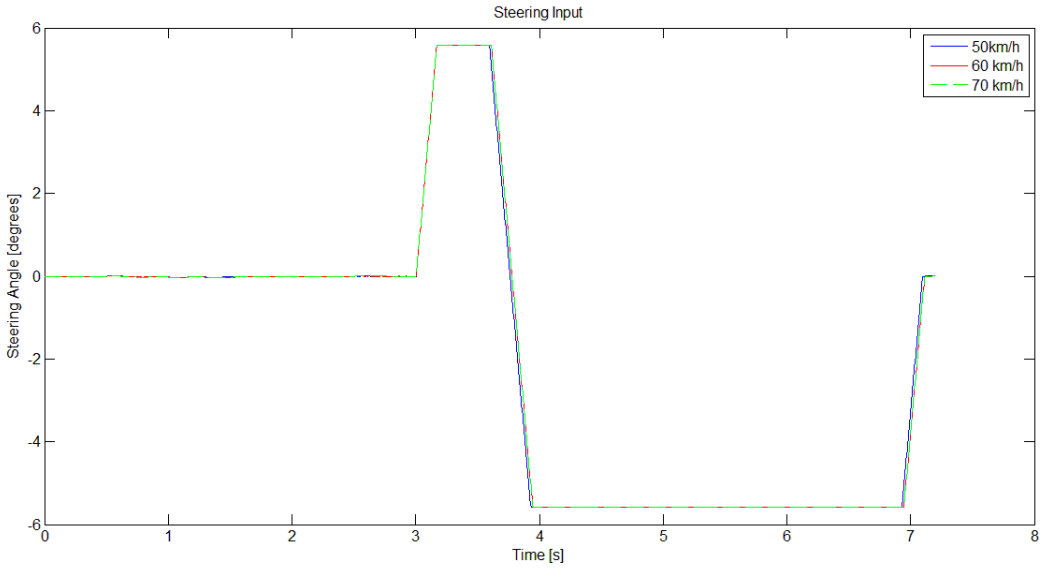

Figure 50 - Fishhook test steering input

The results of the simulations are shown in the following figures. The path followed by the vehicle for different speeds and ESC+RP on and off is shown in Figure 51. The figure shows that the open loop steering input doesn't produce a consistent path, and is mostly dependent on the entry speed. In each case the ESC+RP intervention has led to a tighter path being followed.

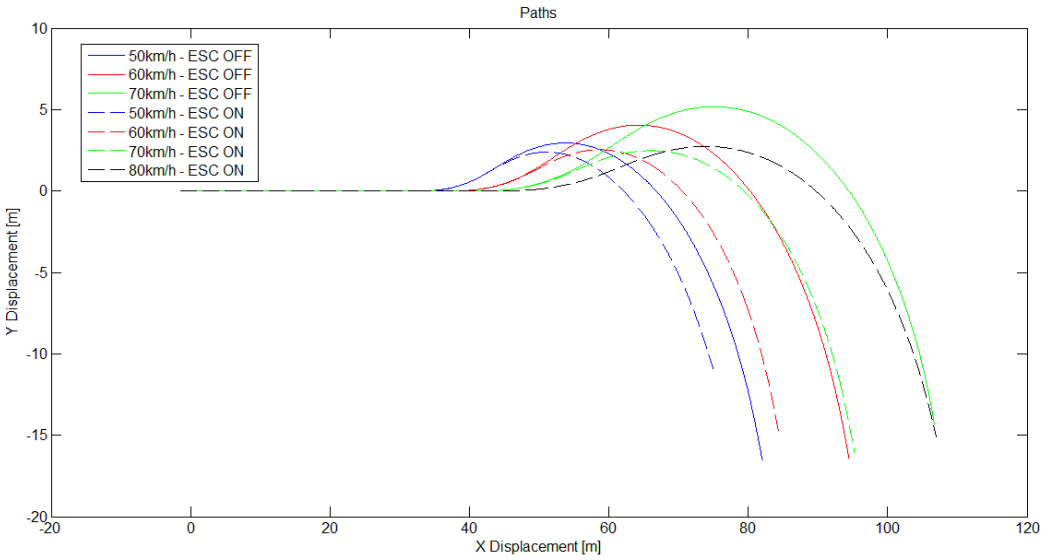

Figure 51 - Fishhook test paths

off. The manoeuver produces large lateral accelerations. The ESC+RP system does however lower the lateral acceleration in each case when the system is triggered. The associated rollover indices are shown in Figure 53 to Figure 56. In each case the zero-moment point based rollover index is shown together with the lateral load transfer ratio.

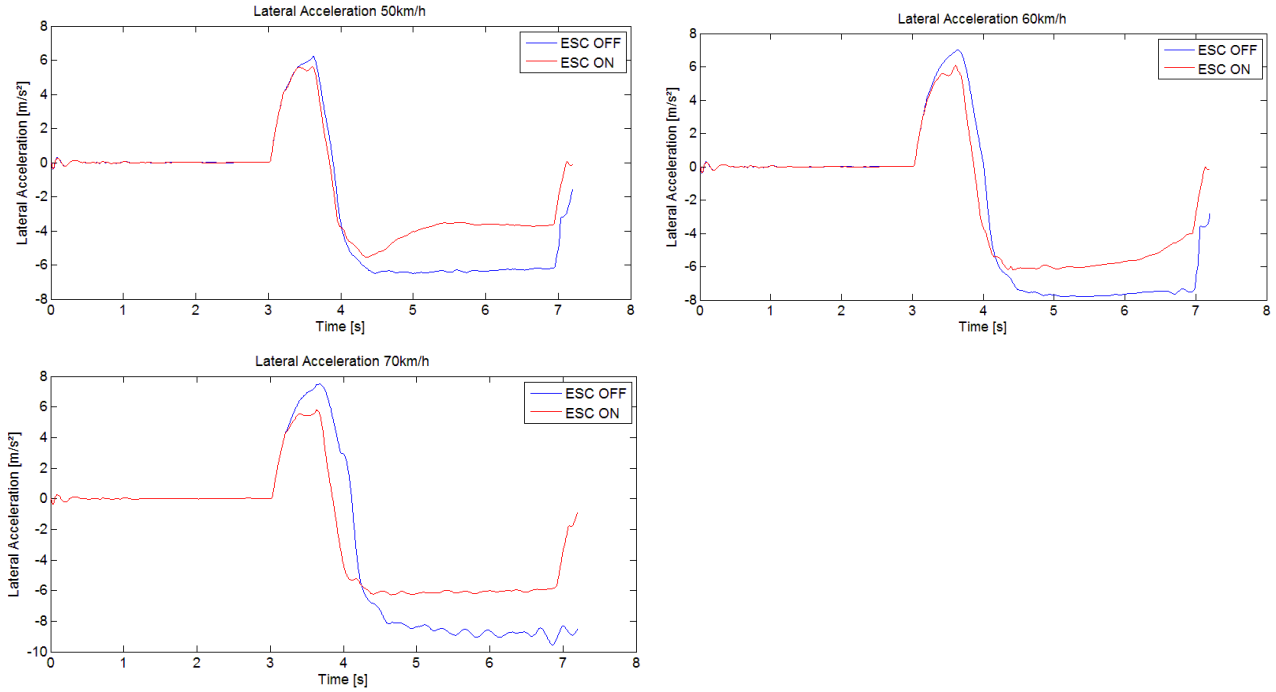

Figure 52 - Fishhook test lateral accelerations

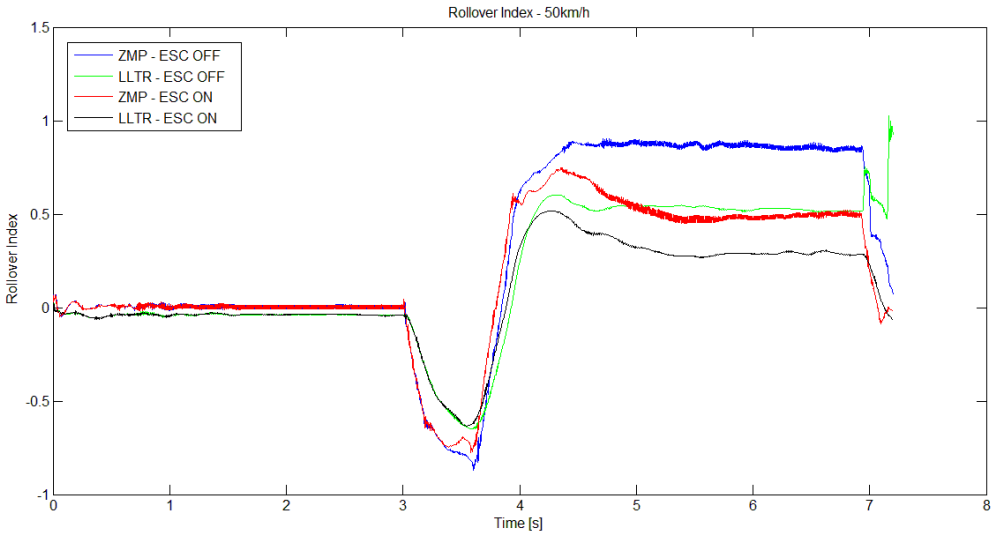

Figure 53 - RI for fishhook at 50 km/h

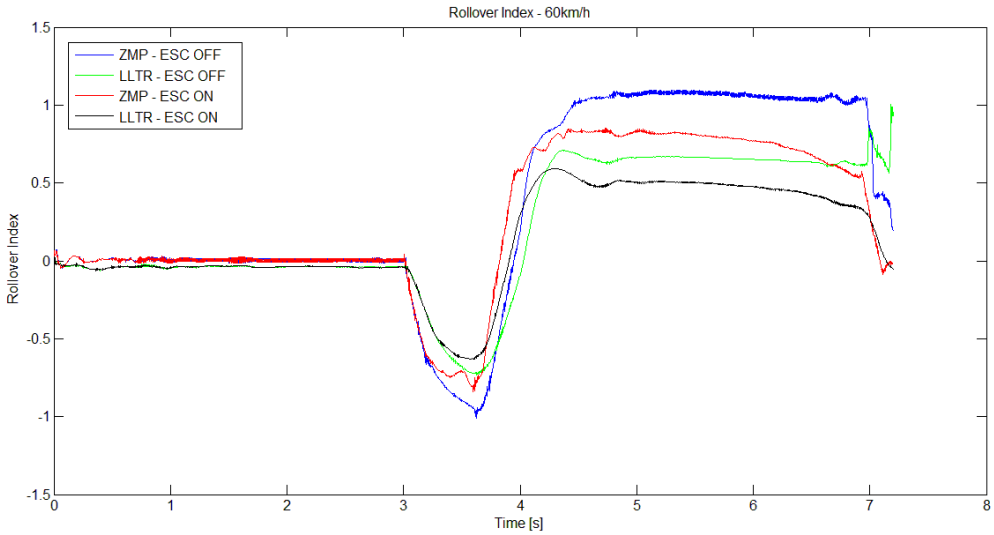

Figure 54 - RI for fishhook at 60 km/h

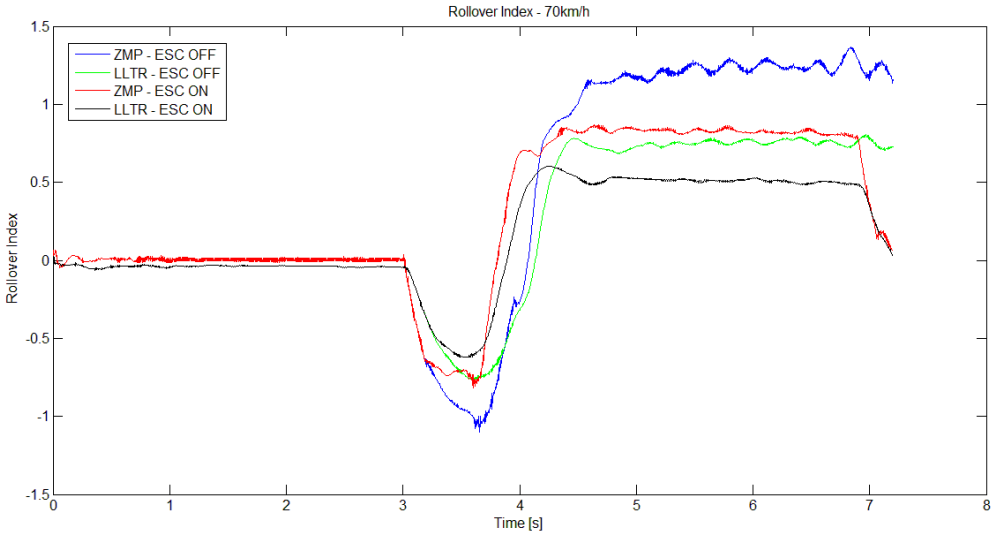

Figure 55 - RI for fishhook at 70 km/h

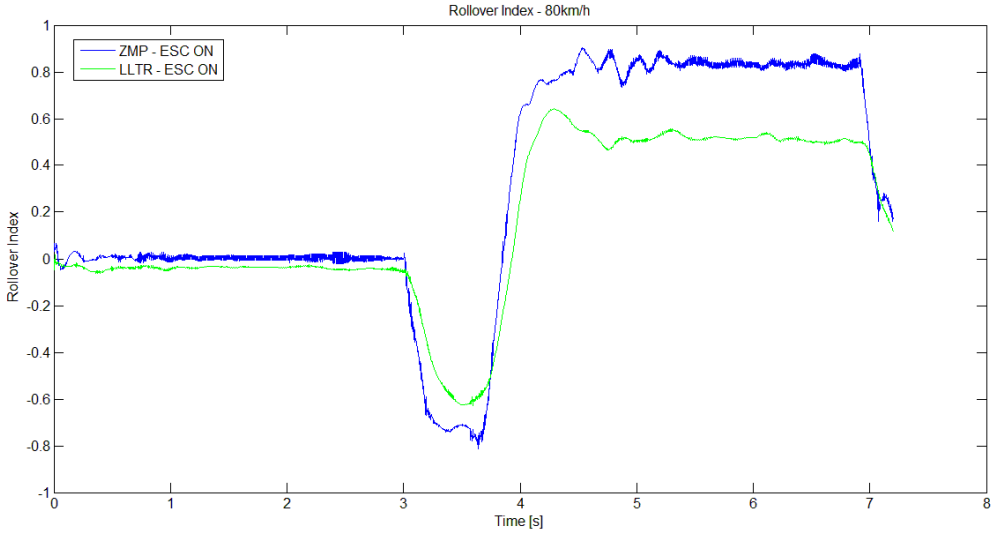

Figure 56 - RI for fishhook at 80km/h

The rollover index figures show how the ESC+RP system reduces the rollover risk in each instance. The system is triggered when the rollover index exceeds the threshold of 0.5. The system allowed the vehicle to enter the fishhook manoeuver at up to 80km/h without rollover, whereas in the non-ESC+RP case the vehicle rolled over. It is also noted that the zero moment point based rollover index is much more sensitive than the lateral load transfer ratio method. What is significant is that the gradient at which the ZMP rollover index grows is much more than the LLTR rollover index. This will allow for earlier detection of an impending rollover.

The effect of the ESC+RP system on the tyre normal loads at a 70km/h entry speed is shown in Figure 57. It can be seen that the reduced lateral accelerations have reduced the load transfer and large loads can be seen on the inner wheels during both parts of the fishhook manoeuver.

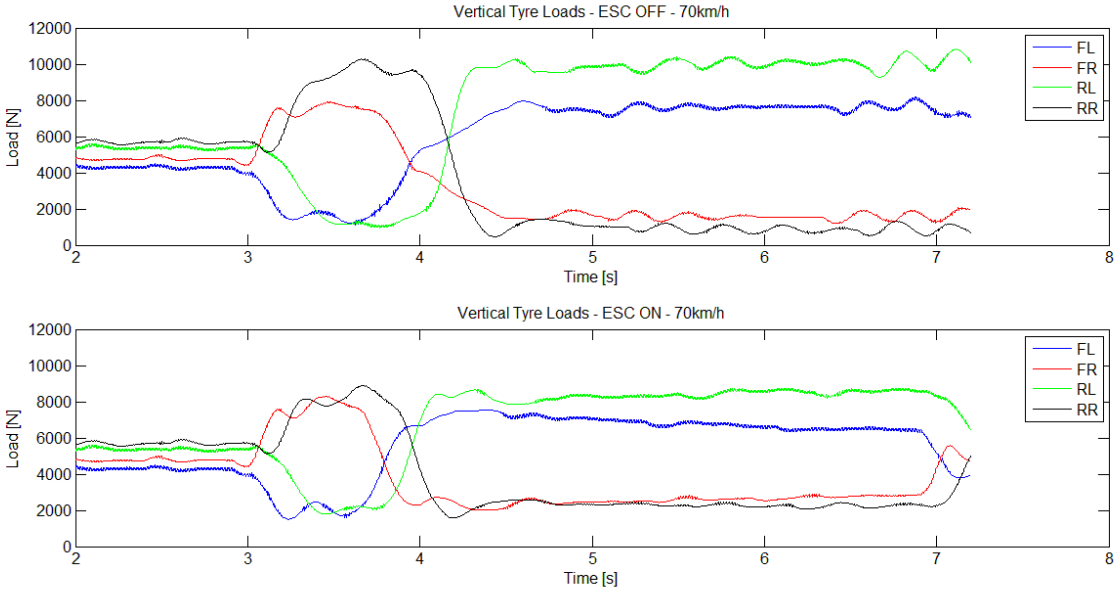

Figure 57 - Tyre normal loads for fishhook at 70 km/h

The vehicle yaw rates at a 70km/h entry speed are shown in Figure 58. The desired yaw rate is calculated from factors such as speed, steering angle and slip angles as described in section 4.2.4. The desired yaw rate is not an absolute measure and varies whenever one of these contributors changes. The desired yaw rate in the non-ESC+RP case becomes quite erratic as the slip angles reach the limits of grip of the tyre. Before the rollover index is exceeded for the first time, both the desired as well as the actual yaw rates of the ESC+RP on and ESC+RP off cases are identical. The system then intervenes and immediately reduces the yaw rate to follow the desired rate. It is evident from the results that yaw rate of the ESC+RP on case has managed to follow the desired yaw rate fairly well.

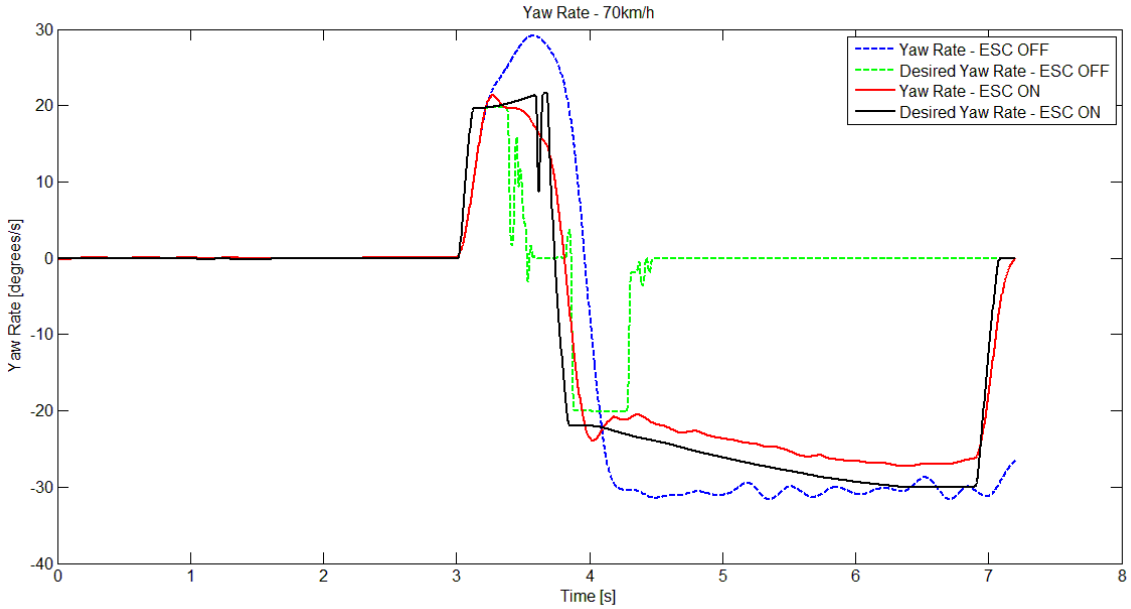

Figure 58 - Yaw rates for fishhook at 70 km/h

The brake pressures generated by the intervention of the ESC+RP system for the 70km/h entry speed case are shown in Figure 59. The desired brake pressures calculated by the control system as well as the simulation generated brake pressures are shown.

The ESC+RP system first starts generating brake pressure to reduce the yaw rate as it approaches the desired value. This is during the left hand turn of the fishhook path and the higher brake pressures produced on the right hand side of the vehicle aims to reduce the yaw rate. During the second phase of the manoeuver the left hand side is initially braked more heavily and the yaw rate overshoot corrected. The pressure on the left hand side gradually reduces to maintain the yaw rate closer to the desired rate. The right hand side brake pressures are limited due to limited grip available from the tyres. This evident from Figure 57 where it is seen that the normal load on the right hand side tyres are quite low and settles to a fairly steady value.

Figure 60 also compares the vehicle speeds during the manoeuver for the 70km/h entry speed case. Even though the vehicle enters at 70km/h, the ESC+RP system brings it down to an eventual safer 44km/h.

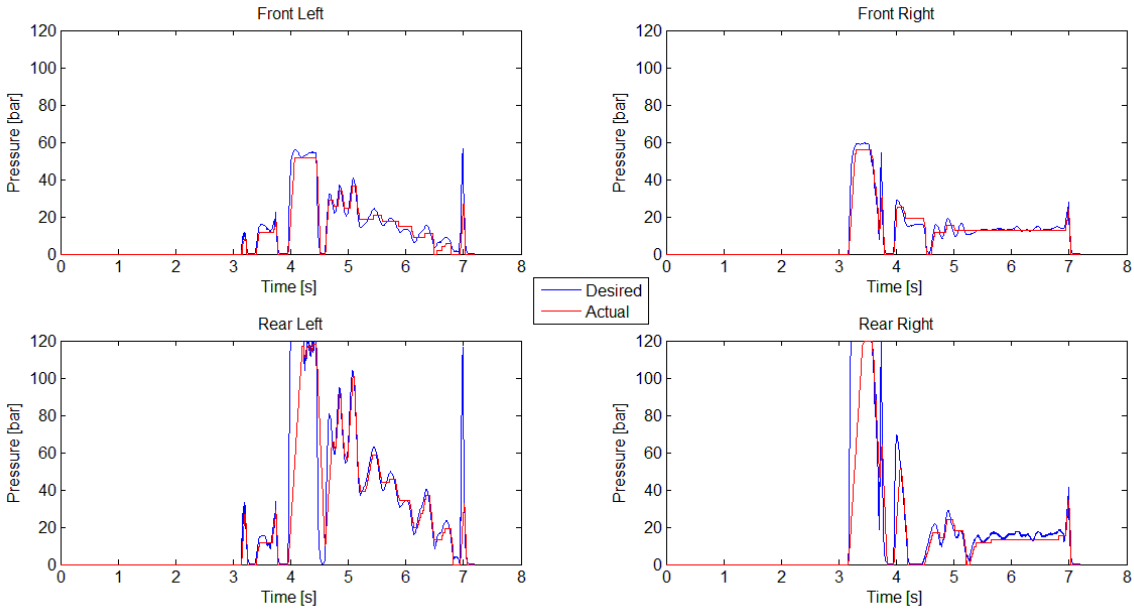

Figure 59 - Brake pressures for fishhook at 70 km/h

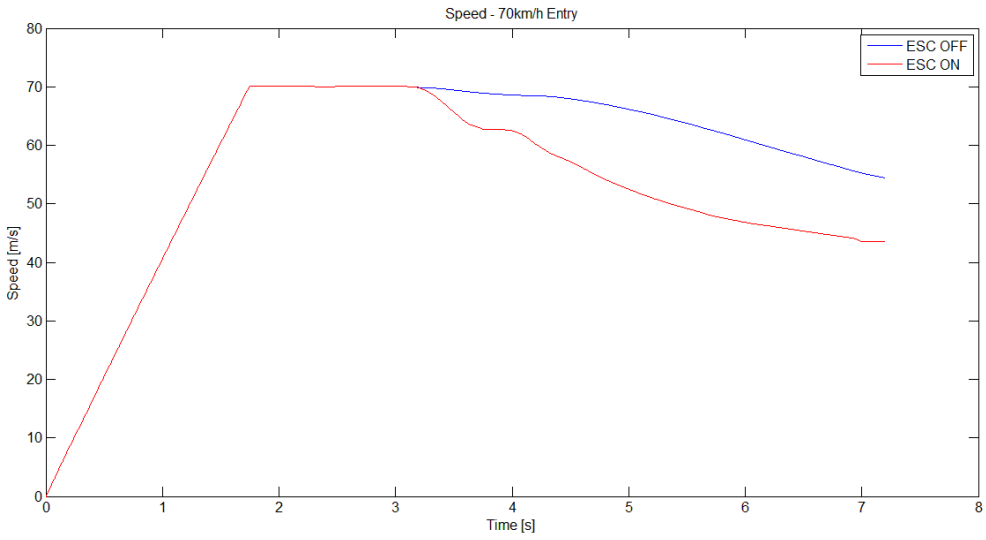

Figure 60 - Vehicle speed for fishhook at entry of 70 km/h

7. Experimental Results

The development and testing of the braking based rollover prevention system in the simulation environment has shown successful results. The system was shown to reduce the rollover propensity of the vehicle significantly as well as improve yaw rate tracking.

The hardware and software required for implementation on the Land Rover Defender test vehicle was prepared and testing conducted at the Gerotek Test Facilities (Gerotek Test Facilities, 2015). The Straight Track at the facility was used to perform the ISO 3888-1 double lane change and ISO 3888-2 obstacle avoidance tests. Experimental testing was conducted to validate the simulations and prove the effectiveness of the system in real world dynamic manoeuvers.

The tests conducted include the following, all conducted with the $4S_4$ suspension set to the handling mode with stiff springs and dampers at the front and rear:

- Double lane change – ESC+RP off – Speeds between 60km/h and 85km/h
- Double lane change – ESC+RP on – Speeds between 68km/h and 85km/h
- Obstacle avoidance – ESC+RP off – Speeds between 40km/h and 60km/h
- Obstacle avoidance – ESC+RP on– Speeds between 40km/h and 60km/h

The $4S_4$ suspension system was also set to stiff springs and damper on the rear and soft springs and dampers on the front and the following tests conducted:

- Obstacle avoidance – ESC+RP off – Speeds of 50km/h and 60km/h
- Obstacle avoidance – ESC+RP on – Speeds of 50km/h and 60km/h

7.1 Double Lane Change

The DLCs with the ESC+RP system off was performed as a baseline comparison. The 60 km/h DLC was found to not exceed the rollover index of 0.5 and does not trigger the ESC+RP system. The DLCs at 68, 77 and 85 km/h entry speeds with the ESC+RP system on are therefore compared to the baseline runs. The 85km/h DLC results are discussed here, while the 68km/h and 77km/h results are shown in Appendix A.

7.1.1 Double Lane Change – 85km/h

Figure 61 shows the ZMP based rollover index for the 85 km/h double lane change. The rollover index threshold for the ESC+RP-on case was exceeded at initial turn-in, at the exit of the second lane and at entry to the final lane. In each instance the peak following the ESC+RP activation was lower than the non-ESC+RP case. The inflection points in the vehicle yaw rate can be seen in Figure 62 at the times where the ESC+RP system was activated. These results are later analysed in more detail

and compared to simulation results. During both runs the vehicle's recorded paths are shown to be within the prescribed lanes, as indicated in Figure 63.

Figure 64 shows the steering inputs, lateral acceleration, roll angle, roll rate and vehicle speed data. The amplitude of the steering inputs for both cases was quite comparable. A counter-steering correction is noted before entry into the final lane, although a correction is also visible for the non-ESC+RP case. There are no other clear indications of steering reaction to the ESC+RP intervention. An important characteristic of a successful vehicle control system is its ability to match the driver's instinct. The change of the vehicle dynamics changes the driver's reactions. The system should therefor act in a way that does not invoke a response from the driver that may result in a loss of control over the vehicle.

As for the RI, the lateral acceleration roll angles and roll rates were generally lower in the ESC+RP-on case. The braking intervention reduced the vehicle speed and exited the manoeuver at about 64 km/h.

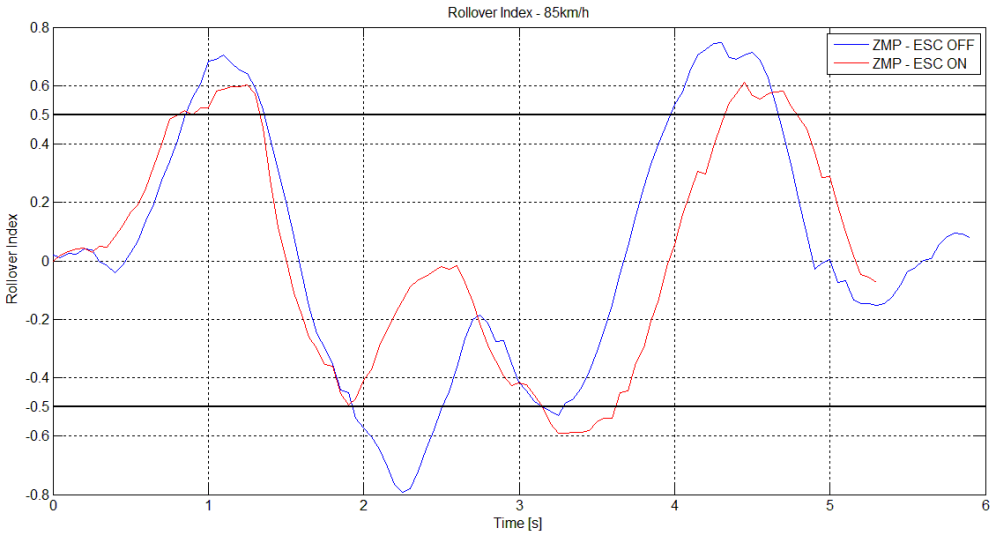

Figure 61 - RI for DLC at 85 km/h

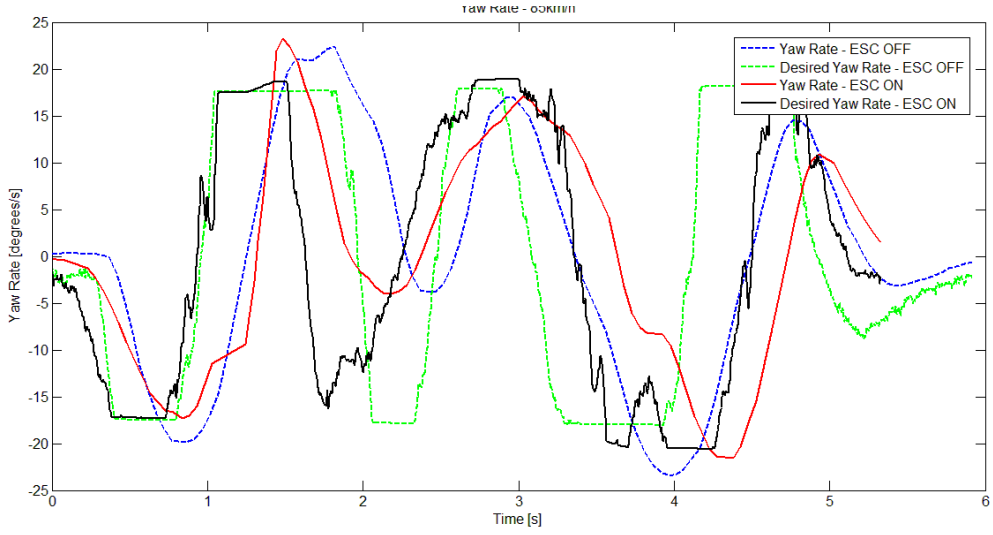

Figure 62 - Yaw rates for DLC at 85 km/h

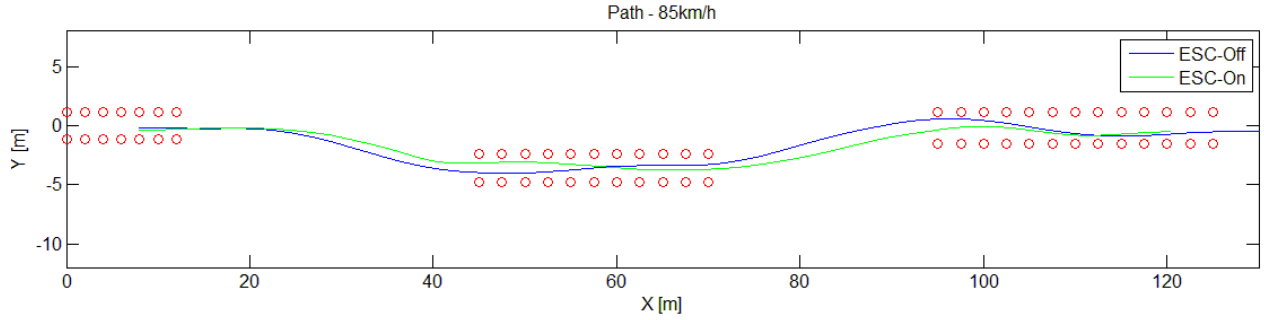

Figure 63 - Paths for DLC at 85 km/h

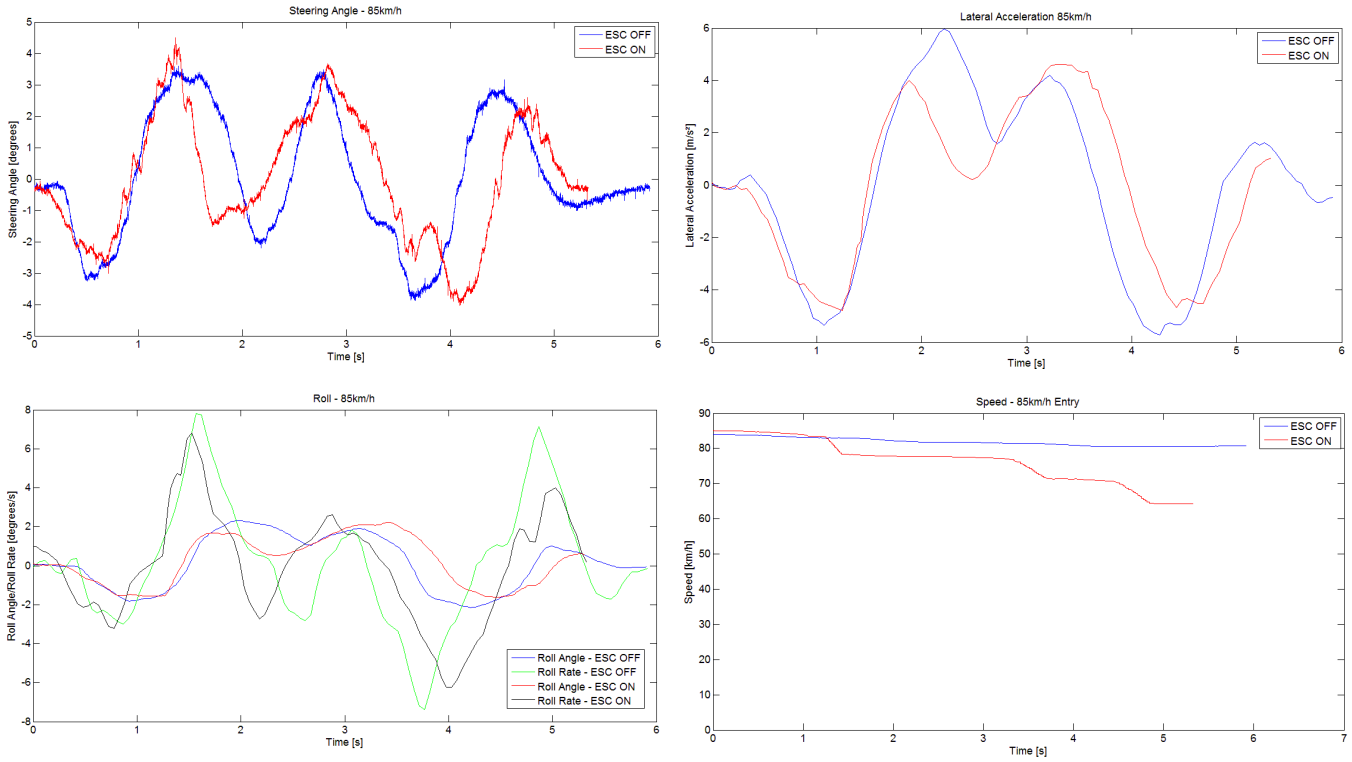

Figure 64 - Steering, lateral acceleration, roll and speed data for DLC at 85 km/h

7.2 ESC+RP Intervention - DLC at 85km/h

The 85 km/h DLC is now compared to simulation results and analysed in more depth. The steering angles recorded during the experimental tests were used as inputs to the ADAMS simulation model and some of the aspects of the control system analysed in more detail.

The steering angle measurements are taken only from the right hand side kingpin. The steering gain from the potentiometer was calibrated to capture the average front axle steering angle as accurately as possible. The Land Rover Defender has a fairly pronounced Ackerman steering effect and therefore measurements on only the one kingpin requires different gains for the different directions

of steering. None the less, the correlation between the measured and simulated data appears reasonably good.

The lateral accelerations and roll angles of the simulation and measured data shown in Figure 65 agree well, although the simulation experienced higher roll rates. Figure 66 shows that the simulation achieved slightly higher rollover index peaks and has an additional ESC+RP activation at the entry to the second lane of the DLC.

The yaw rate as well as the desired yaw rate agrees quite well between the measured and simulation data. The additional early ESC+RP trigger of the simulation model has caused braking of the vehicle and we see the additional drop in speed shown in Figure 68.

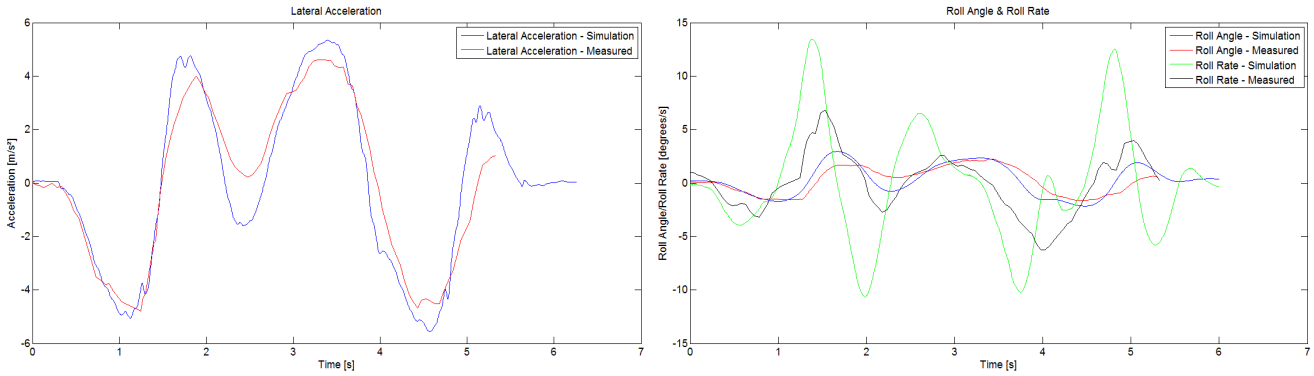

Figure 65 - Lateral acceleration and roll data for DLC at 85 km/h

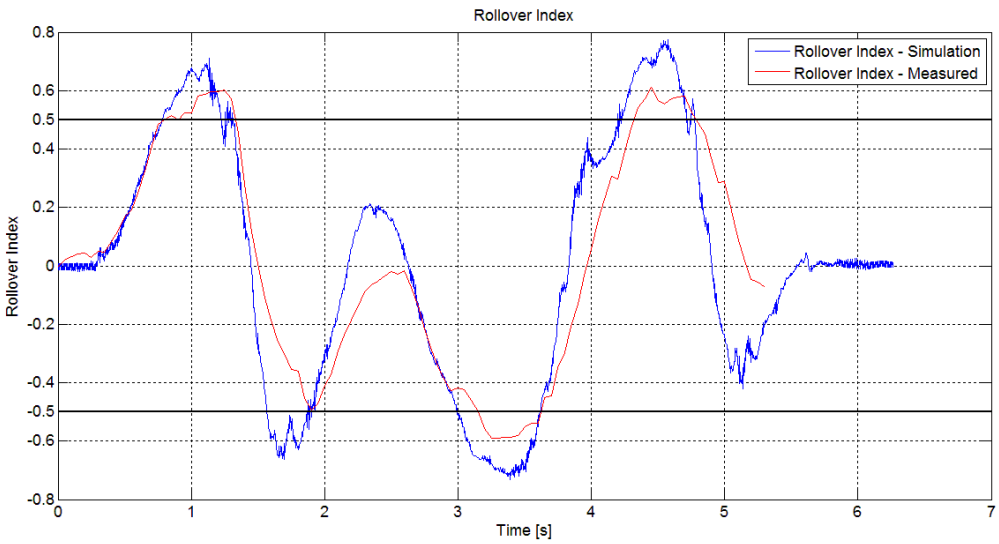

Figure 66 - RI for DLC at 85 km/h

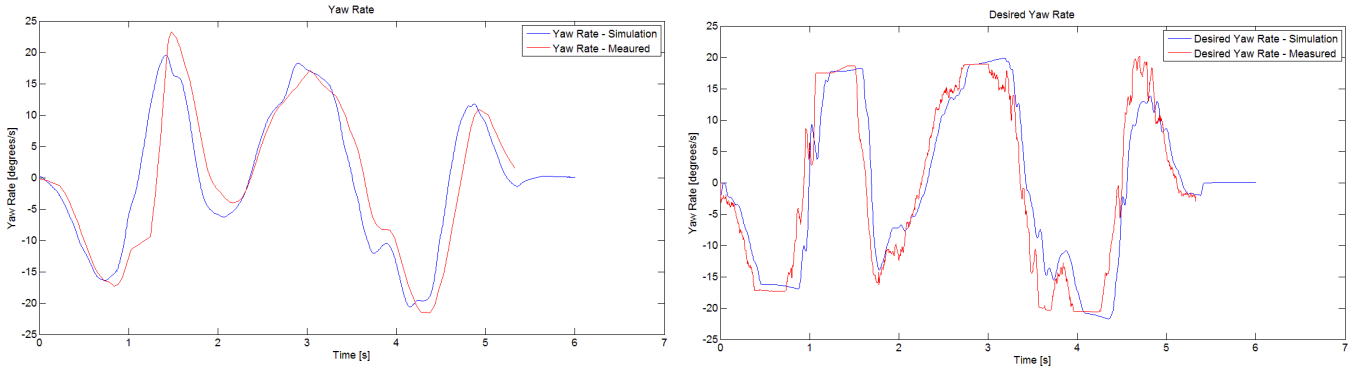

Figure 67 - Yaw rate and desired yaw rate for DLC at 85 km/h

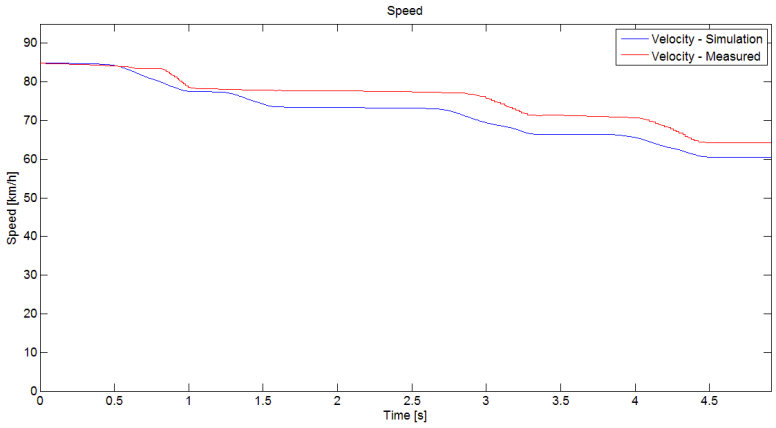

Figure 68 - Speed profiles for DLC at entry of 85 km/h

To gain more insight into the ESC+RP system's response during the dynamic manoeuver, the individual wheel brake pressures are also investigated. Figure 69 to Figure 72 indicate the comparison between the desired and measured brake pressures of the simulation and the actual vehicle.

Looking at the data taken from the test vehicle, there are three main ESC+RP activations of noticeable duration. The first activation produced larger brake pressures on the left of the vehicle in order to reduce the yaw rate as required by the desired yaw rate shown in Figure 73 that also indicates the activation zones. The second main activation around 3.2s favoured the right hand side during the left hand turn and the opposite for the third activation during the right hand turn back into the final lane of the DLC. In all three cases the desired yaw rate required the yaw rate of the vehicle to be reduced and the braking applied accordingly.

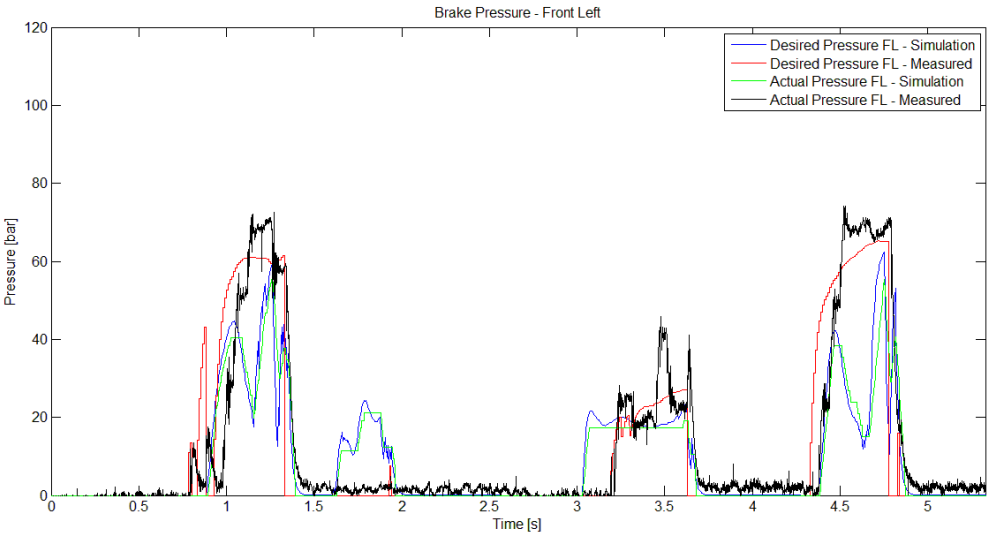

Figure 69 - Brake pressures - front left – 85km/h

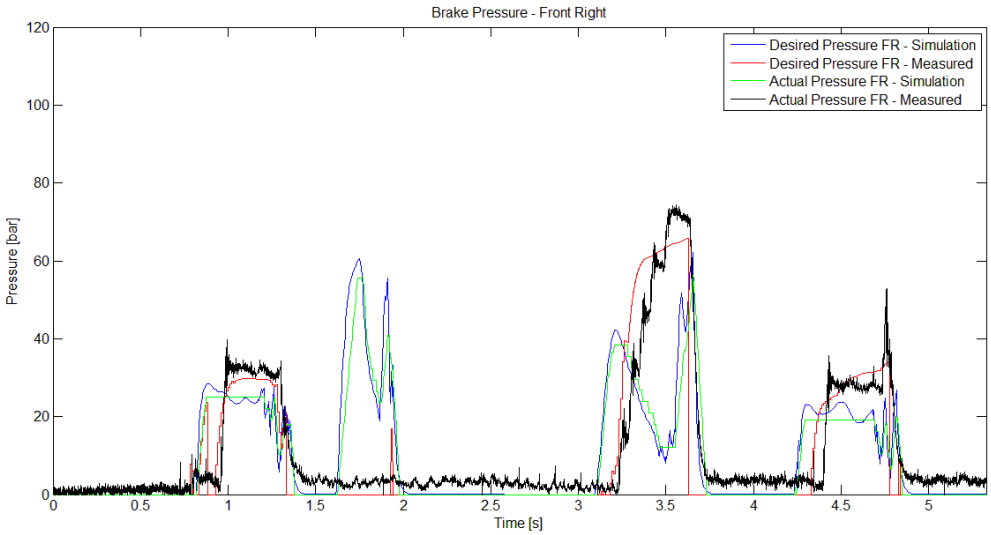

Figure 70 - Brake pressures - front right – 85 km/h

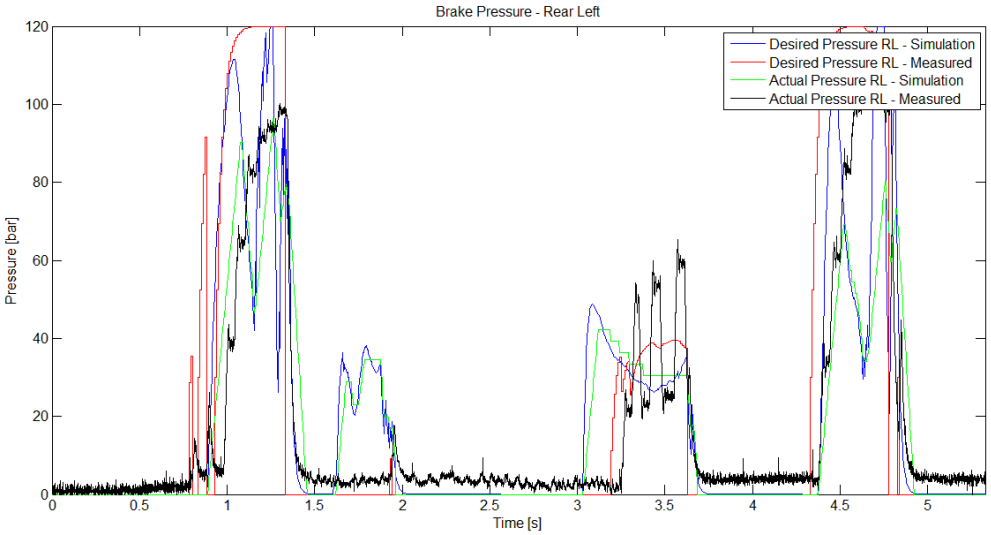

Figure 71 - Brake pressures - rear left – 85 km/h

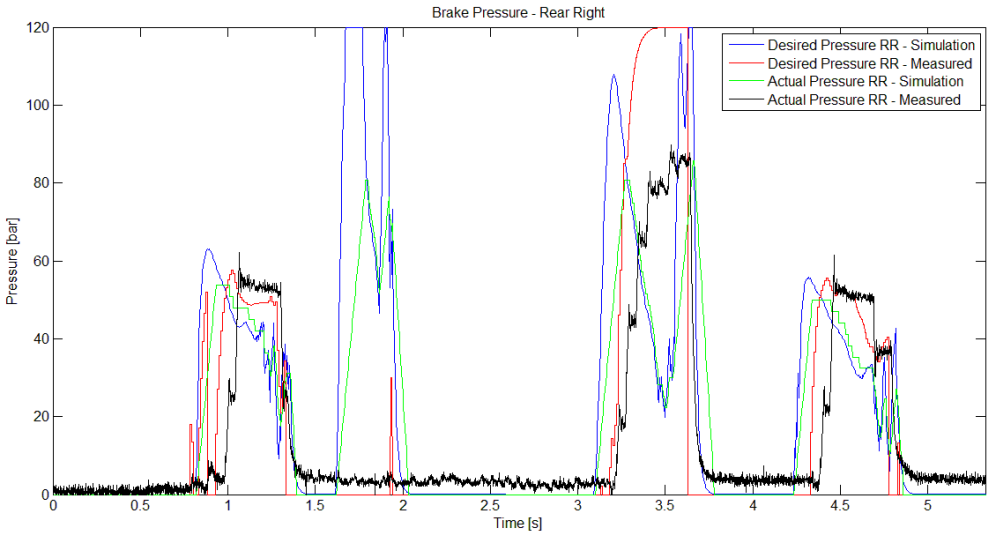

Figure 72 - Brake pressures - rear right – 85 km/h

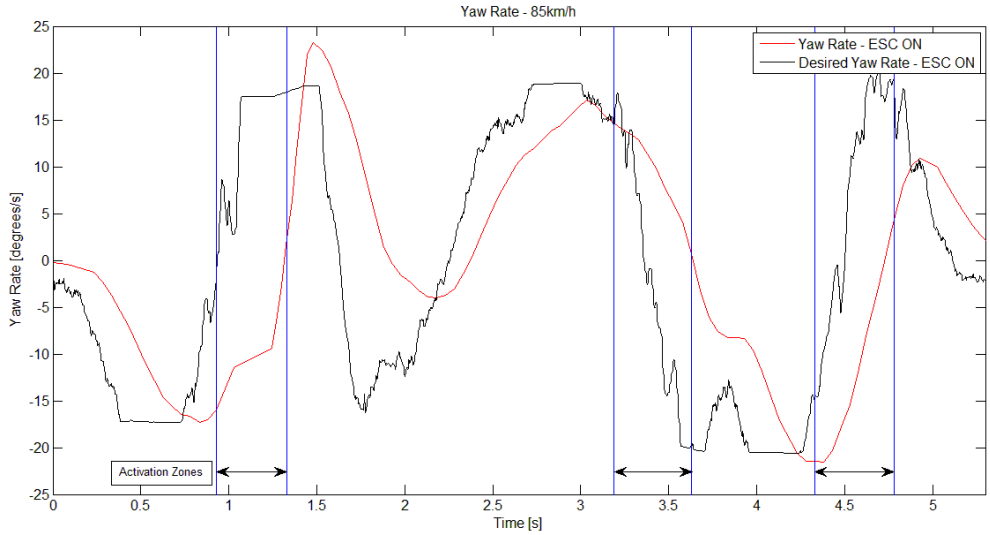

Figure 73 - Desired vs actual yaw rate – 85 km/h

Comparing the actual against the desired brake pressured measured on the vehicle, it is seen that the rate at which the pressure increases tends to be less than what is typically desired. The pump-hold pressure increase approach used increases the pressure more gradually whereas the desired pressure is often a very rapid increase. The desired rate does not take any subjective effects such as a feeling of "unsettling" the vehicle, into account. The system merely reacts to what is required from the desired yaw rate. Whether it would be more beneficial to ramp at the desired brake pressures slower or to allow more rapid actual pressure increases would require further investigation and testing. The former might lead to a perceived more stable vehicle whilst the latter might be more beneficial from a rollover safety point of view due to more aggressive intervention from the ESC+RP system.

Table 7 provides a summary of the accuracy of the actual brake pressures against the desired values. The measures shown are the percentage relative error of the total braking force generated per activation period. The largest errors are experienced at the rear where the required pressures are generally higher.

Table 7 - Percentage relative error - desired vs actual brake pressure

	% Relative Error			
Channel	**Activation 1**	**Activation 2**	**Activation 3**	**Total**
Front Left	-14.09	4.10	-9.24	-11.18
Front Right	8.38	-12.98	-11.03	-9.13
Rear Left	-40.00	-10.06	-35.12	-35.55
Rear Right	-12.61	-40.80	-15.76	-30.28

The brake pressures generated by the ESC+RP system during simulation, show similar trends to the measured results. As mentioned there was an additional activation in the simulation due to the slightly higher rollover index. The magnitudes and duration of the ESC+RP activations compare fairy well, although the exact profiles are obviously very sensitive to the error between measured and desired yaw rate. The higher sampling rate of the simulation compared to the fairly low 20 Hz from the IMU recordings also leads to more noise and possible definition in the simulated desired brake pressure profiles.

7.3 Obstacle Avoidance Test

The ISO 3888-1 double lane change test is generally used as a test of the handling capabilities of a vehicle. The manoeuver consist of two sets of steering inputs although the time spent passing through the second lane allows the dynamics of the vehicle to settle briefly. The modified ISO 3888-2 obstacle avoidance test (OA) does not feature this long second lane and allows the vehicle to spend more time in dynamic states. The results of the effectiveness of the ESC+RP system to intervene when the rollover index threshold is exceeded, is compared to the baseline runs with the system inactive. The initial runs at 40 km/h entry speeds did not produce any intervention from the ESC+RP system and only the results for the 50 km/h and 60 km/h cases are shown.

The 60km/h OA results for both suspension settings are discussed here, while the 50km/h test results are shown in Appendix A.

7.3.1 Obstacle Avoidance – 60 km/h

At a 60 km/h entry speed, very high rollover indices are recorded. Figure 74 indicates the non ESC+RP case peaks at a critical RI of about 1 during the transition through the second lane. The system will already be triggered at the initial turn-in and the intervention brings the rollover index down to below 0.8 with the ESC+RP system in place. The third peak in RI was almost completely avoided. The steering is reduced to a neutral position much earlier in the manoeuver, hence the

shorter data set in the plots. The vehicle reached the third lane of the path at a significantly reduced speed.

The entry speeds of the vehicles were near identical, although the initial steering inputs were quite different, making a direct comparison of yaw response more difficult. It is noted that there was a significant deviation in the yaw rate of the ESC+RP-on case when the vehicle passed through the second gate. The yaw rate was generally followed the desired yaw rate closer (Figure 75).

The baseline vehicle managed to stay within the prescribed course, although counter-steering was required to stay within the lane, indicated in Figure 77. The vehicle with the ESC+RP on arrived in the third lane of the path at a much more sedate 34 km/h.

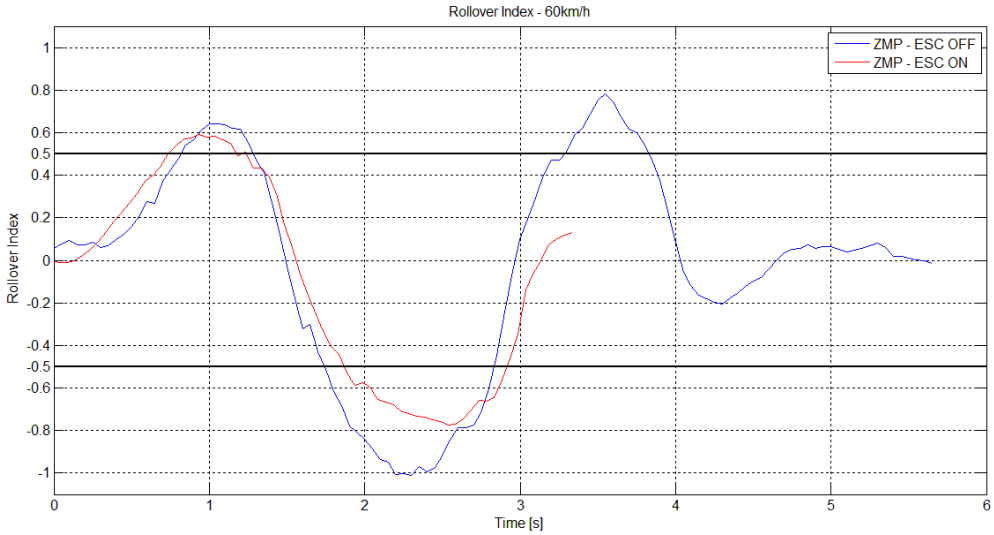

Figure 74 - RI for OA at 60 km/h

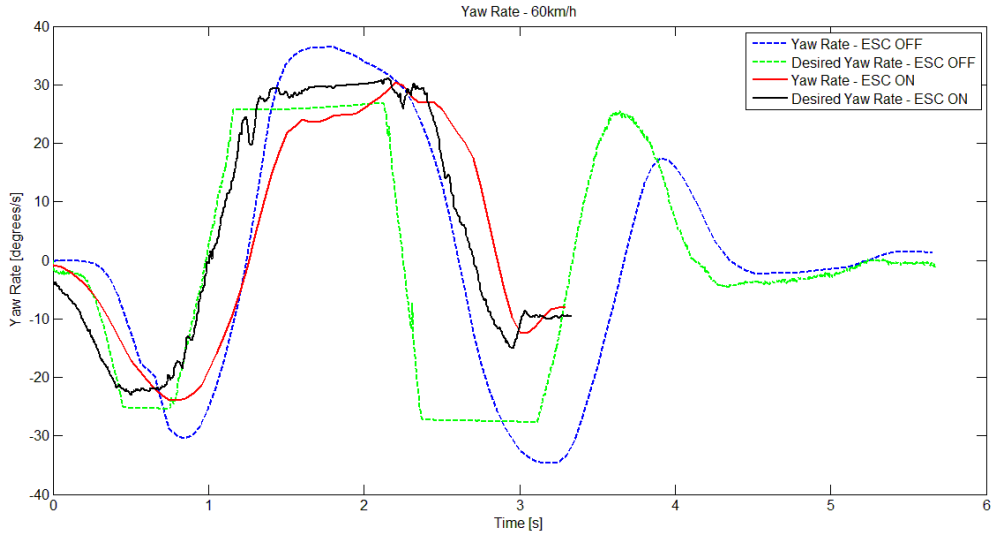

Figure 75 - Yaw rates for OA at 60 km/h

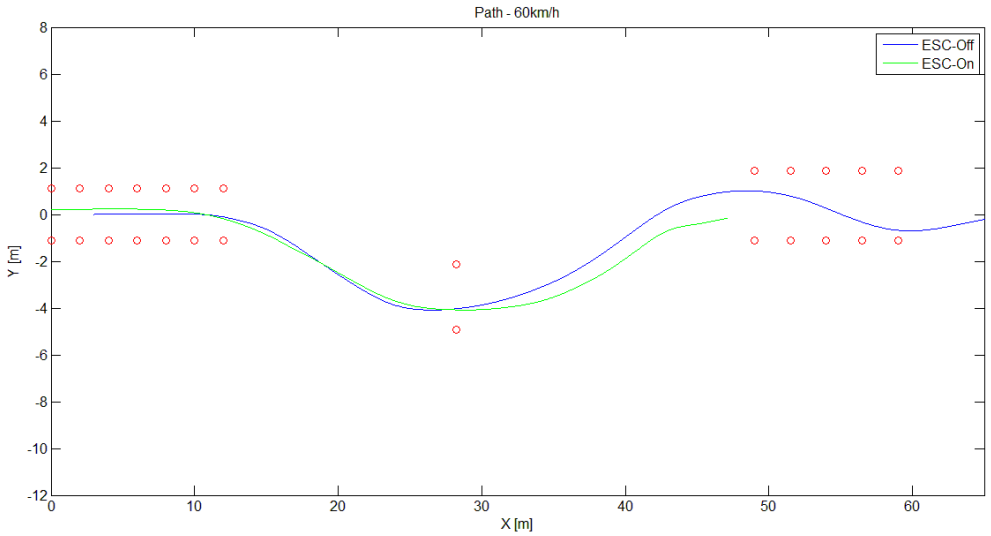

Figure 76 -Paths for OA at 60 km/h

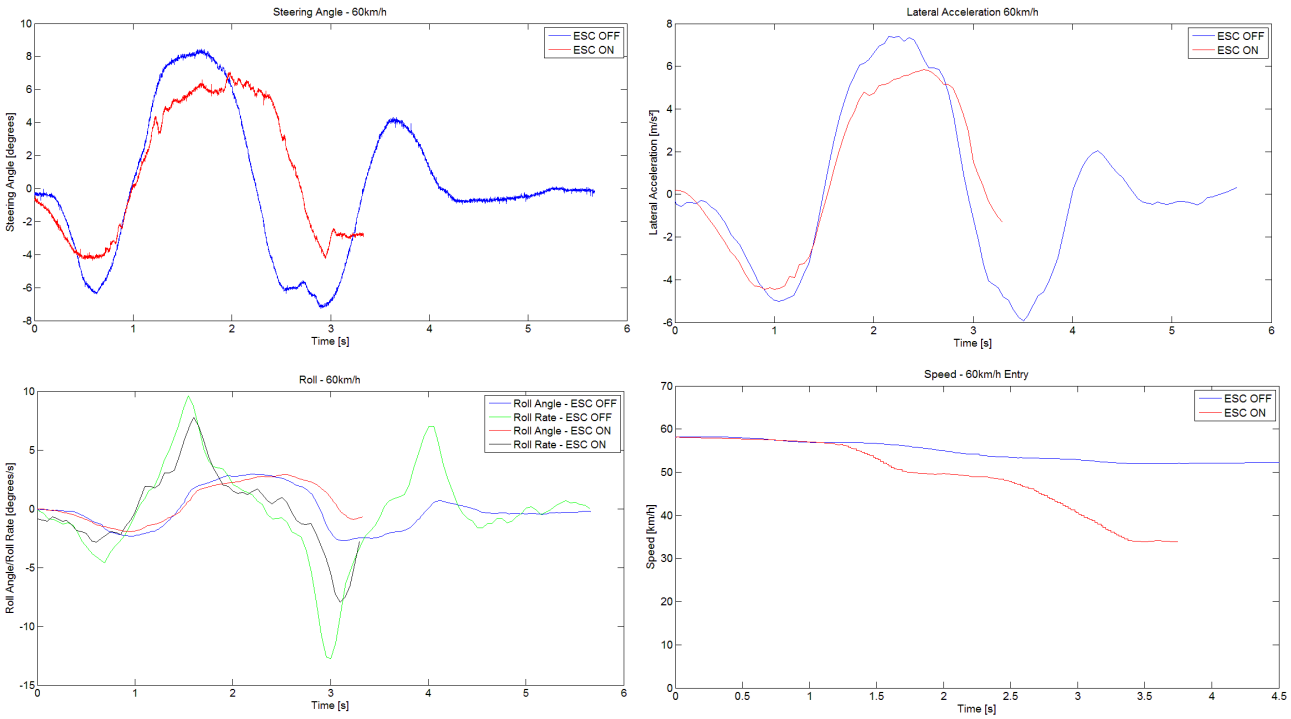

Figure 77 - Steering angle, lateral acceleration, roll and speed data for OA at 60 km/h

7.3.2 Obstacle Avoidance – 60 km/h – Rear Suspension Hard

The same runs through the obstacle avoidance course were repeated after switching the $4S_4$ suspension to a setting with soft springs and dampers at the front and stiff springs and dampers at the rear. The study of the Land Rover Defender by Els (2006) indicated that the vehicle has a natural tendency towards oversteer. The front-to-rear roll moment distribution can be manipulated by

changing the front and rear roll stiffnesses (Milliken & Milliken, 1995). The rear suspension was set to be much stiffer than the front to further provoke the oversteer tendencies of the vehicle.

The results are discussed for the obstacle avoidance test performed at 60km/h with only the rear $4S_4$ suspension on the firm setting. The initial steering inputs were very similar for the baseline and ESC+RP on runs as shown in Figure 81. The initial rollover indices for the two runs were also similar, with the ESC+RP reducing the second RI peak and nearly eliminating the third.

Similar yaw rates were initially recorded for both cases, whereas the ESC+RP system appears to have followed the desired rate much closer. The large yaw rate developed during the turn-in to the final lane of the course as well as the subsequent steering correction and associated yaw rate peak were avoided by the ESC+RP system. This steering reaction was in reaction to loss of grip of the rear tyres and rear wheel lift exhibited during testing as shown in the comparative images in Figure 82.

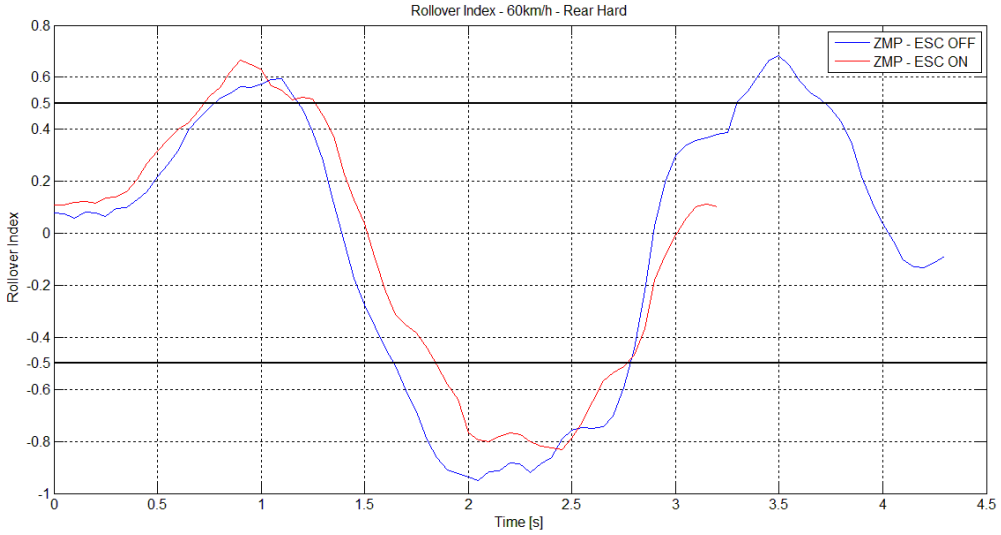

Figure 78 - RI for OA at 60 km/h - Rear suspension hard

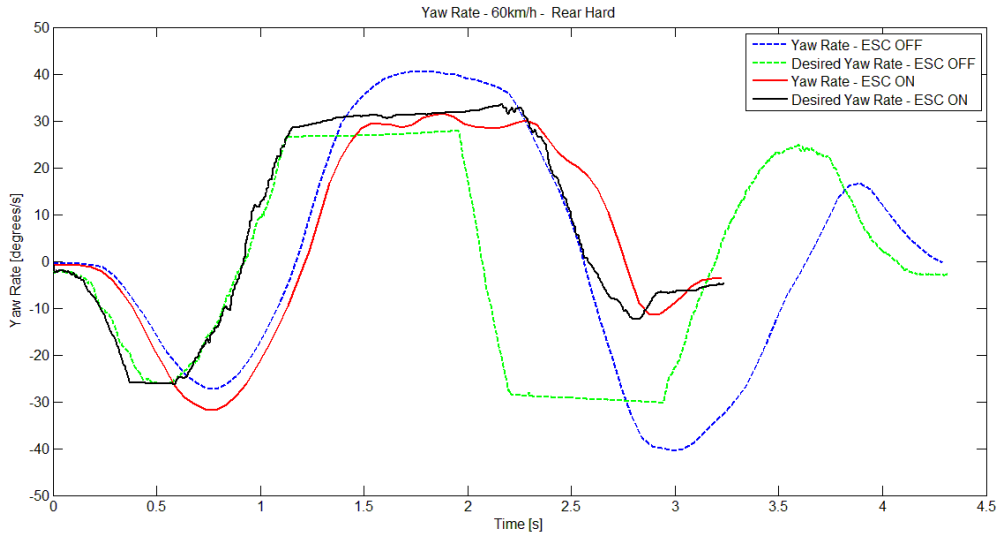

Figure 79 - Yaw rates for OA at 60 km/h - rear suspension hard

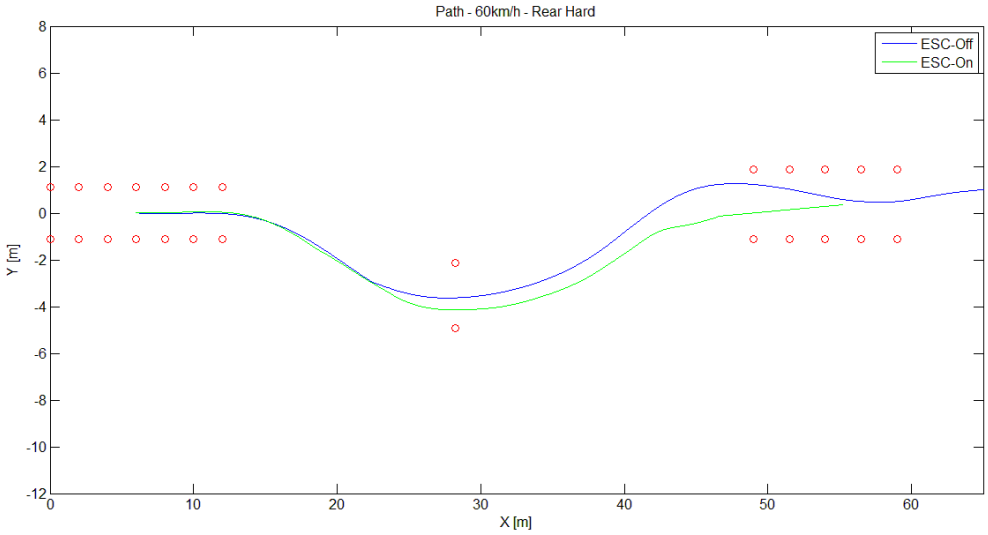

Figure 80 - Paths for OA at 60 km/h - Rear suspension hard

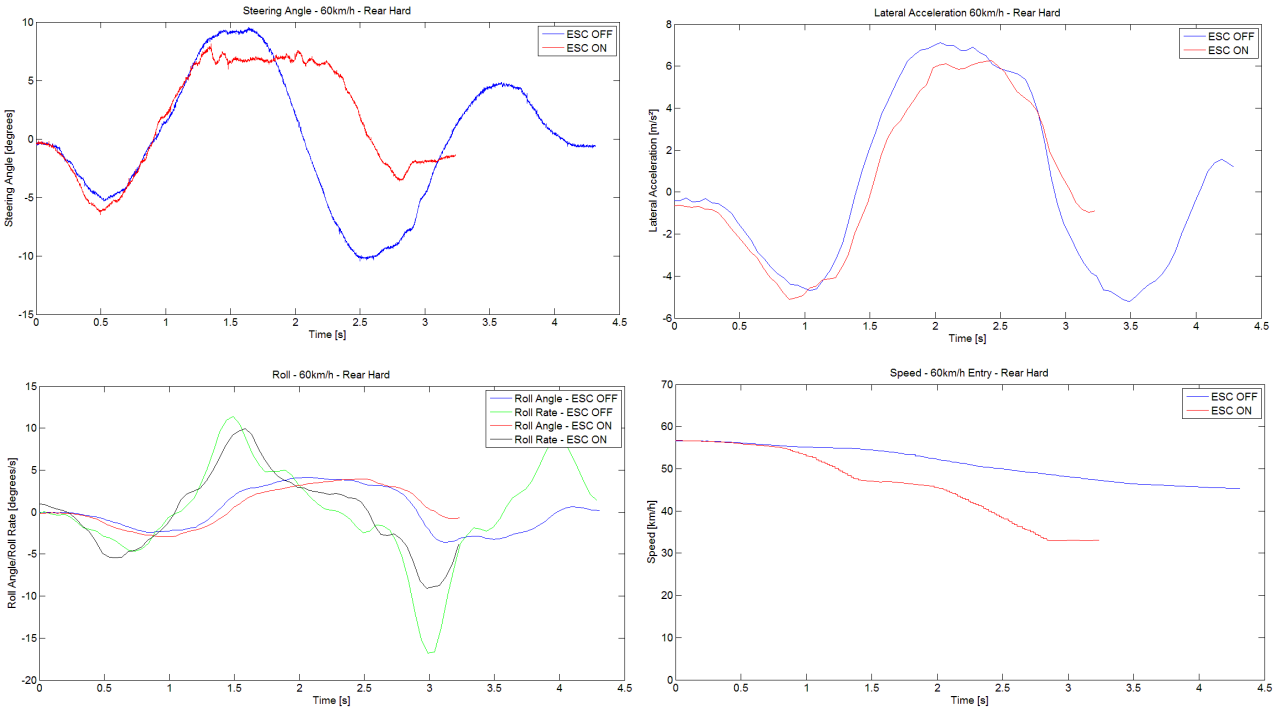

Figure 81 - Steering angle, lateral acceleration, roll and speed data for OA at 60 km/h - Rear suspension hard

The most significant effect of the ESC+RP system was the reduction in dynamics such as lateral acceleration, yaw rate and roll rate during the latter part of the manoeuver. The vehicle speed was reduced to roughly 33km/h at entry to the final lane. The test results show that the vehicle swerved for an obstacle and safely returned to its lane at a controlled speed whilst reducing the rollover risk. With the ESC+RP off the driver still had to provide significant steering inputs to maintain control over the vehicle and return to its original lane after swerving for the obstacle.

Figure 82 - ESC off (top) vs ESC on (bottom) - OA at 60km/h - Rear suspension hard

7.4 ESC+RP Intervention – Obstacle Avoidance at 60 km/h

The recorded steering angles were once again used as input to the simulation model and the results compared for the obstacle avoidance test at 60km/h with the suspension set to firm all round.

The brake pressures plots from Figure 83 to Figure 86 compared the desired and actual pressures from the measured results as well as the simulation results. The measured results from the test vehicle indicate the two main activations during the manoeuver. The first activation favoured the

left hand side of the vehicle during the initial right hand turn. This aims to reduce the yaw rate as required. The activation zones are shown in the yaw rate plot in Figure 87.

The second activation during the left hand turn through the gate first raised the brake pressures on the left hand side before the pressures on the right became dominant. This leads to an initial increase in yaw rate as required and then forcing a reduction in yaw rate.

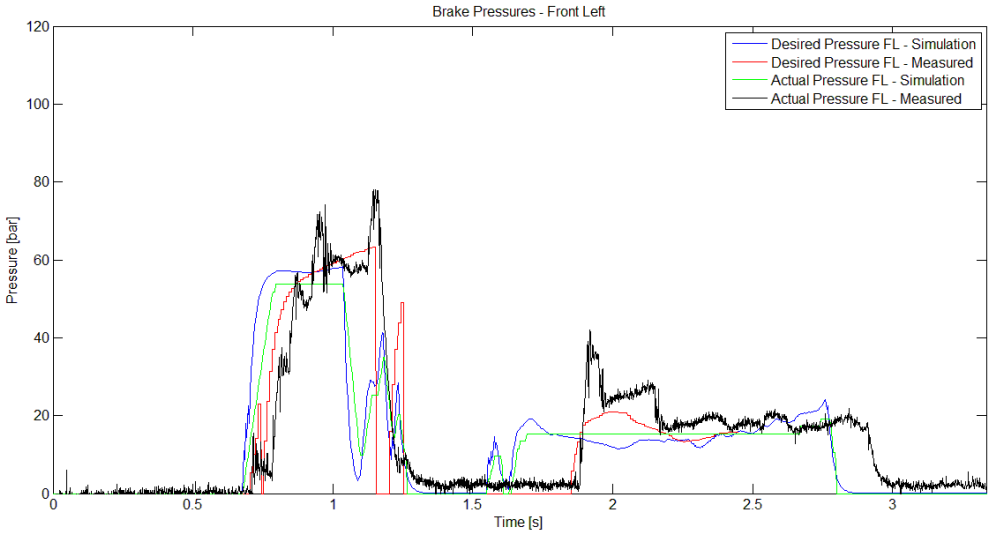

Figure 83 - Brake pressures - front left – 60 km/h

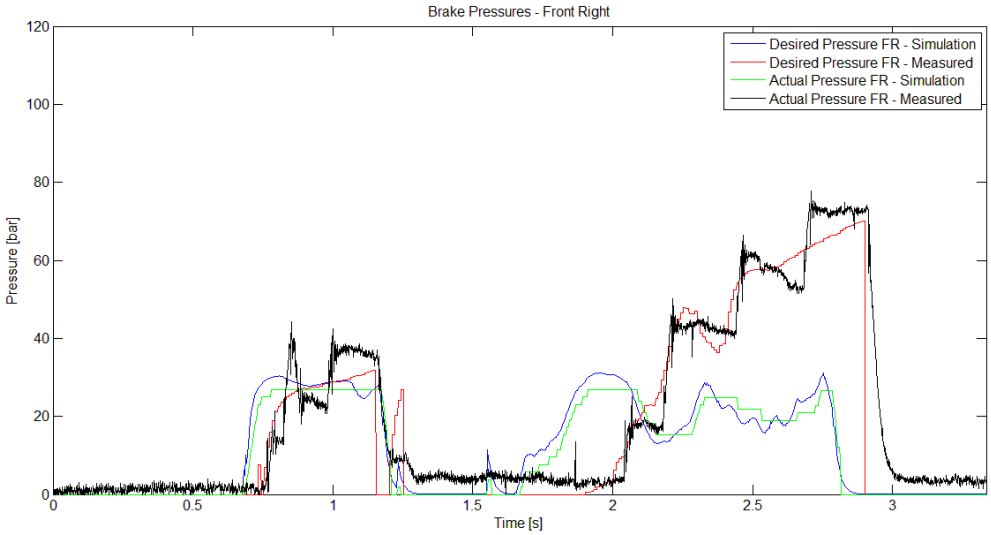

Figure 84 - Brake pressures - front right – 60 km/h

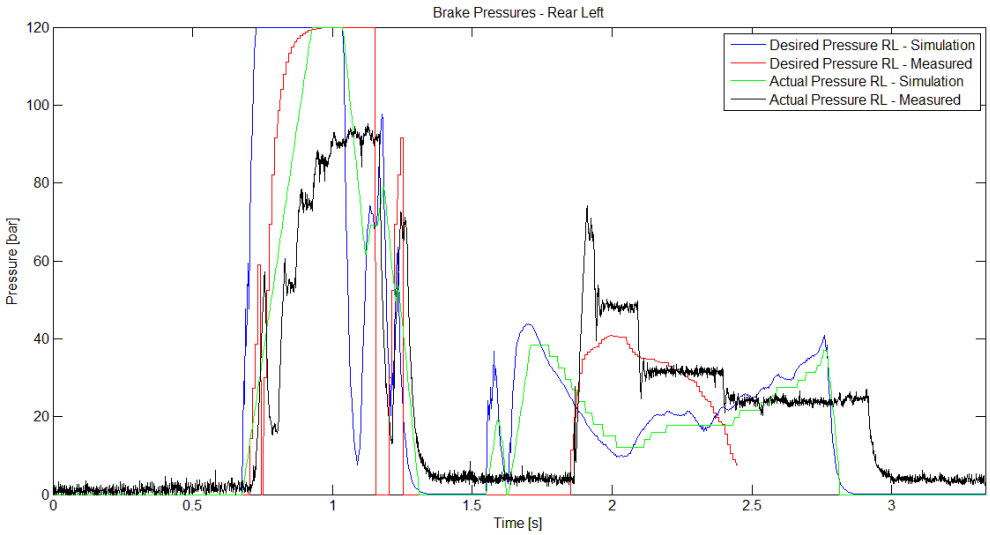

Figure 85 - Brake pressures - rear left – 60 km/h

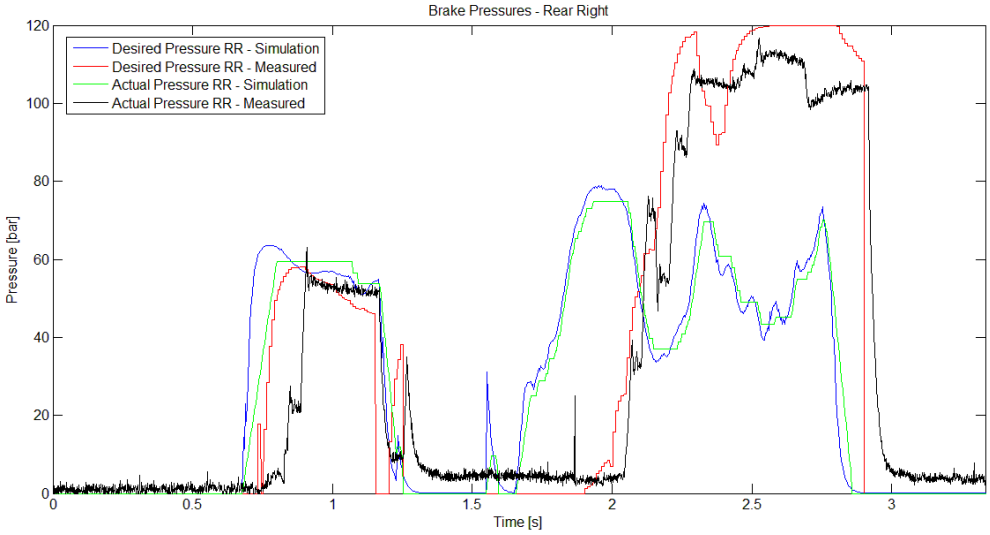

Figure 86 - Brake pressures - rear right – 60 km/h

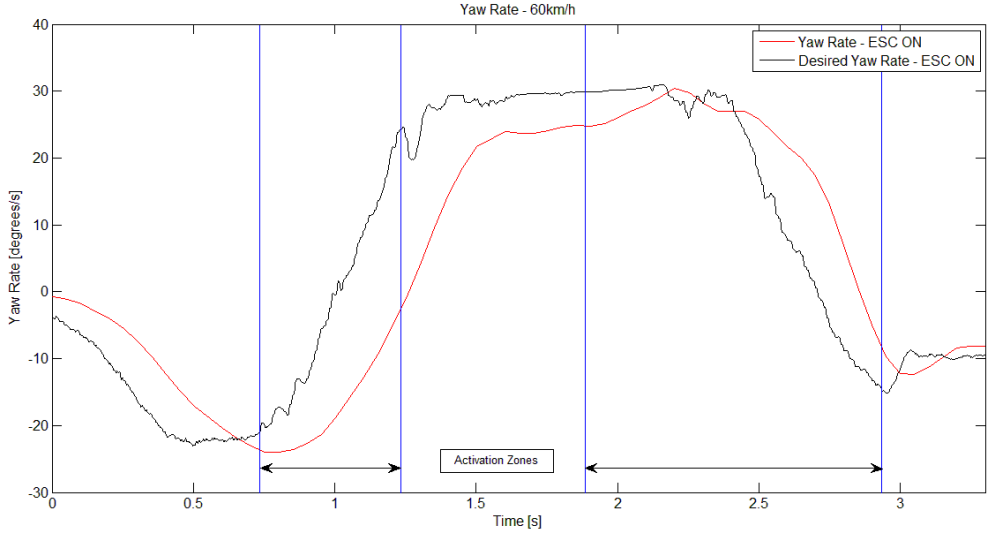

Figure 87 - Desired vs actual yaw rate - OA at 60 km/h

Table 8 provides a summary of the accuracy of the actual brake pressures against the desired values. The measures shown are the percentage relative error of the total braking force generated in the two main activation periods. The total error includes the smaller activations.

The errors seen are generally quite small with the largest errors on the left hand side. The initial activation on the rear left didn't manage to reach the desired pressure for an unknown reason. There are also areas at the end of the second activations on the left hand side where data appears to be missing. This is suspected to only be an unknown data processing error and not an algorithm error, as the simulation results indicate a similar pressure profile.

Table 8 - Percentage relative error - Desired vs actual brake pressures

	% Relative Error		
Channel	**Activation 1**	**Activation 2**	**Total**
Front Left	-7.95	22.89	**1.83**
Front Right	5.38	0.53	**0.44**
Rear Left	-34.66	51.41	**-8.80**
Rear Right	-23.84	-10.80	**-13.94**

The comparative simulation results for the lateral accelerations, roll angle, roll rate, rollover index, yaw rates and vehicle speeds are shown in Figure 88, Figure 89, Figure 90 and Figure 91. The results compare fairly well for the initial part of the manoeuver although a phase shift develops. As mentioned before, this is likely due to the sensitivity of the analysis to the steering angle calibration. The phase shift explains the difference in brake pressure profiles for the second activation, whereas the first correlate quite well to the measured data. The initial velocity profile is subsequently followed very well.

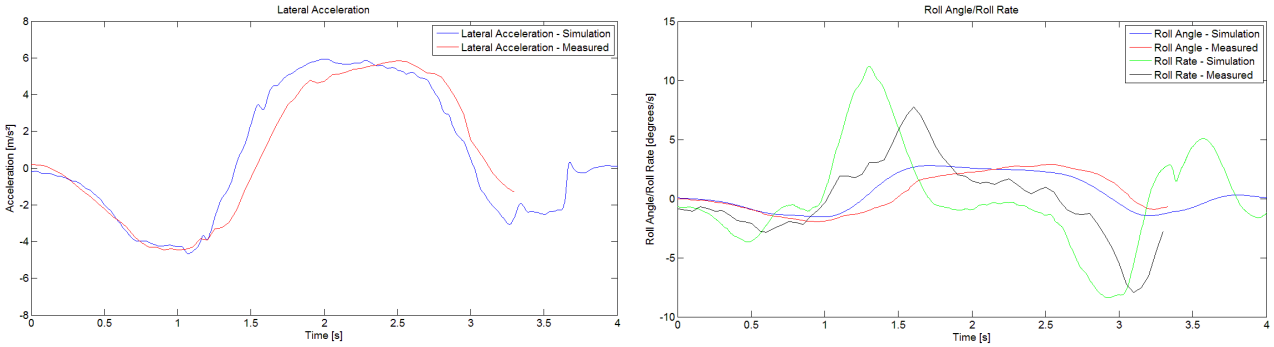

Figure 88 - Lateral acceleration and roll data - 60km/h

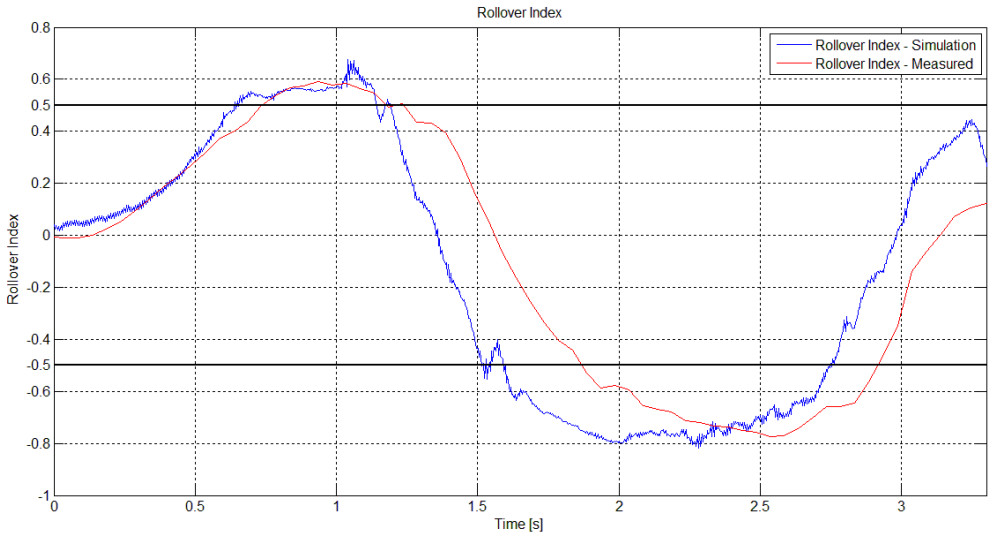

Figure 89 - RI for OA at 60 km/h

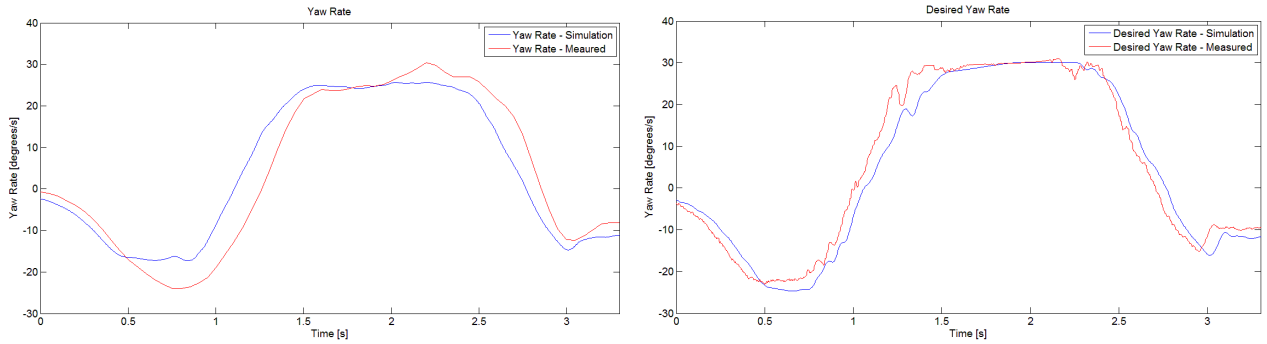

Figure 90 - Yaw rate and desired yaw rate for OA at 60km/h

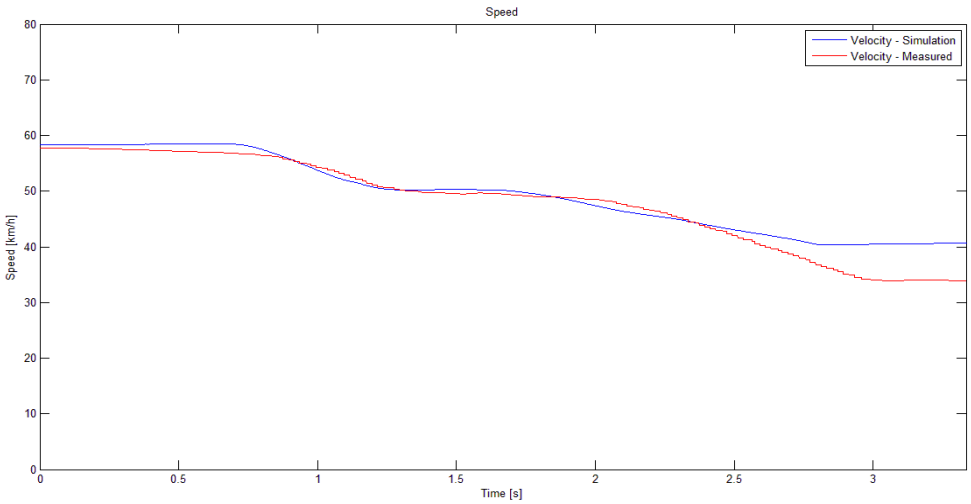

Figure 91 - Speed profiles for OA at entry of 60 km/h

7.5 Summary – ESC+RP Results

In section 6.2 and 6.3 the results from implementing the ESC+RP rollover prevention algorithm in the ADAMS simulation were shown to be very successful in reducing the rollover propensity of the vehicle, whilst maintaining path following and stability. The same ESC+RP system was then tested on the Land Rover Defender test vehicle as described in section 7.1 to 7.4. The variability in steering input often made it difficult to compare results objectively although the effect on the rollover indices and yaw rates mostly show the desired outcomes.

A summary of the achieved rollover indices are shown in Figure 92. Each column pair is the absolute values of the peaks in the rollover index graph for the particular manoeuver.

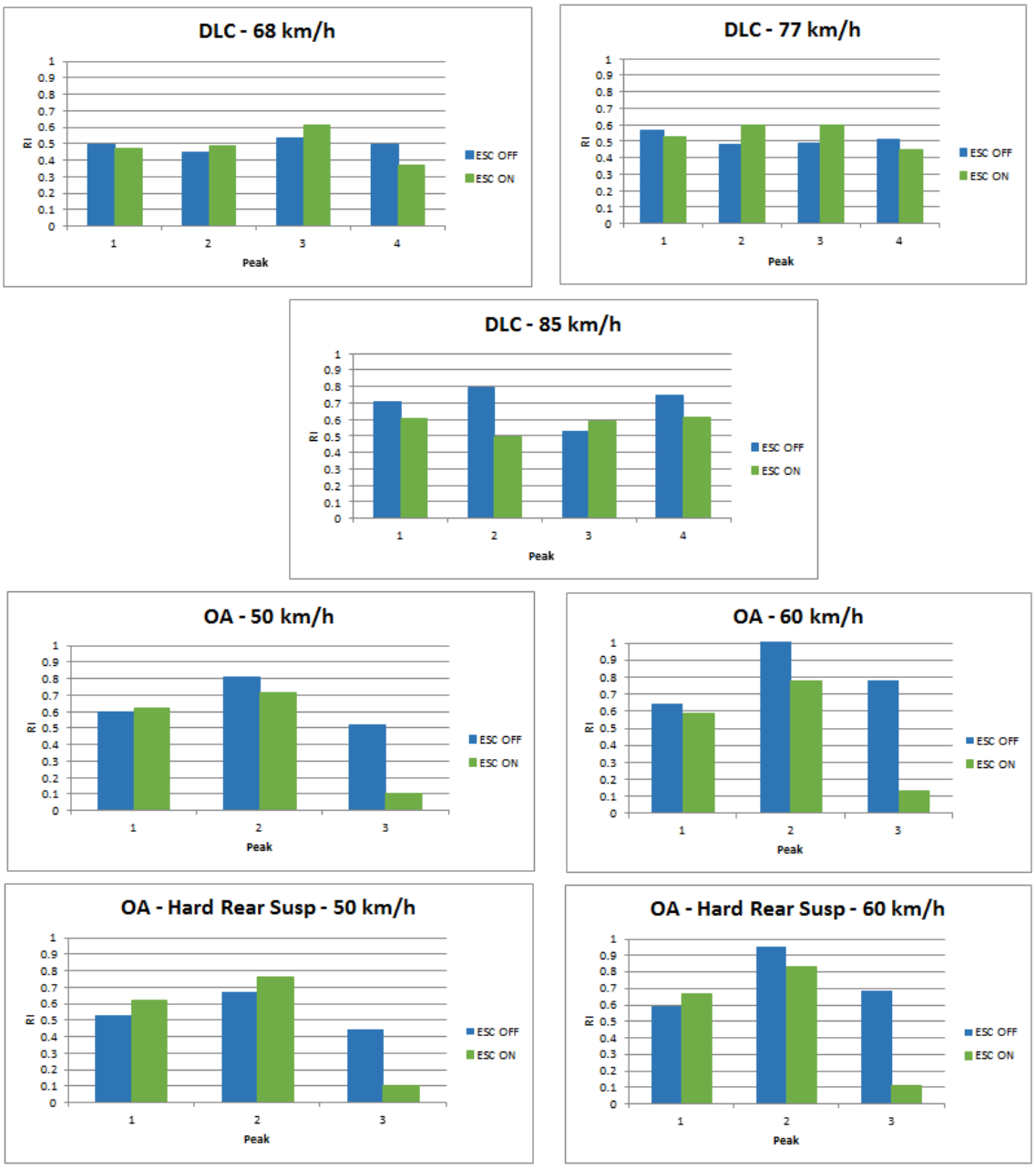

Figure 92 - RI comparison - ESC On vs ESC Off

The graphs illustrate the effect of the ESC+RP system on the RI for different speeds and manoeuvers. At first inspection it appears as if the system did not consistently reduce the RI, although the reasons for this are discussed further by taking the data from Table 9 into account. What is evident is the fact that the final peak in the manoeuver was reduced in each instance. The OA manoeuver produced much higher RI than the DLCs although the ESC+RP system drastically reduced the final RI peaks.

The RI peaks for the higher speed manoeuvers were in general most significantly reduced. For the 85 km/h DLC the 2nd and 4th peaks, which are the steering correcting peaks, the RI peaks were reduced. This is also evident in the 2nd and 3rd peaks for the 50 km/h, as well as both 60 km/h OA manoeuver cases. This observation is significant when it is considered that rollovers are most likely to occur during the steering correction phase, as previously indicated in Figure 16.

Table 9 summarises the experimental results for the rollover index improvements achieved by the ESC+RP system. The table shows the RMS of the rollover index reduced for 4 of the 7 manoeuvers. The first two manoeuvers in the table shows higher average rollover indices and higher peaks on two occasions each. For both these cases the total ESC+RP activation time was less than 1 second and the average steering input was also higher than when the ESC+RP was on. These higher steering inputs lead to larger lateral accelerations and therefore higher rollover indices.

The 50 km/h obstacle avoidance test with the rear suspension hard also showed a higher average rollover index. The third peak of the RI was however dramatically reduced. The higher initial rollover indices could also have been a result of the higher steering inputs.

For each case the final peak of the RI, that occurs when the vehicle returns to the initial lane after the lane change, has been reduced significantly.

Table 9 - RI percentage change - ESC On vs ESC Off

				RI		RI Peak Change				Steering RMS [deg]		Total Activation Time [s]
				RMS		1	2	3	4			
DLC	68 km/h	ESC	OFF	0.28	9%	-5%	9%	16%	-25%	1.407	19%	
			ON	0.30						1.680		0.35
	77 km/h	ESC	OFF	0.30	18%	-7%	24%	23%	-13%	1.438	38%	
			ON	0.36						1.984		0.91
	85 km/h	ESC	OFF	0.43	-11%	-15%	-38%	12%	-18%	2.083	-7%	
			ON	0.38						1.936		1.4
OA	50 km/h	ESC	OFF	0.45	-1%	4%	-11%	-81%		4.630	9%	
			ON	0.45						5.061		1.15
	60 km/h	ESC	OFF	0.49	-8%	-8%	-24%	-83%		5.152	-24%	
			ON	0.45						3.914		1.54
OA - Rear Hard	50 km/h	ESC	OFF	0.41	11%	17%	13%	-78%		3.730	22%	
			ON	0.45						4.560		1.16
	60 km/h	ESC	OFF	0.53	-7%	12%	-13%	-84%		6.156	-22%	
			ON	0.50						4.787		1.5

It can be concluded that in most instances where the steering inputs were comparable, the ESC+RP system succeeded in reducing the rollover risk of the vehicle. It is most noticeable with the obstacle avoidance test where the total activation times are generally longer and the manoeuver more severe. The system created a very large reduction in rollover risk especially during the return of the vehicle to the final lane with an up to 25% RI peak reduction in the latter part of the DLC and up to

84% RI peak reduction for the final part of the OA manoeuver. These reductions in RI were achieved without compromising the path following ability of the vehicle.

The analysis has also indicated that in each case the yaw response of the vehicle reacted to the desired yaw requirement.

8. Conclusions and Recommendations

8.1 Conclusions

An extensive literature study was conducted on the main topics of rollover detection, rollover mitigation techniques and yaw control methods. The zero-moment point (ZMP) method was selected as an accurate, versatile and easily implementable measure of the rollover threat index of a vehicle during a dynamic manoeuver. A braking based rollover system was also selected as the preferred method for intervention during impending rollover.

The results of simulations of the vehicle through the ISO 3888-1 double lane change and NHTSA fishhook manoeuvers have indicated the ESC+RP rollover prevention system developed in this report, has manged to successfully reduce the rollover risk of the vehicle and improved the yaw response of the vehicle. Experimental testing on the Land Rover Defender 110 also showed successful results. The system indicated the most successful results during the ISO 3888-2 obstacle avoidance test. This dynamic manoeuver led to large rollover indices and allowed for longer ESC+RP intervention times. The rollover threat was especially reduced during the latter part of the manoeuver. In all cases the vehicle also successfully maintained its path following ability and showed improved yaw rate tracking.

8.2 Recommendations

Through the study a few areas were identified that allows for further investigation and future improvements to the rollover prevention and yaw control system.

8.2.1 Rollover Index Characterisation

The zero-moment point rollover index proved to be a very easily implementable rollover threat metric that showed a close relationship with the lateral load transfer ratio method, albeit more sensitive and provides earlier warning. Further experimental testing with wheel force transducers fitted to each wheel of the vehicle could be beneficial in better relating the rollover index to the normal loads measured on the wheels during a dynamic manoeuver.

The rollover index could also benefit from incorporating a vehicle preview model such as developed by Linstrom (2015). The previewed metric such as lateral acceleration could benefit the rollover prevention system by allowing more predictive safety intervention.

8.2.2 Side-Slip Angle Control

It was mentioned in section 4.2.4 that the commercial ESP systems usually implement a weighted control of both desired yaw rate as well as desired slip angle. The need for slip control becomes more pronounced on lower friction surfaces, whereas the untripped rollover prevention is more applicable for high friction surfaces. The control methodology is similar for both cases and the ESC+RP system in this report can be expanded to include slip angle control. This also raises the topic of hierarchical control.

The study by Yoon, et al. (2010) also discussed the typical integrated chassis control hierarchy for a vehicle. It was shown how metrics such as rollover index, yaw rate error and slip angle error can be integrated to alter the characteristics of the ESC+RP intervention. The ESC+RP will then either give preference to rollover index reduction and yaw tracking as opposed to slip angle control and visa versa.

The implementation of slip angle control does however require an accurate slip angle estimator to be effective. This topic was briefly discussed in section 5.6.

8.2.3 Parameter Estimation

The control algorithm for the ESC+RP currently includes a few hard coded estimated parameters that are required to determine factors such as desired yaw rate and maximum available tyre grip. Both these factors require an estimation of the friction available on the road surface. Accurate estimation of the friction available on the road surface will allow more accurate control over the required braking torques.

8.2.4 Subjective – Objective Evaluation

The control algorithm of the ESC+RP system includes various parameters that are user defined and allows for the tuning of the characteristics and behaviour of the system. These factors include:

- RI threshold for ESC+RP activation can be adapted to conditions.
- Gain relationship between rollover index and desired vehicle deceleration.
- Tolerance band of sliding mode controller for both desired vehicle speed and yaw control.
- Pump-hold and dump-hold duty cycles for the low level brake pressure control.

The ESC+RP system has shown good performance with the current set of parameters, although tuning of the characteristics could be very beneficial. The primary objective of this process will be to improve the way in which the system intervention is experienced subjectively.

As important as it is for the system to reach the target quantifiable objectives such as desired rollover index and desired yaw rate, it is equally important to be as minimally unsettling to the

driver. The system intervention should be as progressive as required so as to not induce sudden steering reaction from the driver and further unsettle the vehicle. The vehicle should meet its control objectives whilst also making the driver aware that certain limits have been exceeded but then stabilise the vehicle without the driver reacting to the control inputs and fighting against it.

Bibliography

Abe, M., 2009. *Vehicle Handling Dynamics.* Oxford: Elsevier.

Blundell, M. & Harty, D., 2004. *The Multibody Systems Approach to Vehicle Dynamcis.* New York: Elsevier.

Bodie, M. O. & Hac, A., 2000. *Closed Loop Yaw Control of Vehicles Using Magneto-Rheological Dampers,* Detroit: SAE.

Bosch, 2013. *ESP Value Added Functions.* [Online]
Available at: http://www.bosch-automotivetechnology.com/
[Accessed 12 11 2013].

Botha, T. R., 2011. *High Speed Autonomous Off-Road Vehicle Steering,* Pretoria: University of Pretoria.

Budynas, R. G. & Nisbett, J. K., 2008. *Shigley's Mechanical Engineering Design 8th Edition.* Singapore: McGraw Hill.

Cao, J., Jing, L., Guo, K. & Yu, F., 2013. Study on Integrated Control of Vehicle Yaw and Rollover Stability Using Nonlinear Prediction Model. *Mathematical Problems in Engineering.*

Carlson, C. R. & Gerdes, J. C., 2003. *Optimal Rollover Prevention with Steer by Wire and Differential Braking.* Washington, ASME International.

Cheli, F., Sabbioni, E., Pesce, M. & Melzi, S., 2007. A methodology for vehicle sideslip angle identification: comparison with experimental data. *Vehicle System Dynamics,* 45(6), pp. 549-563.

Chen, B. C. & Peng, H., 1999. *A Real-time Rollover Threat Index for Sport Utility Vehicles.* San Diego, s.n.

Chen, B. C. & Peng, H., 2010. Differential-Braking-Based Rollover Prevention for Sport Utility Vehicles with Human-in-the-loop Evaluations. *International Journal of Vehicle Mechanics and Mobility.*

Cosin Scientific Software, 2015. *Cosin.* [Online]
Available at: https://www.cosin.eu/prod_FTire
[Accessed 9 September 2015].

Cronjé, P. H., 2008. *Improving off-road vehicle handling using an active anti-roll bar,* Pretoria: University of Pretoria.

Els, P. S., 2006. *The Ride Comfort vs. Handling Compromise for Off-Road Vehicles,* Pretoria: University of Pretoria.

Forkenbrock, G. J., Elsasser, D. & O'Harra, B., 2005. *NHTSA's Light Vehicle Handling and ESC Effectiveness Research Program,* s.l.: National Highway Traffic Safety Administration.

Forkenbrock, G. J., O'Harra, B. C. & Elsasser, D., 2004. *A Demonstration of the Dynamic Tests Developed for NHTSA's NCAP Rollover Rating System - Phase VIII of NHTSA's Light Vehicle Rollover Research Program,* Washington: National Highway Traffic Safety Administration.

Gerotek Test Facilities, 2015. *Gerotek Test Facilities.* [Online]
Available at: http://www.armscordi.com/SubSites/Gerotek1/Gerotek01_landing.asp
[Accessed 24 November 2015].

Gillespie, T. D., 1992. *Fundamentals of Vehicle Dynamics.* Warrandale: SAE International.

Hac, A., 2002a. Influence of Active Chassis Systems on Vehicle Propensity to Maneuver-Induced Rollovers. *Vehicle Dynamics and Simulation.*

Hac, A., 2002b. Rollover Stability Index Including Effects of Suspension Design. *Vehicle Dynamics and Simulation.*

Hac, A., Brown, T. & Martens, J., 2004. Detection of Vehicle Rollover. *Vehicle Dynamics & Simulation.*

Heyring, C., 1995. USA, Patent No. US5447332 A.

International Organisation for Standarisation, 1999. *International Standard ISO 3888-1: Passanger cars - Test track for severe lane-change manoeuver - Part 1: Double lane-change,* s.l.: ISO 3888-1:1999.

International Organisation for Standarisation, 2011. *International Standard ISO 3888-2: Passanger cars - Test track for severe lane-change manoeuver - Part 2: Obstacle avoicance,* s.l.: ISO 3888-2:2011.

Lapapong, S., 2010. *Vehicle Rollover Prediction for Banked Surfaces,* University Park: Pennsylvania State University.

Linstrom, B. V., 2015. *Real-time Non-linear Vehicle Preview Model,* Pretoria: University of Pretoria.

Li, Y. et al., 2013. Effect of vertical and lateral coupling between tyre and road on vehicle rollover. *Journal of Vehicle Mechanics and Mobility.*

Milliken, W. F. & Milliken, D. L., 1995. *Race Car Vehicle Dynamics.* Warrandale: SAE international.

NHTSA, 1991. *Technical Assessment Paper: Relationship between Rolloverand Vehicle Factors,* s.l.: s.n.

NHTSA, 2013. *Rollover.* [Online]
Available at: http://www.safercar.gov/Rollover
[Accessed 11 November 2013].

Penny, W. C. W., 2015. *Anti-lock Braking Systems on rough terrain.* Rome, International Society for Terrain Vehicle Systems.

Phanomchoeng, G. & Rajamani, R., 2011. *New Rollover Index for Detection of Tripped and Un-Tripped Rollovers.* Orlando, s.n.

Rajamani, R., 2006. *Vehicle Dynamics and Control.* Minnesota: Springer.

Road Traffic Management Corporation, 2009. *Road Traffic Report for the Calender Year 2009,* s.l.: Road Traffic Management Corporation.

Robert Bosch GmbH, 2005. *Driving Stability Systems.* Stuttgart: Robert Bosch GmbH.

Slotine, J. & Li, W., 1991. *Applied Nonlinear Control.* New Jersey: Prentice Hall.

Teknikens Varld, 2014. *Porsche Macan behaves strangely in the moose test.* [Online] Available at: http://teknikensvarld.se/porsche-macan-behaves-strangely-in-the-moose-test-162276/ [Accessed 15 October 2015].

Thoresson, M. J., 2007. *Efficient Gradient-Based Optimisation of Suspension Characteristics for an Off-Road Vehicle,* Pretoria: University of Pretoria.

Uys, B. P., 2007. *Omrol van Veldvoertuie,* Pretoria: University of Pretoria.

Uys, P., Els, P. & Thoresson, M., 2007. Suspension settings for optimal ride comfort of off-road vehicles travelling on roads with different roughness and speeds.. *Journal of Terramechanics.,* pp. Vol. 44, pg. 163-175.

Van der Westhuizen, S. & Els, P., 2014. Comparison of different gas models to calculate the spring force of a hydropneumatic suspension. *Journal of Terramechanics.*

Van Der Westhuizen, S. F., 2012. *Slow Active Suspension Control for Rollover Prevention,* Pretoria: University of Pretoria.

Wielenga, T. J., 2000. United States of America, Patent No. 6,065,558.

Wu, J., Wang, Q., Wei, X. & Tang, H., 2010. Studies on improving vehicle handling and lane keeping performance of closed-loop driver–vehicle system with integrated chassis control. *Mathematics and Computers in Simulation.*

Yoon, J. et al., 2010. Design and evaluation of a unified chassis control system for rollover prevention and vehicle stability improvement on a virtual test track. *Control Engineering Practice.*

Yoon, J., Cho, W., Koo, B. & Yi, K., 2009. Unified Chassis Control for Rollover Prevention and Lateral Stability. *IEEE Transactions on Vehicular Technology.*

Yoon, J., Kim, D. & Yi, K., 2007. Design of a rollover index-based vehicle stability control scheme. *Vehicle System Dynamics: International Journal of Vehicle Mechanics and Mobility.*

Appendix A

A.1 Double Lane Change – 68 km/h

Figure 93 shows the ZMP based rollover index for the 68km/h double lane change. It can be seen that there was only one activation of the ESC+RP system when the rollover index threshold of 0.5 was exceeded. Even though this RI peak was higher than the non-ESC+RP case, the following peak was reduced to below the threshold.

The comparison of the yaw rates and desired yaw rates in Figure 94 show that very similar results were achieved for both runs. A slight inflection point is however visible at the point where the ESC+RP system is triggered. The yaw rate is reduced to minimize the error to the desired yaw rate. During both runs the vehicle's recorded paths are shown to be within the prescribed lanes, as indicated in Figure 95.

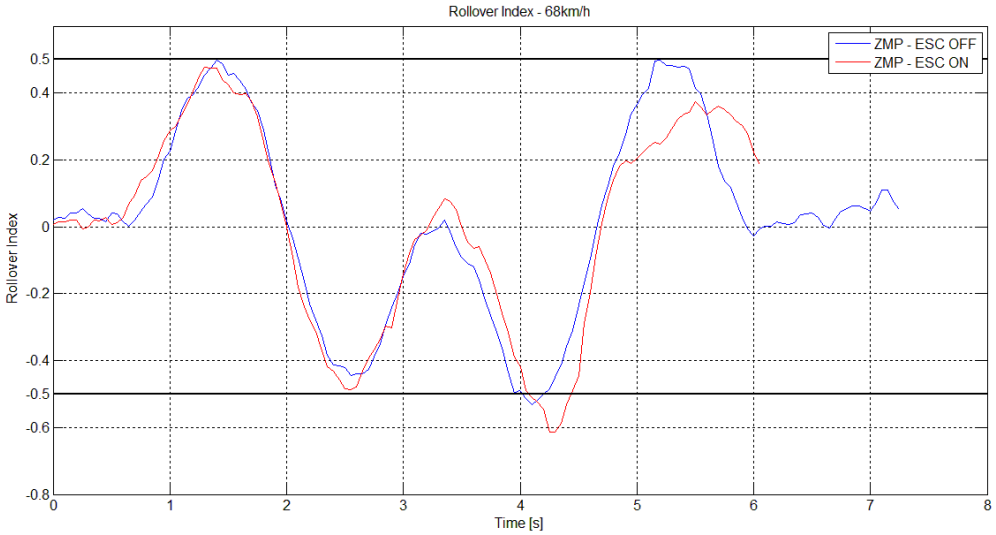

Figure 93 - RI for DLC at 68km/h

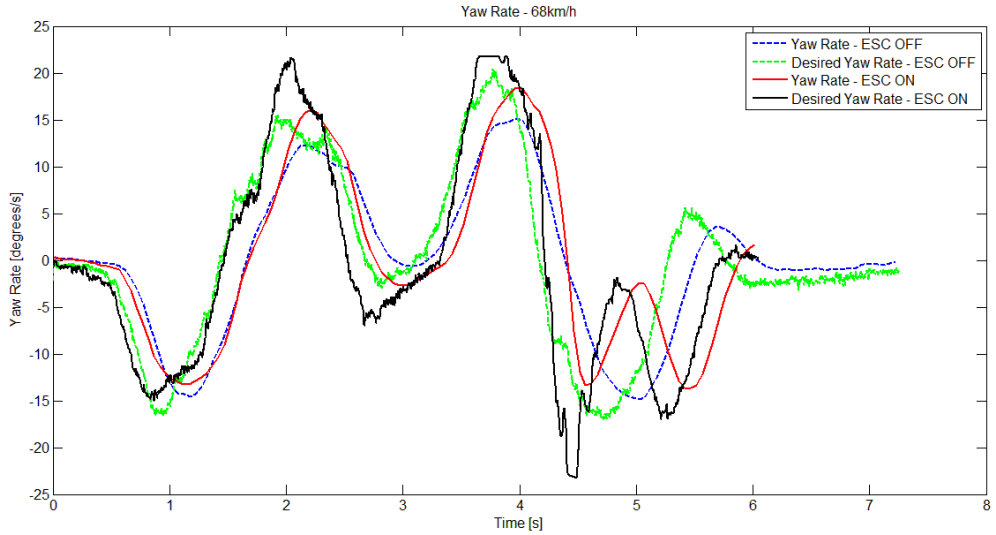

Figure 94 - Yaw rates for DLC at 68 km/h

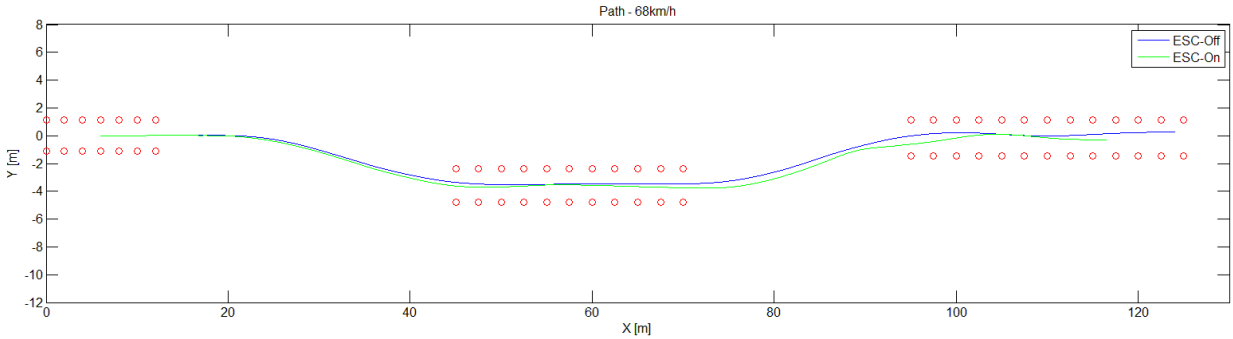

Figure 95 - Paths for DLC at 68 km/h

Figure 96 shows the steering inputs, lateral acceleration, roll angle, roll rate and vehicle speed data for the 68km/h entry speed run. Most noticeable is the larger spike in steering angle after the second lane of the manoeuver. This spike has led to the larger RI and lateral acceleration of the ESC+RP-on case. It is also apparent that there was a counter steering reaction from the driver before entry into the final lane. There was no ESC+RP activation at this point although it could be in reaction to the earlier reduction in yaw rate.

It is shown that the speed through the manoeuver has been reduced to about 62 km/h.

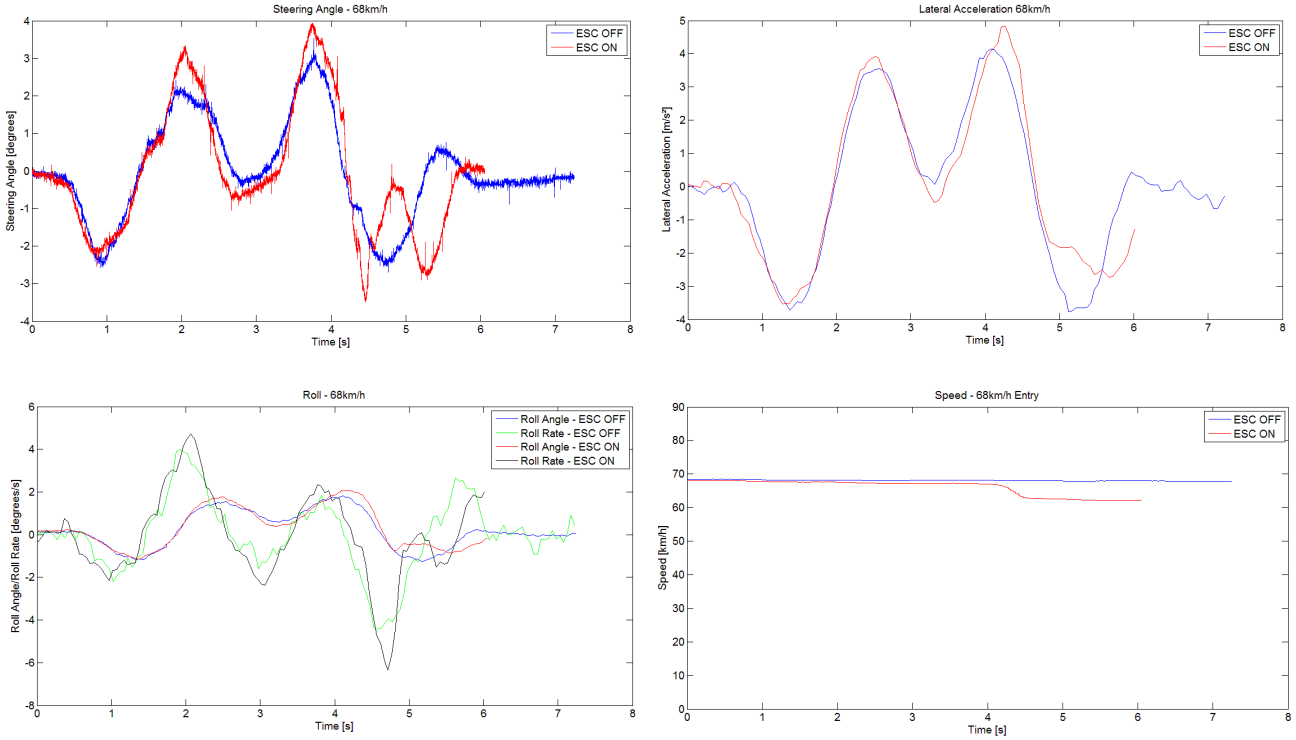

Figure 96 - Steering, lateral acceleration, roll and speed data for DLC at 68 km/h

A.2 Double Lane Change – 77 km/h

The results of the rollover index, yaw response and path for the 77km/h run are shown in Figure 97, Figure 98 and Figure 99. During the run with the ESC+RP on a short trigger is noted at initial turn in and the RI threshold is then exceeded at entry to and exit from the second lane. The RI peaks are generally higher than the non ESC+RP case, although tis can possibly be attributed to the sharper steering inputs. The inflection points in the vehicle yaw rate can once again be noted at activation of the ESC+RP, where the yaw rate is reduced in both instances.

The sharper steering inputs are indicated in Figure 100 and could possibly be the reason for the generally higher lateral acceleration, roll angles and roll rates for the ESC+RP-on case. A steering correction is once again noted before entry into the final lane, although a counter steering action is also visible for the non ESC+RP run. No noticeable steering reactions were induced at the earlier activations of the ESC+RP system.

The vehicle speed was once again reduced to about 62 km/h at the exit of the manoeuver.

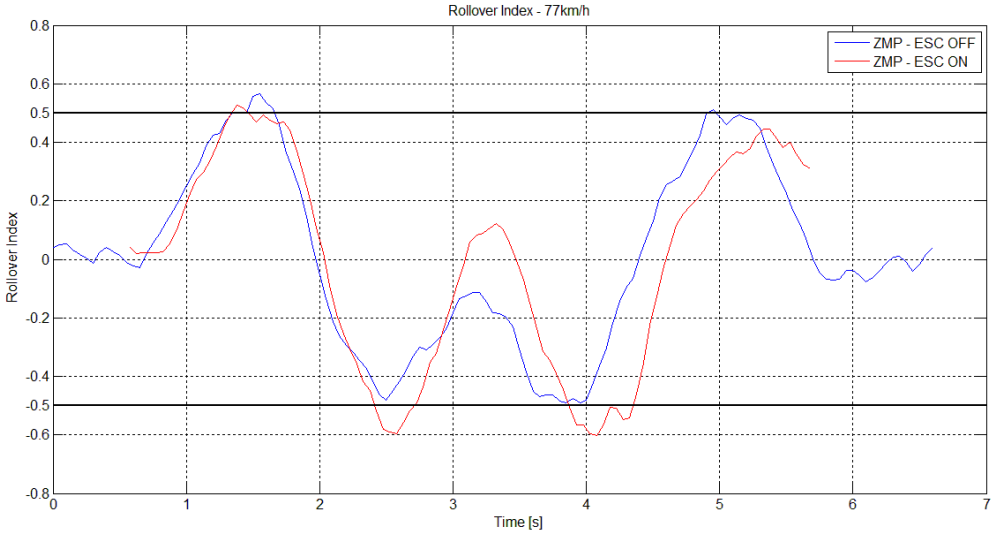

Figure 97 - RI for DLC at 77km/h

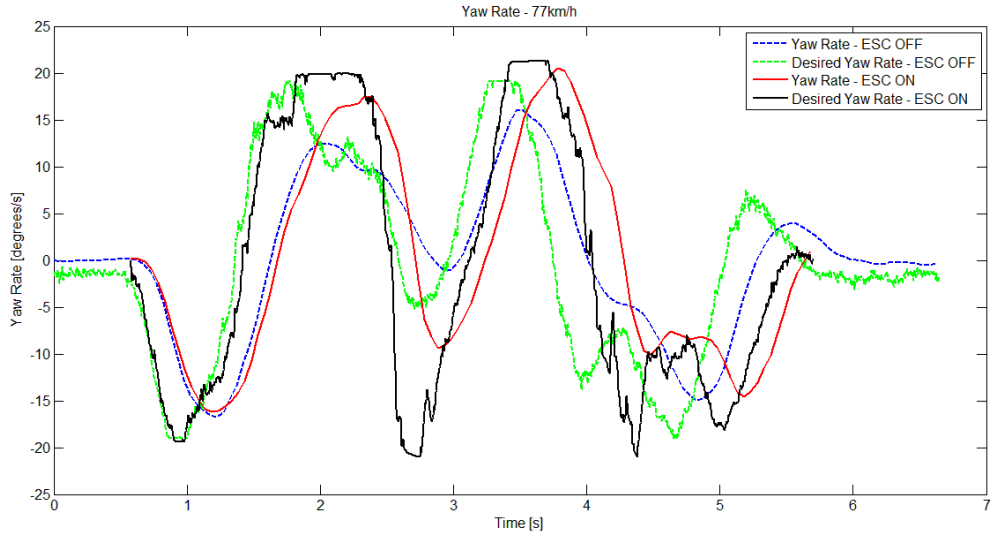

Figure 98 - Yaw rates for DLC at 77 km/h

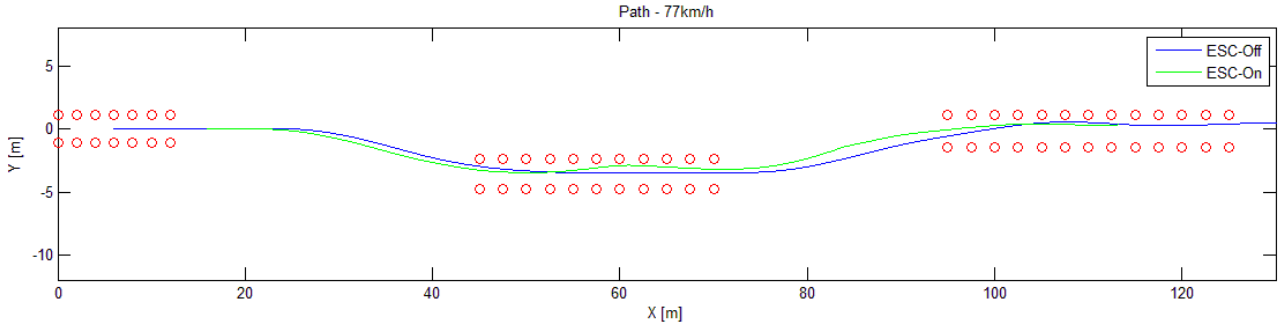

Figure 99 - Paths for DLC at 77 km/h

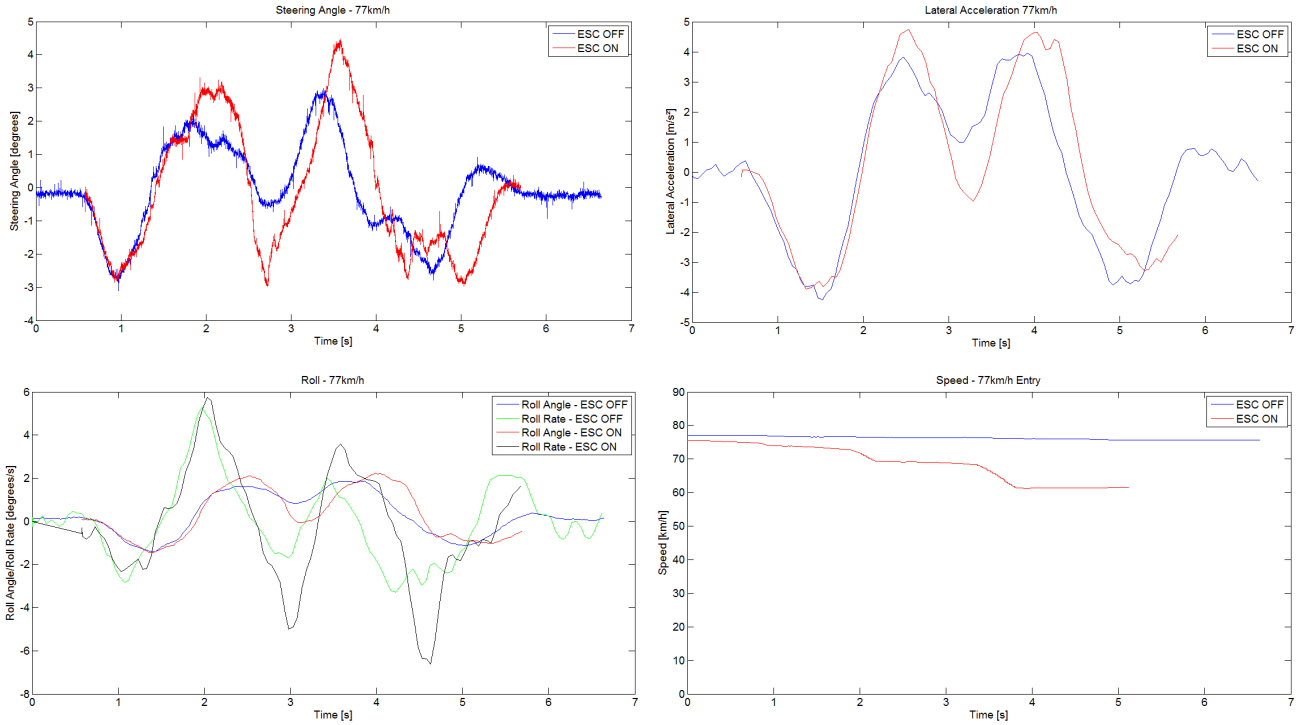

Figure 100 - Steering, lateral acceleration, roll and speed data for DLC at 77 km/h

A.3 Obstacle Avoidance – 50 km/h

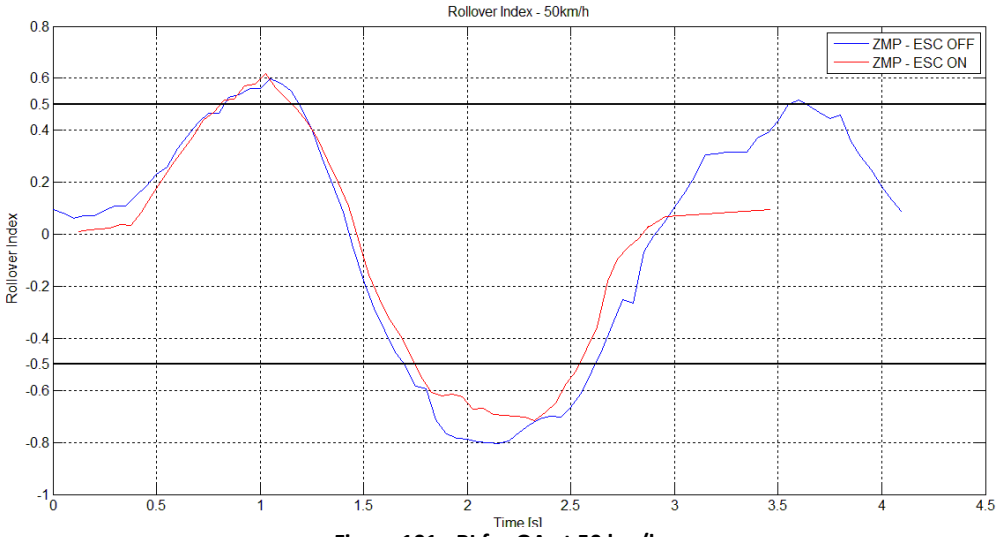

Figure 101 - RI for OA at 50 km/h

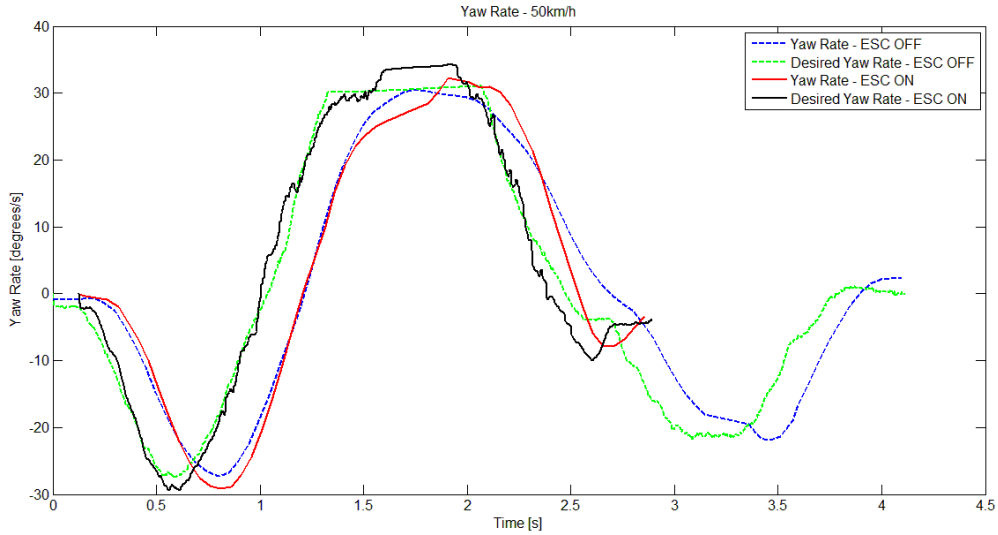

Figure 102 - Yaw rates for OA at 50 km/h

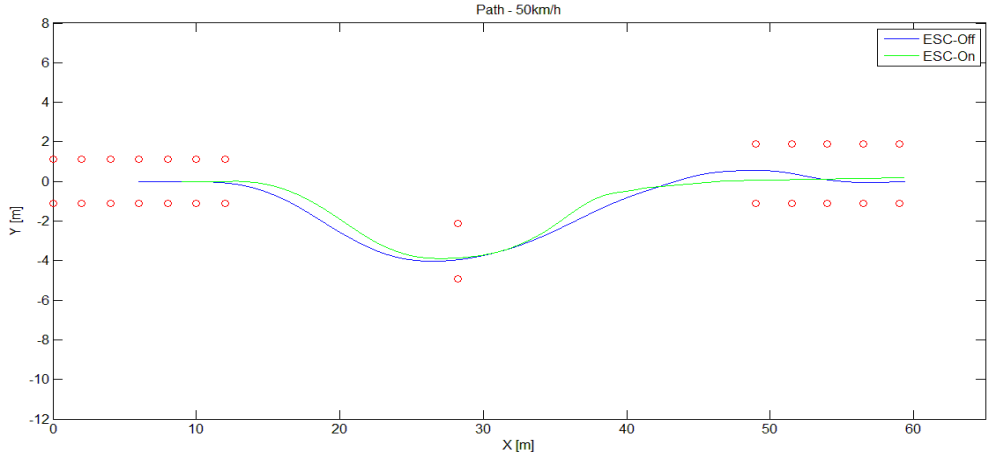

Figure 103 - Paths for OA at 50 km/h

It is seen from the rollover index in Figure 101 that the RI threshold of 0.5 is exceeded twice, with the manoeuver producing much higher peaks than the DLC manoeuver. It is noticeable that the initial RI and yaw rates of the both cases were very similar before the ESC+RP intervention. The RI during the left turn through the middle lane has been reduced and the third peak nearly completely eliminated. The yaw rate results indicate that the ESC+RP system appears to have forced the yaw rate closer to the desired yaw rate, with a larger deviation seen in the non-ESC+RP case.

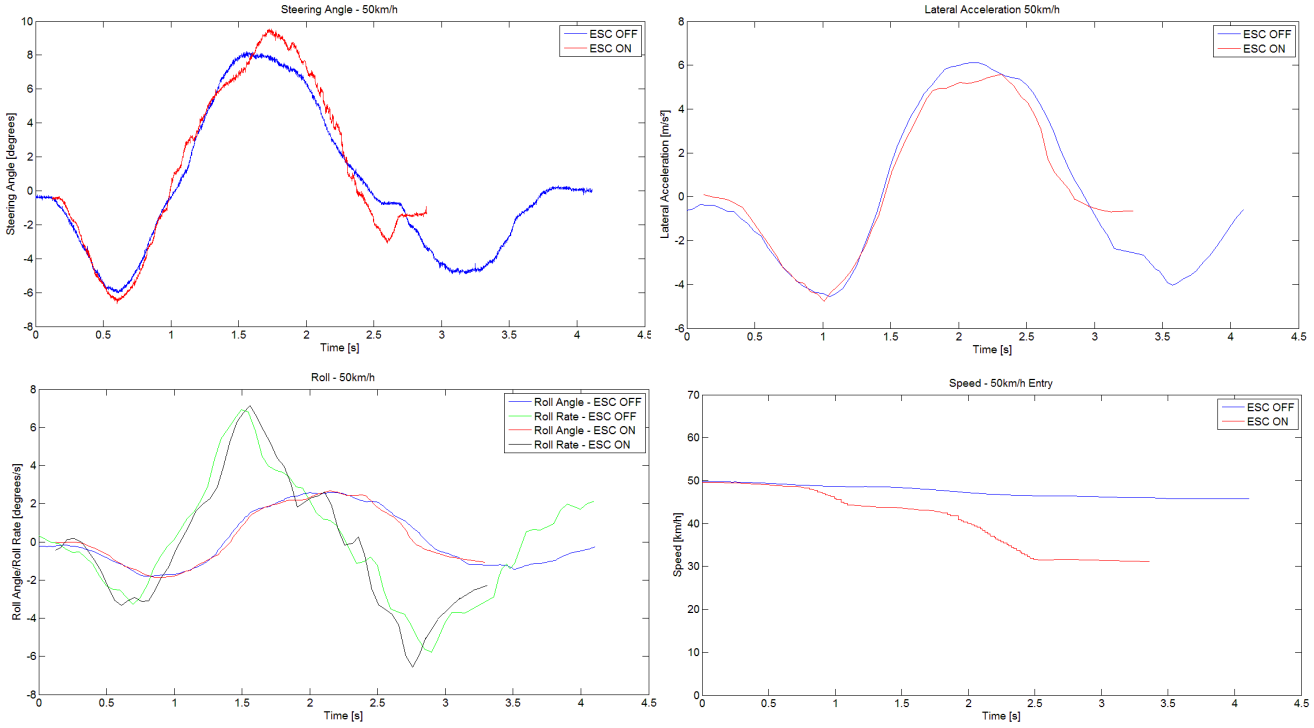

Figure 104 - Steering angle, lateral acceleration, roll and speed data for OA at 50 km/h

Figure 104 shows the steering inputs for the two manoeuvers, which are very similar for both runs and were also done at near identical entry speeds. The initial roll angles, roll rates and lateral accelerations were subsequently comparable. The braking from the ESC+RP system has reduced the vehicle speed to about 32km/h at exit.

During both runs the vehicle successfully stayed within the predefined course, whilst the vehicle with the ESC+RP on recorded a lower rollover index and exited the manoeuver at a safer speed.

A.4 Obstacle Avoidance – 50 km/h – Rear Suspension Hard

The results for the 50 km/h runs indicate very similar rollover indices with and without the ESC+RP on. The steering angles in Figure 108 do indicate that slightly larger steering angles and rates were initially applied in the ESC+RP-on case.

Looking at the yaw rate data in Figure 106 there is a more rapid decline in the yaw rate at the first ESC+RP intervention as opposed to the non-ESC+RP case. It is also interesting to note at the second activation that initially the desired yaw rate is actually higher than the actual yaw rate. The brake pressure data indicate that the wheels on the inside of the turn are braked before the outer wheels and hence we see the rise in yaw rate at about the 2s mark. As the outer wheels are braked the yaw rate declines more sharply. The last yaw rate peak is avoided with the ESC+RP on.

For both runs the vehicle completed the manoeuver without exceeding the course limits. The most noticeable aspect of the runs with the ESC+RP on is the fact that the dynamic aspects of the entry into the final lane of the manoeuver are almost completely eliminated. The steering correction seen in the non-ESC+RP case, to get the vehicle to stay within the lanes, produces another peak in RI which is not seen with the ESC+RP on.

The vehicle entered the final lane at a very safe speed of about 31 km/h while not allowing the vehicle to leave the desired path.

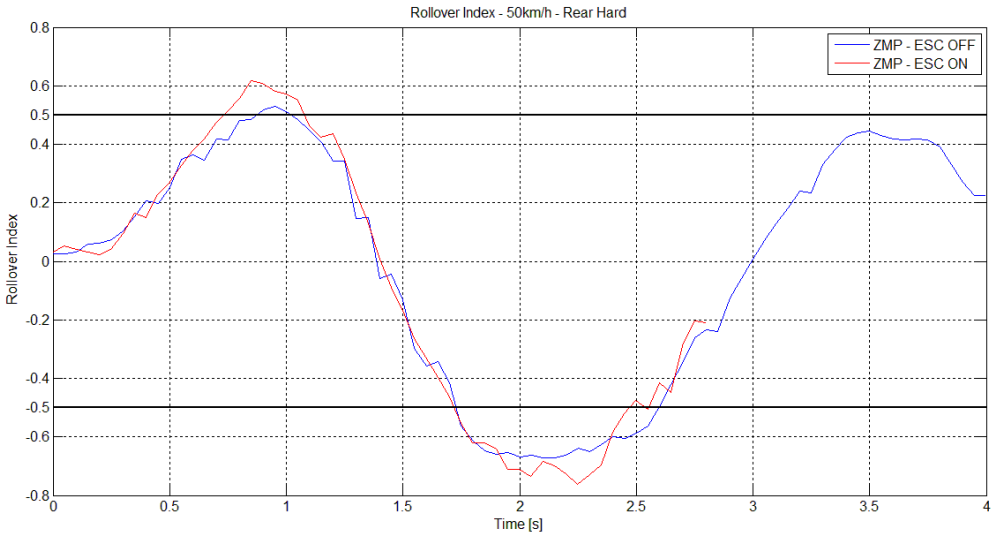

Figure 105 - RI for OA at 50 km/h - Rear Suspension Hard

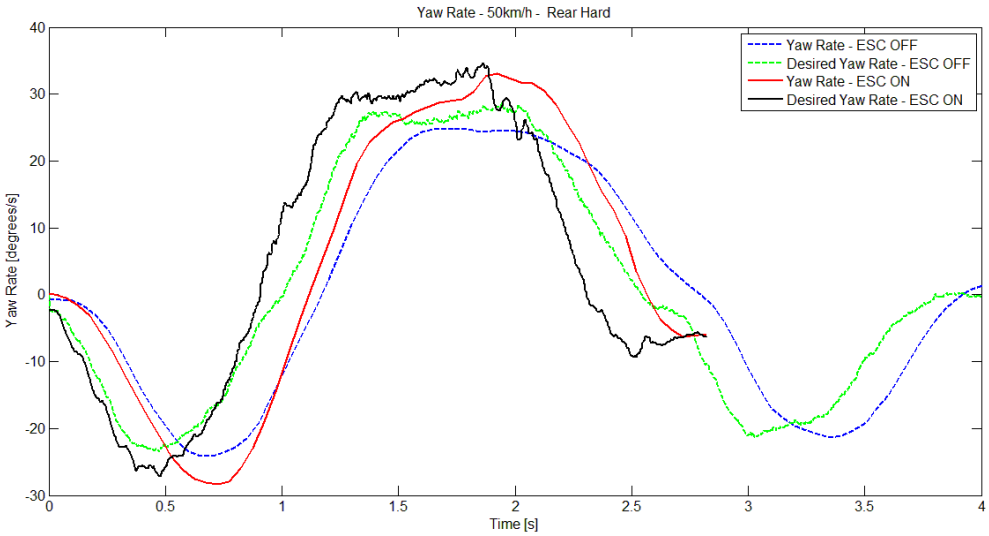

Figure 106 - Yaw rates for OA at 50 km/h - Rear suspension hard

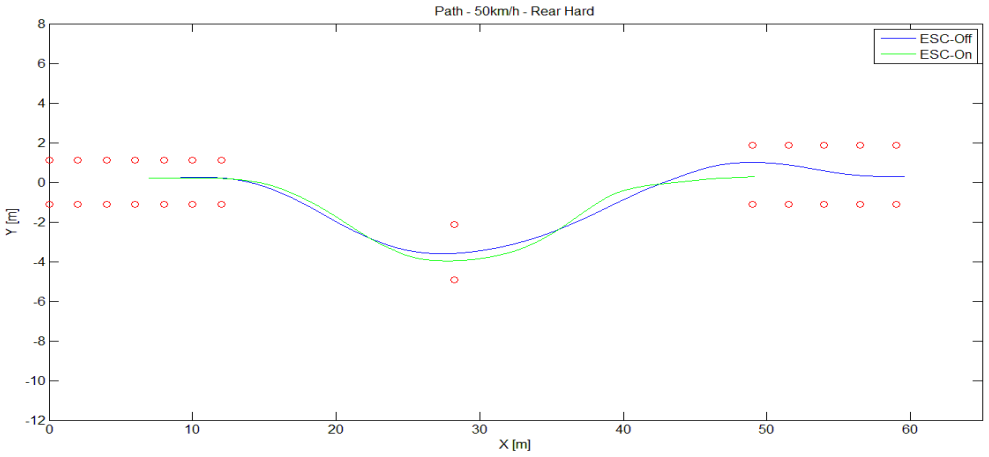

Figure 107 - Paths for OA at 50 km/h - Rear suspension hard

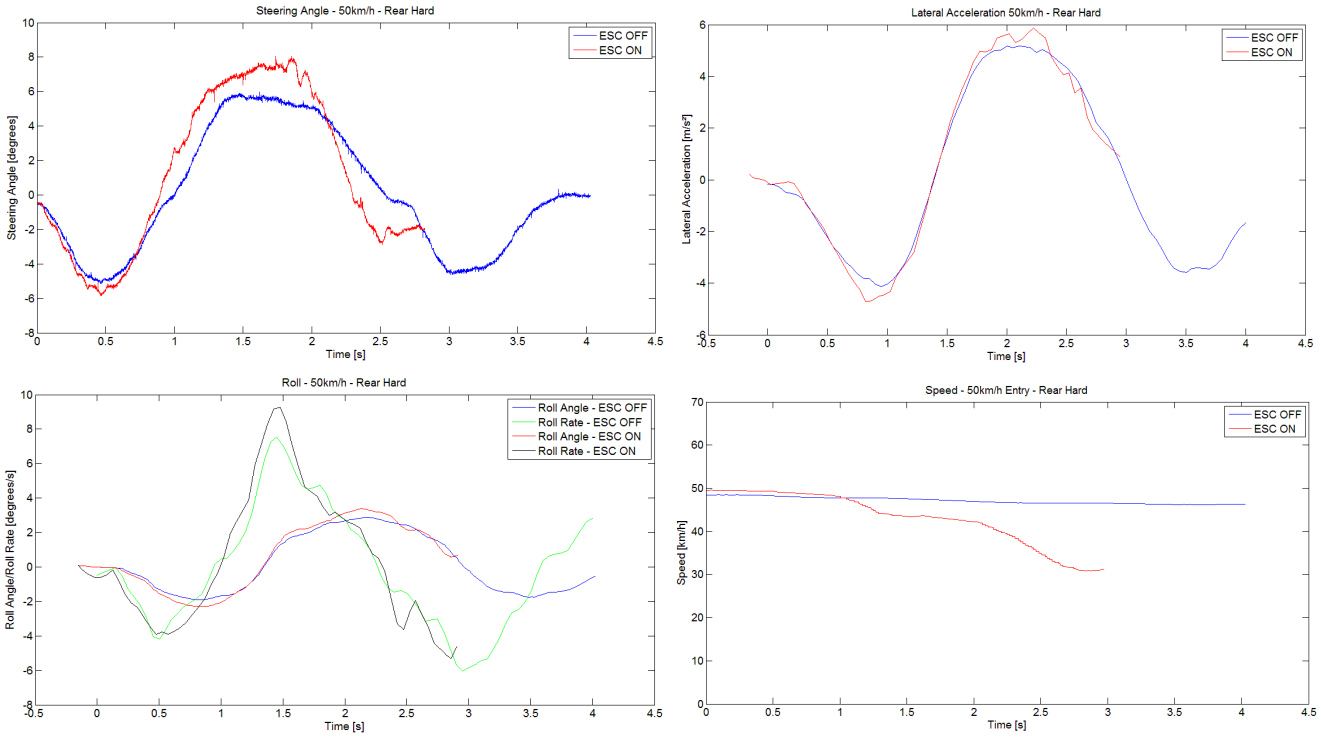

Figure 108 - Steering angle, lateral acceleration, roll and speed data for OA at 50 km/h - Rear suspension hard